Cement and Concrete Research 202 (2026) 108150

Contents lists available at ScienceDirect

Cement and Concrete Research

journal homepage: www.elsevier.com/locate/cemconres

Insights into the nano- and microstructures of cementitious materials using synchrotron X-rays☆

Miguel A.G. Aranda [a,b,*], Angeles G. De la Torre [a,b], Susan A. Bernal [c], John L. Provis [d]

[a] Departamento de Química Inorgánica, Cristalografía y Mineralogía, University of Malaga, Malaga, 29071, Spain
[b] Instituto Universitario de Materiales y Nanotecnología, IMANA, Ada Byron Building, University of Malaga, 29071, Malaga, Spain
[c] Department of Architecture and Civil Engineering, University of Bath, Bath, United Kingdom
[d] PSI Center for Nuclear Engineering and Sciences, Paul Scherrer Institut, Forschungsstrasse 111, 5232, Villigen PSI, Switzerland

ARTICLE INFO

Keywords:
Synchrotron radiation
Diffraction
Rietveld analysis
Spectroscopy
Tomography
Imaging
Segmentation

ABSTRACT

Synchrotron X-ray techniques have been extensively applied to characterise the mineralogy of anhydrous cementitious materials, the hydration processes and products in cementitious systems, and the alterations induced by different environmental exposure conditions. However, with changes in cement compositions and performance requirements, and an increased focus on materials design for sustainability, there is now strong emphasis on the use of advanced analytical tools to bring fundamentally based, multi-scale, multi-modal, spatially-resolved and/or time-resolved understanding of the physico-chemical factors influencing cementitious materials in the fluid, hardening and cured states. Beamline-based analysis complements conventional laboratory techniques, bringing unique capabilities to develop high-level insights. Here we provide a critical overview of the application of synchrotron radiation-based techniques to cementitious materials, and the opportunities and research needs to unlock their full potential for their use in future cement materials research, including issues related to handling and processing the very large datasets that can be generated.

Abbreviations

Synchrotron radiation techniques

3DXRD	3D X-ray Diffraction (microscopy)
abs−μCT	Absorption contrast micro−Computed Tomography
BCDI	Bragg Coherent Diffraction Imaging
B−PXnCT	Bragg−Ptychographic X-ray nano−Computed Tomography
CDI	Coherent Diffraction Imaging
EDXRD	Energy Dispersive X-ray Diffraction
EXAFS	Extended X-ray Absorption Fine Structure
FCDI	Forward Coherent Diffraction Imaging
ff−PXnCT	far-field−Ptychographic X-ray nano−Computed Tomography (forward)
HX−nCT	Holographic X-ray nano−Computed Tomography
HX−μCT	Holographic X-ray micro−Computed Tomography
nCT	nano−Computed Tomography
nf−PXnCT	near-field Ptychographic X-ray nano−Computed Tomography (forward)
PDF	Pair Distribution Function
ph−nCT	Phase contrast nano−Computed Tomography
ph−μCT	Phase contrast micro−Computed Tomography
PXnCT	Ptychographic X-ray nano-Computed Tomography (forward)
PXμCT	Ptychographic X-ray micro-Computed Tomography (forward)
s3DXRD	scanning 3D X-ray Diffraction (microscopy)
SANS	Small Angle Neutron Scattering
SAXS	Small Angle X-ray Scattering
SCXRD	Single Crystal X-ray Diffraction
SR−μCT	Synchrotron Radiation micro−Computed Tomography
SXRPD	Synchrotron X-Ray Powder Diffraction
TEDDI	Tomographic Energy-Dispersive Diffraction Imaging
WAXS	Wide Angle X-ray Scattering
XANES	X-Ray Absorption Near Edge Spectroscopy
XAS	X-ray Absorption Spectroscopy
XRD−μCT	X-Ray Diffraction micro−Computed Tomography
XRF	X-Ray Fluorescence
XRPD	X-Ray Powder Diffraction
μCT	micro−Computed Tomography

☆ This article is part of a Special issue entitled: 'Low-carbon cement science' published in Cement and Concrete Research.

* Corresponding author at: Departamento de Química Inorgánica, Cristalografía y Mineralogía, University of Malaga, Malaga, 29071, Spain.
E-mail address: g_aranda@uma.es (M.A.G. Aranda).

https://doi.org/10.1016/j.cemconres.2026.108150
Received 29 June 2025; Received in revised form 12 January 2026; Accepted 23 January 2026
Available online 27 January 2026
0008-8846/© 2026 The Authors. Published by Elsevier Ltd. This is an open access article under the CC BY license (http://creativecommons.org/licenses/by/4.0/).

μXRD micro-X-Ray Diffraction

Cement terminology

AFm	Aluminate/Ferrite-mono substituted (hydrocalumite-like calcium aluminate)
AFt	Aluminate/Ferrite-Tri-sulfate or ettringite
ASR	Alkali-Silica Reaction
BCSA	Belite Calcium SulfoAluminate
BFS	Blast Furnace Slag
CSA	Calcium SulfoAluminate
C-S-H gel	Calcium Silicate Hydrate (with variable stoichiometry) gel
FA	Fly Ash
LC^3	Limestone Calcined Clay Cement
LDH	Layered Double Hydroxide
MKPC	Magnesium Potassium Phosphate Cement
PC	Portland Cement
PCE	PolyCarboxylate Ether
SCMs	Supplementary Cementitious Materials
SP	Superplasticiser
w/b	water to binder mass ratio
w/c	water to cement mass ratio
w/s	water to solids mass ratio

Other acronyms

AI	Artificial Intelligence
BL	BeamLine
CNR	Contrast-to-noise ratio
DLS	Diamond Light Source
$D_{v,50}$	Median particle size by volume
EPMA	Electron Probe Micro-Analyse
ESEM	Environmental Scanning Electron Microscopy
ESRF	European Synchrotron Radiation Facility
FoV	Field of View
HEMC	HydroxyEthyl Methyl Cellulose
ML	Machine Learning
PSI	Paul Scherrer Institut
RH	Relative Humidity
RQPA	Rietveld Quantitative Phase Analysis
SEM	Scanning Electron Microscopy
SLS	Swiss Light Source
SNR	Signal to Noise Ratio
SR	Synchrotron Radiation
STXM	Scanning Transmission X-ray Microscopy
UV	Ultra-Violet
WS	Watershed segmentation

1. Brief introduction to the properties of synchrotron X-rays

Synchrotron light source facilities are a type of circular particle accelerator built to produce electromagnetic radiation with exceptional features. These large facilities are user-oriented, where personnel from very different backgrounds (*photon scientists*: physicists, chemists, materials scientists, geologists, biologists, etc.; and *supporting scientists and technologists*: accelerator physicists, mechanical/vacuum/computing/control engineers, data scientists, technicians, etc.) work together with the goal of providing the best possible service to the users. A synchrotron source typically contains three types of electron accelerators: i) the linear accelerator (i.e. linac), ii) the booster, and iii) the storage ring. The electrons are produced and accelerated in the linac. Then, they are injected into the booster to be further accelerated, before being transferred to the storage ring. This storage ring is a circular accelerator where the kinetic energy of the electrons is kept constant (at relativistic speeds, within a fraction of a percent of the speed of light) and the desired SR is generated within the photon sources comprising, or inserted into, the ring. More information about synchrotron light sources can be found in [1–3].

From the user's perspective, everything starts at the photon source, where the SR is produced by manipulating these relativistic electrons using magnetic devices in a suitable (technique-dependent) manner. Each change of direction of the electrons generates electromagnetic radiation, in the form of photons. These photons are of a variety of wavelengths (i.e. polychromatic; either white or pink beam), and they must be conditioned before they can be used to analyse cementitious, or any other, samples. For a description of the optics components that are employed to do this, interested readers can find more information in [1–3], or in selected reviews on the use of SR for material analysis such as [4–6].

The main properties of SR are briefly summarised here. Some other potentially useful properties of SR, such as its intrinsic picosecond time-structure (that allows researchers to follow ultra-fast processes) and polarisation features (that permit the study of magnetic samples) are not discussed here as they are not of interest for cementitious materials research.

I. Very high flux. This characteristic leads to the following key uses: — Yields data with very high SNRs, allowing: (i) high quality analyses, (ii) studies with very low limits of detection and limits of quantification, and (iii) to study weakly scattering samples; — Permits very fast data collection for time-lapse studies; and — Allows complex sample environments (that absorb many photons) such as high-temperature or high-pressure cells.
II. Parallel geometry. This feature allows: — To improve full-field reconstruction for imaging/tomography; — To minimise the errors in powder diffraction; and — Grazing incidence techniques.
III. Energy tunability. It is noted that this property is at the heart of SR techniques. On the one hand, hard X-rays (i.e. energies higher than approximately 6 keV) permit bulk sample studies. Much higher energies allow for cell (and sample) penetration and complex sample environments. On the other hand, soft X-rays (i.e. energies lower than approximately 2 keV) offer surface sensitivity and allow the study of light elements. X-ray energies between 2 and 6 keV are usually labelled as tender X-rays. Specifically, — It permits spectroscopic techniques; — It yields chemical sensitivity through tuning to absorption edges; — Tuning to high energy (hard X-rays) minimises absorption in complex sample environment experiments; — High-energy SR allows access to large momentum transfer values, very useful for techniques such as total scattering or high-pressure studies; and — Tuning to low, i.e. soft, energy SR allows enhanced contrast for imaging, surface-specific analysis due to low penetration depth, and spectroscopy of lighter elements.
IV. Beam size tunability (from nanometres to centimetres). — It enables a very large range of imaging techniques, from centimetres in concretes to nanometres in pastes; — It allows matching the size of the beam to the sample/experiment requirements; — It allows easier design of sample environments.
V. Partial transverse coherence. — Permits several modalities of phase-contrast imaging; — Allows coherent diffraction imaging.
VI. Spatial and time stability. — Guarantees high resolution and high reproducibility.

To end this subsection, review papers partly addressing the use of SR techniques for investigating cementitious materials include [7–9]. Those studies also include information about other analytical techniques that can be applied to cementitious materials, such as electron microscopy and nanoindentation, which are often complementary and/or necessary for the accurate multi-modal interpretation of SR derived results. It is noted that since 2016, there have not been review publications solely devoted to the use of SR to investigate cementitious materials [5], with only a perspective review on 4D synchrotron X-ray nanoimaging for

early-age cement studies published in 2025 [10]. This paper is therefore timely in providing updates on progress in this fast-moving field.

2. Brief introduction to synchrotron radiation techniques applied to cementitious materials

Fig. 1 displays a schematic summary of the most common SR techniques that have been employed for studying cementitious systems. These techniques range from scattering/diffraction for the analysis of components (crystalline or nanocrystalline) to spectroscopic tools for characterisation of chemical species, and to spatially-resolved approaches for multiscale characterisation including macro-, micro-, meso- and even nano-structures. This review is not intended to be a thorough compilation of works dealing with the characterisation and analysis of building materials by SR techniques. Rather, the scope of this overview is to briefly introduce some of the most useful tools and chiefly, to illustrate, through selected examples, the type of relevant scientific information that can be gained by applying these techniques. A brief overview of the scope of the review is as follows:

Concerning the elastic interaction of SR X-ray photons with cementitious materials, three broad types of techniques are being used:

(i) SXRPD allows analysis of both anhydrous cements and hydrating/hydrated binders. The powder patterns are usually analysed by the Rietveld method (in some cases with additional plug-in like PONKCS [11,12] or mass balance calculations [13,14]) to also determine the presence of poorly diffracting components. With this general approach, the dissolution (i.e. reaction) of pristine crystalline phases, the crystallisation of hydrates and even the formation/precipitation of amorphous phases are quantitatively measured. Selected uses of this method, i.e. SXRPD, will be elaborated in Section 3.1 for early-age analysis, and Section 4.1 for later-age samples. Moreover, SXRPD can be implemented using very small beam sizes, yielding the synchrotron X-ray microdiffraction techniques that have been employed in cementitious systems [15], detailed in Section 4.1.2. SCXRD has also been applied to determine new crystal structures in cementitious materials [16], but its application is far less common in this field.

(ii) SAXS has been applied to study the size, shape and arrangement of the building blocks constituting the cement pastes at early hydration ages including multiscale investigations [17–19]. This technique, and its counterpart WAXS (which is another name for XRPD), are described in Section 4.1.3.

(iii) Total scattering synchrotron patterns, mainly analysed by the PDF approach [20], take advantage of the information in Bragg peaks and also the diffuse scattering in the powder patterns. This is being used to further characterise nanocrystalline gels arising from the hydration of PCs and also from alkaline activations, see for instance [21–23] and Section 4.1.4.

There are several spectroscopic techniques based on SR, see Fig. 1. Initially, a distinction should be made between SR photons of infrared energies and those of X-ray ones. Moreover, for X-rays, hard and soft-based X-ray techniques are quite different from the experimental point of view as soft (and tender) X-rays require the use of vacuum to minimise the interaction/absorption/scattering with the environment. Discussion of selected spectroscopic applications relevant to cementitious materials is presented in Section 4.2. Combining scattering and spectroscopy can also yield additional valuable information, which has recently been reviewed in the context of nanomaterials characterisation [24].

Fig. 1 also displays most of the SR techniques that have been employed to gain spatially-resolved information in cementitious materials research [5]. These techniques can be categorised into two broader clusters. On the one hand, we consider those techniques that can study features in 2D, i.e. mapping. Often (but not always), the specimens are thin slabs, and the information is obtained by scanning the flat samples with a synchrotron beam of the correct size for acquiring the corresponding signal. The types of recorded signal can be very diverse, ranging from an X-ray diffraction powder pattern to an IR spectrum, or absorption-contrast radiographs can be collected through a thick sample for use in monitoring the evolution of void, liquid, and solid phases

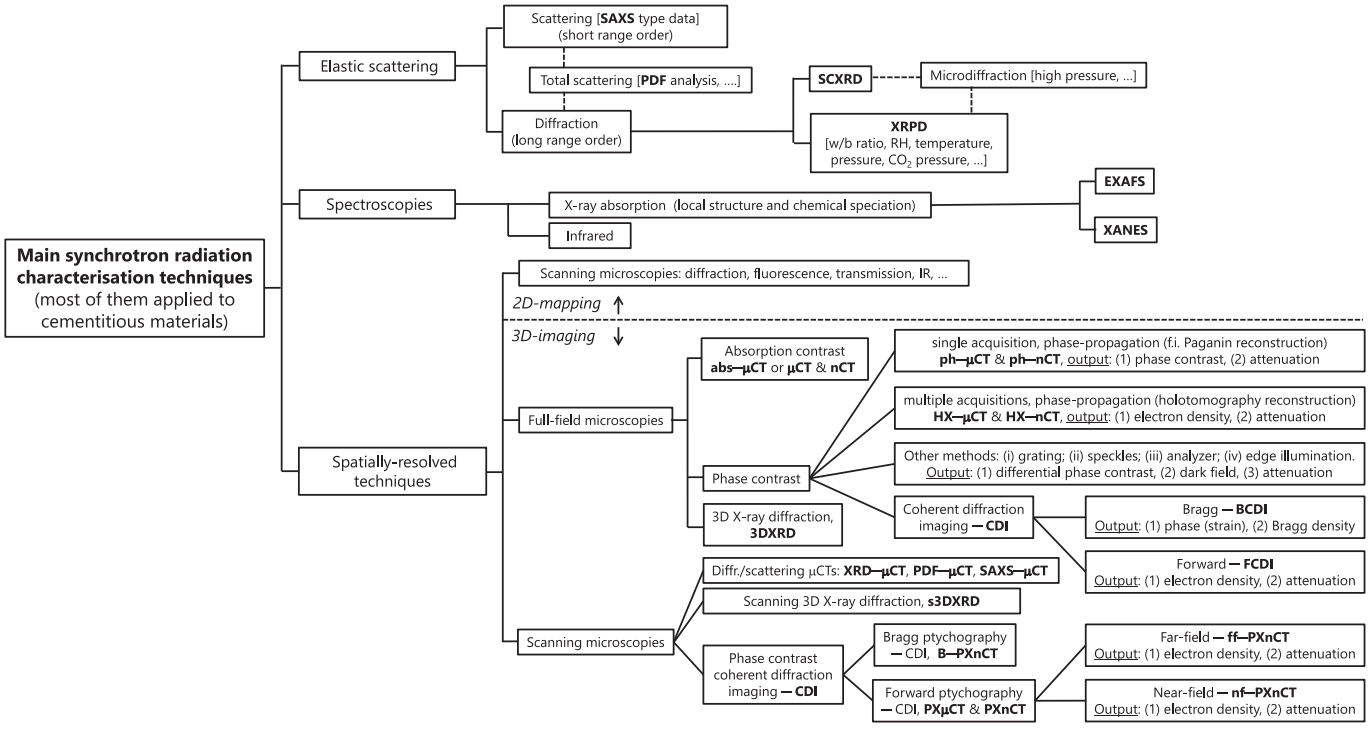


Fig. 1. Scheme illustrating the main SR techniques used for materials characterisation. Many of these techniques have been applied in the study of cementitious materials. The most commonly used acronyms are given in bold and are defined at the 'abbreviations' list of the manuscript.

within a flowing sample of paste, Section 3.4. On the other hand, there are tools that permit the extraction of 3D information by a CT approach, where a virtual volume is reconstructed from thousands of angular projections; Sections 3.2, 3.3, and 4.3. In turn, as is shown in Fig. 1, 3D imaging techniques can be classified into full-field approaches, where an entire angular projection is taken at once, and scanning microscopies, where an angular projection is obtained by combining many data points through scanning the specimen with a synchrotron beam with the appropriate size and divergence. The sizes of the SR beam and sample (usually cylindrical) can be adjusted considering the resolution required for the analysis of the material.

Information about 3D SR imaging techniques that have been used to characterise cementitious materials, as well as their advantages and disadvantages, can be found in [5]. More detailed information about the generalities of SR imaging/tomography can be found in [6,25–28], and general overviews of tomography applied to cementitious materials are also available [7–9,29–32].

As detailed in Section 4.3.2, μCT data can be acquired in two general modalities: (i) absorption-contrast, placing the detector as close as possible to the sample and using X-ray attenuation as the contrast mechanism, and (ii) phase-contrast, where the coherence features of the synchrotron X-ray beams are exploited. The second modality can be implemented experimentally using various configurations, with the most common being in-line phase-propagation CT. In this approach, the detector is positioned at an optimised distance from the sample, to enhance contrast by exploiting phase shifts arising from refraction at material interfaces. The X-ray phase shifts are usually retrieved using the Paganin algorithm, which has become the standard practice [33]. This experimental configuration (and data processing pipeline) is available at most, if not all, μCT BLs.

When X-rays pass through a sample, they can be absorbed, refracted or scattered. These interactions encode distinct physical and chemical properties of the sample. Multi-modal X-ray imaging methods can access complementary information through different imaging channels retrieved from the same measurement: (1) attenuation, (2) differential phase contrast and (3) dark field, see Section 4.3.2. These imaging methods are mainly based on the use of: (i) analyser; (ii) edge illumination; (iii) grating interferometry and (iv) speckles. Multi-modal imaging has rarely been used [34,35] for cements, probably due to the modest spatial resolution attained in the early studies. This is evolving and much better spatial resolution is now available, see for instance [36].

Concerning other techniques mentioned in Fig. 1, it is noted that some techniques such as XRD−μCT and forward ptychotomography are discussed in Section 4.3.1. However, there are others such as 3DXRD [37,38], s3DXRD [39] and BCDI [40,41] which are not further discussed in this review due to their limited use in cementitious materials studies and space restrictions in this work.

As mentioned above, the objective of this review is to provide potential users with relevant information that can be extracted from each technique. However, identifying the appropriate synchrotron BL for a given technique or experiment can be challenging, particularly for non-specialist users. At least two online platforms facilitate this process by helping to align specific scientific questions with the available infrastructure. The Lightsources.org website [42] provides a global interactive map of more than 50 synchrotron facilities, each offering direct access to BL descriptions and user portals. For a more targeted search within the European landscape, the Way for Light portal [43] allows users to filter BLs by technique (e.g. X-ray tomography, XRD, XAS) and by sample environment. As an example, just for 'imaging', this website provides links for 128 BLs in 20 European facilities (including but not limited to synchrotrons). Filtering the search to only consider 'synchrotrons' results in 91 BLs in 12 facilities. Further filtering of the search by adding 'X-ray tomography' yields 37 BLs in 11 facilities. Although beamtime allocation via a competitive application system applies in all cases, access to those facilities and software for data processing comes at no cost to the users, and in many instances financial support for travelling and accommodation is also provided.

3. Early-age cementitious materials hydration studies

PC hydration [44,45] is a complex, multi-stage process initiated upon mixing cement with water, which triggers a series of chemical reactions. After partial cement particle dissolution, mass transport and supersaturation, interconnected reactions of crystallisation and precipitation take place. These reactions progressively transform the initially anhydrous, and predominantly crystalline, clinker phases into a combination of crystalline hydration products such as portlandite and ettringite, and nanocrystalline or disordered (often termed "amorphous") phases such as C-S-H gel. Partially-ordered layered hydrous calcium aluminates, and (at later ages) iron-siliceous hydrogarnets also are formed. The time-evolution of crystalline and amorphous phases implies changes in the microstructure of the cement paste as capillary pore space is progressively filled by hydrated phases. Critically, the evolution of the microstructure during hydration and/or other processes such as CO_2 mineralisation modifies the movement of species through the evolving pore structure. Therefore, phase assemblages (type and reaction products forming) and microstructural development (including the pore structure) are intimately interconnected and linked to engineering properties and durability. This partly justifies why the curing behaviour of cementitious materials is so complex.

Thus, in-situ analysis of the time-evolution of phases and microstructures is key to predicting and optimising the potential performance of cementitious products. In this context, a multiscale/multimodal picture is essential [46]. Electron microscopy can yield data with very high spatial resolution, but cannot follow changes with time in relevant conditions, i.e. w/b ratios used in field applications, and with commercial cementitious materials which have $D_{v,50}$ values of 10–20 μm. These materials should not be further milled if researchers are seeking to investigate kinetics and microstructural evolution, as the fineness of cement has a very significant influence on measured reaction kinetics and microstructures [47]. In the next subsections, selected recent examples of early-age in-situ SXRPD (for phase evolution determination) and in-situ SR-μCT (in different modalities for microstructure evolution determination) are presented. It should first be clarified that the terms 'in-situ' and 'time-lapse' are used indistinctly in the literature, and both are referring to studying the same specimen over time.

3.1. *In-situ SXRPD applied to analyse evolution of crystalline compounds*

SXRPD offers many advantages compared to standard laboratory measurements [5] because of the properties highlighted in Section 1. For this technique, the key benefits are: (i) rapid acquisition because of the high intensity of the beam at the sample position; (ii) high-resolution (i.e. reduced overlap of diffraction peaks) due to the use of an incident monochromator and long sample-detector distances; and (iii) the potential to collect high-quality data because of the use of a parallel X-ray beam. Hydration in PC systems begins within seconds of water addition, making sample preparation a critical step to ensure accurate capture of the earliest hydration processes. The time dependence of these reactions also renders the data acquisition strategy essential. BL optical components, particularly crystal analysers and mirrors, enhance angular resolution and improve the SNRs [48], which is especially important for cementitious systems due to extensive peak overlap from the numerous coexisting phases. A high acquisition speed is required to track the rapid transformation of the initial anhydrous phases into hydration products [49]. This subsection starts with a discussion on sample preparation for early-age time-lapse studies, followed by selected examples of SXRPD data acquisition and data analysis.

Sample preparation presents significant challenges in terms of acquiring data from the very onset of the hydration reaction while enabling meaningful comparisons among various analytical techniques.

To achieve this, highly consistent preparation protocols are essential. Several experimental procedures have been implemented in which water is remotely introduced into the capillary using syringe injection pumps, see Fig. 2a. This setup is often coupled with external vibration or overhead homogenisation systems, enabling the preparation of cement pastes with w/s values ranging from 0.4 to 1.0. To ensure complete wetting of the powder, a small amount of glass wool is typically inserted into the capillary tube. This methodology enables data acquisition within seconds of water addition, thereby allowing the earliest hydration stages to be monitored with minimal delay [50,51]. The use of an acoustically-levitated cement pellet (to which water is applied by a syringe) instead of a capillary has also been demonstrated in a study which achieved sub-second time resolution [52], but this is a complex methodology and was observed to yield rather variable peak intensity between successive scans.

An alternative, yet related, approach involves the manual addition of water directly to the capillary after it is aligned in the sample holder, Fig. 2b. In such cases, data collection typically starts approximately 3 min after water addition. However, this strategy generally employs a significantly higher w/s ratio (e.g. close to 10:1) to ensure paste homogeneity throughout the probed volume within the capillary [53]. This high w/s ratio substantially deviates from conventional cement hydration conditions and may limit the representativeness of the hydration processes so observed.

A third alternative is to prepare the paste in the laboratory by mixing water with the cement. This mixing can be mechanically performed and the resulting paste is then introduced into the capillary using a syringe, Fig. 2c. This procedure takes more time but it ensures that mixing step is carried out in exactly the same conditions as for other techniques such as isothermal calorimetry or ultra-sound pulse velocity. To prevent water loss and CO_2-ingress the end of the capillaries/tubes must be sealed before placement on the (goniometer head) sample holder. The complete procedure, including paste preparation, capillary filling, sealing, and alignment on the sample holder, typically takes approximately 10–15 min before data acquisition can start [54–56]. In addition to ensure the paste homogeneity, the main advantage of this approach is that it allows strict control over the w/s ratio, although information corresponding to the first minutes of hydration is inevitably lost.

In time-lapse (i.e. in-situ) SXRPD experiments, two main types of detectors are typically employed: 2D detectors and 1D position-sensitive detectors such as the Mythen system [57,58]. 2D detectors simultaneously capture a large area of diffraction data, facilitating the very fast collection of medium-resolution diffraction rings and enabling the analysis of complex samples, avoiding issues related to preferred orientation. In this context, single-photon counting detectors have many advantages for diffraction applications [59]. The 2D images are then processed into 1D diffraction data using software such as Fit2D [60], heXRD [61], or Dawn Workbench [62], see Fig. 3.

In contrast, 1D detectors like the Mythen type provide high temporal resolution and precise angular information along a single axis, making them very well-suited for fast, time-lapse measurements. These detectors offer real-time data acquisition and are often integrated with BL automation, thereby increasing the throughput of kinetic studies. To improve particle statistics and minimise artefacts such as preferred orientation, capillary spinning is essential. Additionally, it is recommended to acquire multiple diffraction patterns (typically 3–4) at different positions along the capillary and merge them with the appropriate software. In this way, not only is sample-averaging notably improved, but chiefly, radiation damage is minimised while having very good SNRs.

A common strategy for studying cement hydration mechanisms involves the use of pure phases as model systems. The main advantage of this approach is that it reduces the complexity of data analysis, facilitating mechanistic interpretation. However, this comes at a price: this type of studies cannot account for the potential synergistic interactions among coexisting phases, as pore solution chemistry is inevitably different. In any case this approach is often followed, and in-situ SXRPD is particularly well-suited for investigating phases that exhibit rapid hydration kinetics, such as C_3A [50], $C_4A_3\overline{S}$ [54] or C_3S [55].

The hydration of C_3A in the absence and presence of sulfate has been extensively investigated because of its fast dissolution rate and its critical influence on the early reactivity of cement systems. This phase plays a key role in controlling/delaying silicate dissolution, and in inducing flash setting in systems with insufficient early-age sulfate availability [45,64]. In this context, the hydration of C_3A with different sulfate sources ($MgSO_4$, Na_2SO_4, K_2SO_4, and $CaSO_4$) was monitored by in-situ SXRPD [50]. Time-lapse SXRPD data revealed the initial formation of the AFm-type phase C_4AH_{19}, followed by its transformation into C_3AH_6. These transformations are consistent with known hydration sequences but are more clearly resolved due to the high temporal resolution. Notably, all sulfate salts, regardless of cation type and even at low concentrations, delayed the formation of crystalline hydration products. This highlights that precipitation kinetics are predominantly governed by sulfate ions rather than the nature of the accompanying cation [50].

AFt is the primary crystalline phase formed during the early hydration of C_3A in the presence of calcium sulfate(s). The impact of different SPs on ettringite formation was investigated in [53]. In particular, naphthalene-based SP promoted the faster and more extensive formation of crystalline AFt, whereas PCE-based SPs slowed the precipitation kinetics and reduced the degree of crystallinity. Two commercial PCs

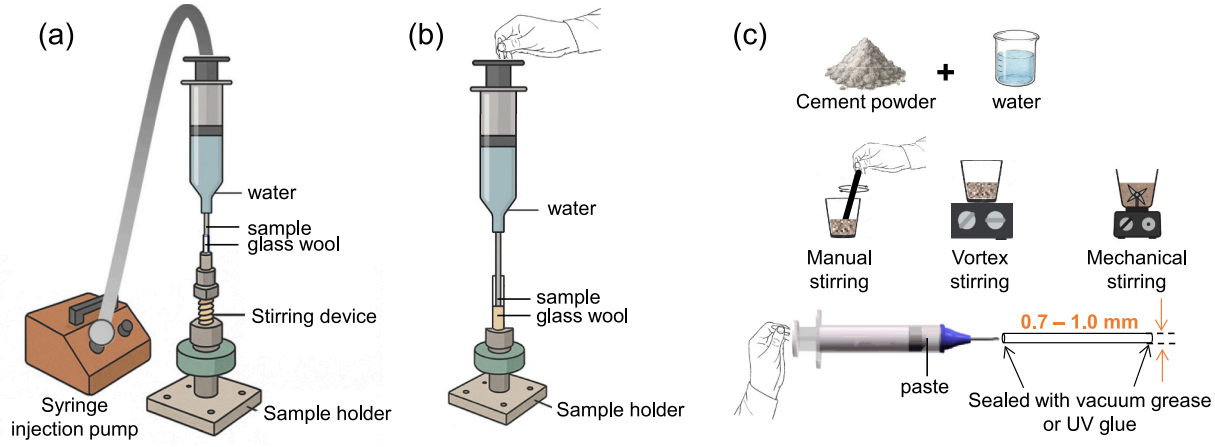


Fig. 2. Sketches of sample preparation for time-lapse SXRPD measurements. (a) Remote in-situ water addition by a syringe injection pump, (b) manual in-situ water addition, and (c) ex-situ paste preparation and injection into the capillary, immediately followed by sample mounting and time-lapse data acquisition.

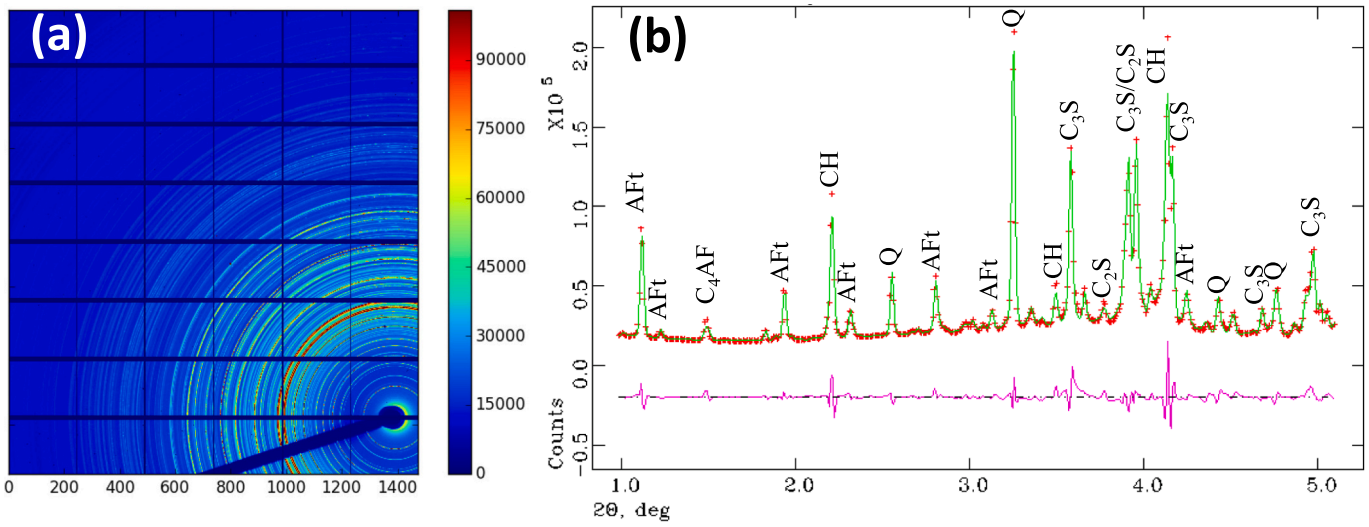


Fig. 3. (a) SXRPD raw 2D data (λ = 0.19 Å) obtained for a PC paste after 12.8 h of hydration. A Pilatus3 X CdTe 2 M hybrid photon counting detector with pixel size 172 × 172 μm^2 was used, off-centred with respect to the incident beam and placed 999.505 mm from the sample. (b) Selected low-angle region of the Rietveld plot for the corresponding integrated 1D pattern, with the main peaks due to a given phase labelled in standard cement notation (Q stands for quartz used as internal standard). Used under the terms of the Creative Commons CC-BY-NC-ND licence [63].

with similar overall compositions but different early-age mechanical strengths were also examined and compared with model systems. In these PCs, faster and more complete crystallisation of AFt was observed. Larger AFt crystallites were identified by ESEM and SXRPD, and the lattice parameters converged more rapidly to the final values. These results highlight the capabilities of in-situ SXRPD to resolve, in real time, the crystallographic and kinetic evolution of ettringite during the early hydration of C_3A. Moreover, this technique enables a detailed assessment of how chemical admixtures influence both the crystal structure(s) of cement hydrates, and the kinetics of hydration [50,52,53].

In-situ SXRPD analysis of C_3S hydration faces the limitation of the nanocrystalline nature of the C-S-H gel. As a result, SXRPD alone is insufficient to comprehensively resolve the structural and compositional features of this primary hydration product. The poor long-range crystallinity of C-S-H hampers conventional diffraction techniques, which can analyse phases with long-range periodic atomic arrangements. To (partly) overcome this limitation, a multi-technique approach is essential. A comprehensive study by Cuesta et al. [55] exemplifies this strategy by employing multiscale characterisation of C_3S hydration. The employed methodology combined in-situ SXRPD during the first 48 h, with ex-situ measurements of previously prepared samples with the same pastes, enabled the monitoring of phase evolution for up to 100 days. Fig. 4 illustrates the temporal evolution of crystalline phases for two alite samples with different average particle sizes. Not only were C_3S hydration and portlandite crystallisation mapped out, but C-S-H formation could also be (indirectly) monitored by mass balance calculations. As expected, the alite sample with finer particles yielded faster kinetics, see Fig. 4. Moreover, from additional (synchrotron) PDF studies (see Section 4.1.4 for discussion of this technique), it was suggested that C-S-H gel forms as a nanocomposite comprising defective tobermorite and monolayers of calcium hydroxide [55].

The role of admixtures in the hydration of model phases can also be investigated. Qoku et al. [65] focused on how HEMC admixtures affect early hydration of C_3S, up to 48 h. The in-situ SXRPD and PDF studies revealed that HEMCs retard both the dissolution of C_3S and the precipitation of hydration products. While portlandite formation was significantly delayed, the local atomic structure of C-S-H remained unchanged. The PDF analysis showed consistent short- and medium-range order among all samples, implying that HEMCs primarily affect the kinetics rather than the structure of C-S-H. This work highlights the importance of synchrotron-based analysis in identifying the surface

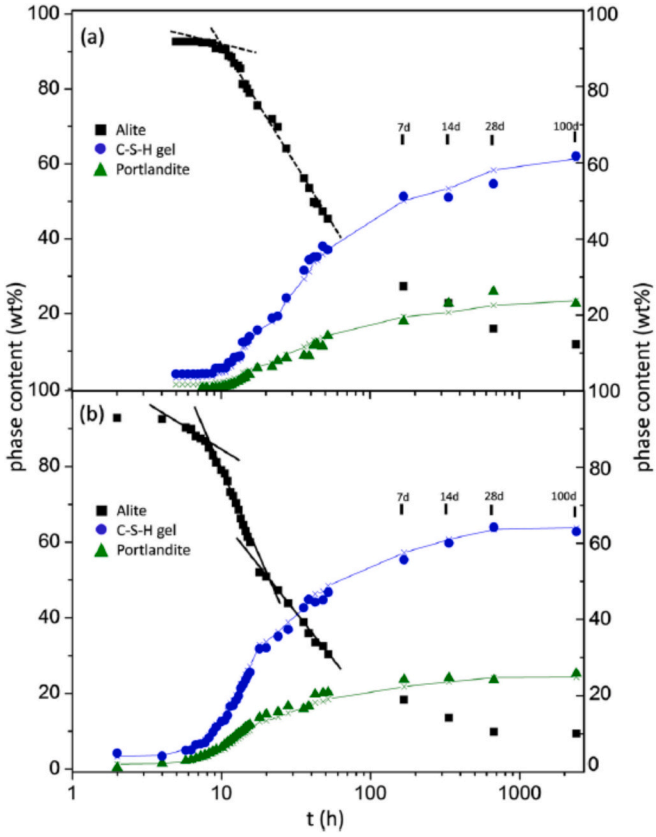


Fig. 4. Quantitative phase analysis results from SXRPD data. (a) Phase evolution for a C_3S sample with $D_{v,50}$ = 21 μm. (b) Idem, for C_3S with $D_{v,50}$ = 7 μm. Both pastes had w/s = 0.80. The lines for C-S-H gel (blue) and portlandite (green) show the expected amounts from the measured dissolution of alite according to the reaction $C_3S + 5.2H \rightarrow 1.2CH + C_{1.8}SH_{4.0}$. Used under the terms of the Creative Commons CC BY licence [55]. (For interpretation of the references to colour in this figure legend, the reader is referred to the web version of this article.)

interaction of HEMCs with hydrating particles as the primary

mechanism of retardation.

It has been mentioned above that the reductionist approach of using single phases for studying cement hydration has advantages and disadvantages. The same occurs when studying commercial Portland cements to understand general cement hydration behaviour(s). Several factors must be considered when interpreting the results for commercial samples, including the presence of minor elements in the clinker phases, variations in cooling rates that influence polymorphism, particle sizes and specific surface areas, the generalised use of grinding aids during production which affect hydration, etc. Each of these parameters can substantially impact hydration and may introduce biases that are difficult to assess independently. In any case, early-age SXRPD studies of commercial cement samples have also been conducted. In such cases, the principal advantage over pure phase studies lies in the ability to evaluate synergistic (i.e. coupled) interactions between coexisting clinker phases. Two recent extensive studies involving up to 40 clinkers [66,67], with diverse compositions and production parameters, were carried out to assess the influence of these variables on the hydration features of the resulting cements. The results indicate that the observed trends are broadly representative of modern Portland clinkers. However, such conclusions should still be considered approximations, given the inherent variability of clinker properties and processing conditions. In spite of the limitations associated with studying commercial cements, a few available works do provide valuable insights and report meaningful results. Notably, Morales-Cantero et al. [63] evaluated two commercial PCs at various w/c ratios over the first 16 h of hydration, quantifying the degree of hydration of individual phases, i.e., C_3S, C_3A and C_4AF, as a function of both w/c ratio and hydration time. These results were correlated with calorimetric data and setting times determined using the Vicat method. The main conclusion was that C-S-H gel, rather than AFt, is the primary phase responsible for the setting of PC; this topic has been under discussion for a long time in the scientific community. A similar study was carried out by Vigor et al. [68] who evaluated the phase changes in blast furnace slag blended cements, and identified the influence of the interactions between PC and slag on the rate and extent of formation of various hydrates.

A related system characterised by rapid hydration kinetics and pronounced AFt formation is CSA cements. Investigations into the early-age hydration behaviour of CSA and BCSA cements, considering variations in the amount and type of calcium sulfate as well as the presence of chemical admixtures, provide valuable complementary insights [69,70]. These studies shed light on several key aspects, including the influence of ye'elimite polymorphism, the role of slow-reacting phases such as belite, and the impact of dopants such as boron, which delay AH_3 precipitation and alter the early hydration pathways [71]. Furthermore, the interaction with admixtures is critical, as it can significantly alter dissolution-precipitation pathways and modify the kinetics of AFt formation [69,70]. In all these studies, the amount of nanocrystalline aluminium hydroxide has to be indirectly quantified by either the internal standard methodology [72], mass balance calculations [13,14] or the PONKCS approach [11,12], as it plays an important role in the hydrate assemblage of CSA-type cements but does not show sufficiently long-range order for Bragg peaks to be observed.

In-situ SXRPD is especially well-suited to study the role of admixtures in early age cement hydration. As an example, the effect of C-S-H nucleation seeding on the initial hydration of one commercial PC and two industrial belite-rich cements was studied [73], and the results were connected with those obtained by isothermal calorimetry and ultrasonic pulse velocity measurements. In this study, SXRPD was not limited to monitoring only the first few hours of hydration, but also enabled the collection of diffraction data up to 60 h. A synergistic effect was observed when C-S-H nucleation seeding was combined with alkanolamines. While the hydration rates of alite and belite were not significantly influenced by the C-S-H seeding after one day, an acceleration in the dissolution of sulfate and aluminate phases was clearly detected, which in turn facilitated the early formation of ettringite and modified the setting times and the early mechanical strengths [74].

Additional recent work employed in-situ SXRPD to investigate the role of admixtures (two different SPs, C-S-H nucleation seeding and triisopropanolamine) on the early age hydration of limestone-calcined clay blended binders [75]. The pozzolanic reaction in these cements started as soon as 7 h after water mixing. The stagnation of portlandite content, despite the continuous C_3S hydration, provided direct evidence of the pozzolanic reaction, see Fig. 5. Moreover, other kinetic phenomena became evident, such as the faster dissolution of C_3A and C_4AF by the addition of the C-S-H nucleation seeding admixtures. This effect was SP-dependent. It is also worth noting that for the PC used as reference, gypsum was consumed at 10 h but AFt continued crystallising beyond 18 h, see Fig. 5. The authors speculated that the sulfate source for ettringite crystallisation was desorpted from C-S-H gel. In addition, RQPA in combination with mass balance calculations was used to quantify the formation of C-S-H and C-A-S-H gels and to estimate the reaction degree of metakaolin [75].

Finally, this review also elaborates on the evolution of hydration reactions with time under moderate pressures at mildly elevated temperatures (for studies at high pressures using diamond anvil cells, the reader is referred to [8], and to the brief discussion in Section 4.1.1). In-situ SXRPD under non-ambient conditions provides valuable insights for systems such as oil-well cements, which are exposed to elevated temperatures and pressures. The experimental configuration typically involves the use of sapphire capillaries or triple-walled Kapton tubes [76,77]. The hydration behaviour of a Class-G PC incorporating a phosphonate retarder was examined under relevant conditions (165 °C, ~70 bar), revealing a substantial delay in the formation of 11 Å tobermorite and α-C_2SH due to the presence of the retarder [77]. Additionally, a novel high-resolution in-situ SXRPD approach employing a spinning capillary cell was implemented to monitor the hydration of Class-G PC at 150 °C and 150 bar. This setup enabled phase quantification using Rietveld analysis [78], indicating that alite achieved 90% hydration degree within 7 h, while belite achieved 42% after 14 h. Minor quantities of α-C_2SH and jaffeite were also detected. This study uniquely demonstrated the ability to resolve the hydration kinetics of individual clinker phases under realistic wellbore conditions. The same cell was employed at 180 bar and 160 °C to study the hydration behaviour of pure alite, pure belite, their mixtures and a belite-rich cement [79]. The main finding was that, under these conditions, the degree of hydration of belite exceeded that of alite. This behaviour is attributed to the rise in pH induced by alite hydration, which appears to play a crucial role in accelerating belite hydration at moderated pressures and temperatures.

3.2. *In-situ SR−μCT studies on the hydration of cementitious materials*

Understanding the chemical or physical changes cementitious materials experience as a function of hydration time and/or exposure to specific environmental conditions is fundamental to ensure their longevity and stability during service life. This has motivated the adoption of time-lapse X-ray CT approaches as effective non-destructive tools for the evaluation of undisturbed samples. Time-lapse tomographic experiments in cementitious materials have centred on evaluating two key aspects: (i) space-filling evolution of hydrated cements particularly during the first hours of reaction, and (ii) identifying microstructure alterations as a function of exposure time to aggressive environments. In-situ experiments, where the same specimen, without [80,81] or with fibres [82], is subjected to varying loads or different pressures [83] have also been conducted. This to identify preferential crack formation patterns and fracture mechanism of cementitious materials. Such results are often used as inputs for developing performance predicting models, see for example [84], and are discussed in more detail in Section 4.3.2.

Prior to hardening, hydrated PC is in a liquid plastic state, and can be better described as a fluid concentrated suspension. During the first hours of hydration the unrestricted movement of relatively dense

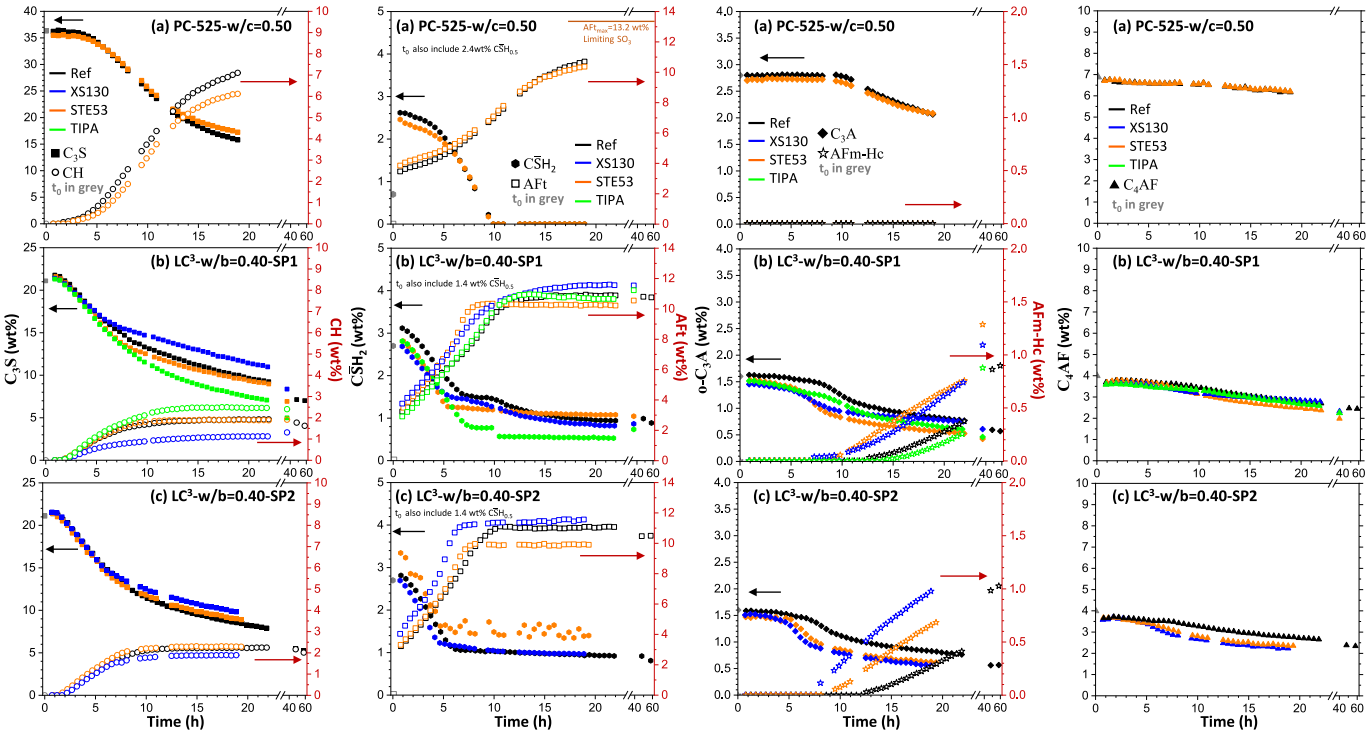


Fig. 5. Phase content evolutions from time-lapse SXRPD for (a) PC-52.5 pastes, w/c 0.50; (b) LC^3-SP1 pastes, w/b = 0.40; and (c) LC^3-SP2 pastes, w/b = 0.40. Two different PCE based SPs (SP1 and SP2) were investigated, and three strength enhancing admixtures: XS130, STE53 and TIPA; more details in the original publication [75]. Left-hand vertical axes of each panel: dissolution/hydration of cement phases (alite, gypsum, tricalcium aluminate and ferrite). Right-hand vertical axes of each panel: crystallisation of hydrates (portlandite, AFt and hemicarbonate). The symbols in grey indicate the starting amounts, i.e. $t = 0$. Adapted from [75], published under the Creative Commons CC-BY-NC-ND licence.

particles can lead to sedimentation and segregation before the materials fully harden. This is one of the reasons why most studies applying X-ray tomography techniques to evaluate cementitious materials have been conducted on hardened specimens. However, automated volume tracking procedures such as the one developed by Vigor et al. [85] can be adopted during data processing, to make the necessary corrections for identification and monitoring of specific hydrating cement grains in SR−μCT datasets collected during the first minutes of hydration of PC.

In-situ SR−μCT experiments from ~1.5 h to 3 days of age have also been conducted for plain PCs formulated with and without superplasticisers [86]; changes in unreacted clinker fractions and the evolution of hydrate phase formation were reported, along with the variations in porosity of the samples. Challenges in data collection and processing were acknowledged and a procedure for analysis of CT data was proposed. It is noted that this early SR−μCT study employed a relatively large sample-detector distance, i.e. 24 mm, which resulted in edge enhancement (i.e. propagation-based phase-contrast). However, the phases were not retrieved and the data were treated as just abs−μCT.

Evaluation of the effect of FA and limestone addition on the pore evolution of PC-blended binders has also been explored [87]. Time-lapse μCT results were collected between 30 min and 12 h of hydration, and it was identified that the empty space was continuously reduced as hydration progressed over the first 2 h of reaction, which in this case corresponded to the induction period. This was more noticeable in plain PC samples, compared to those blended with FA or limestone [87,88]. Beyond 2 h of hydration, significant changes in the void fraction were observed until 6 h of hydration, where a plateau was identified with no significant changes in the total porosity, independent of the cement type evaluated. In-situ ph−μCT experiments have revealed, for the hydration of plain PC pastes, the formation of hydration product layers from the first minutes of hydration, corresponding to the induction period, see Fig. 6 [56]. With continued reaction, the hydrate products gradually begin to grow both from particle surfaces into the initially fluid-filled region, and into the space originally occupied by the cement particles, forming an observable density gradient within the microstructure. During the acceleration period, interconnection of agglomerated low density outer hydrates is observed.

In-situ μCT studies have also been conducted for other cement types. Liu et al. [89] evaluated the pore structure evolution of a Class G well-cement slurry from 90 to 600 min of hydration, where sedimentation of particles at a hydration time < 145 min was identified. It was hypothesised that sedimentation can induce hydrostatic pressure gradients which might influence water movement, altering hydration rates and pore development at this early stage of hydration, however, this was not explored in detail. Nevertheless, the interconnectivity of pores as well as the overall porosity was reported to reduce during the hydration time evaluated, most notably between 180 and 600 min of reaction. In-situ ph−μCT has also been recently employed to study the hydration of blast furnace slag-PC blends with and without a $CaCl_2$ accelerator [90], and the bassanite-gypsum transformation [91].

In-situ SR−μCT can be used for evaluating cementitious materials, beyond their hydration and pore structure evolution. For instance, it is worth noting recent studies monitoring the behaviour of building materials under mechanical load [92,93].

3.3. *In-situ hard SR−nCT to probe evolution of submicrometre microstructural features*

Concerning the early-age hydration of cementitious materials, some pertinent features are submicrometric in size, which requires the use of 4D synchrotron X-ray nanoimaging. These features can be broadly categorised in three types: (i) related to the dissolution of cement particles, such as etch-pits growth or spatial dissolution rates (which are time-dependent but they can also be dependent on the initial particle size); (ii) related to the growth of the hydrates, such as C-S-H gel shells and needles growth rates and densification, or AFt growth rate; and (iii)

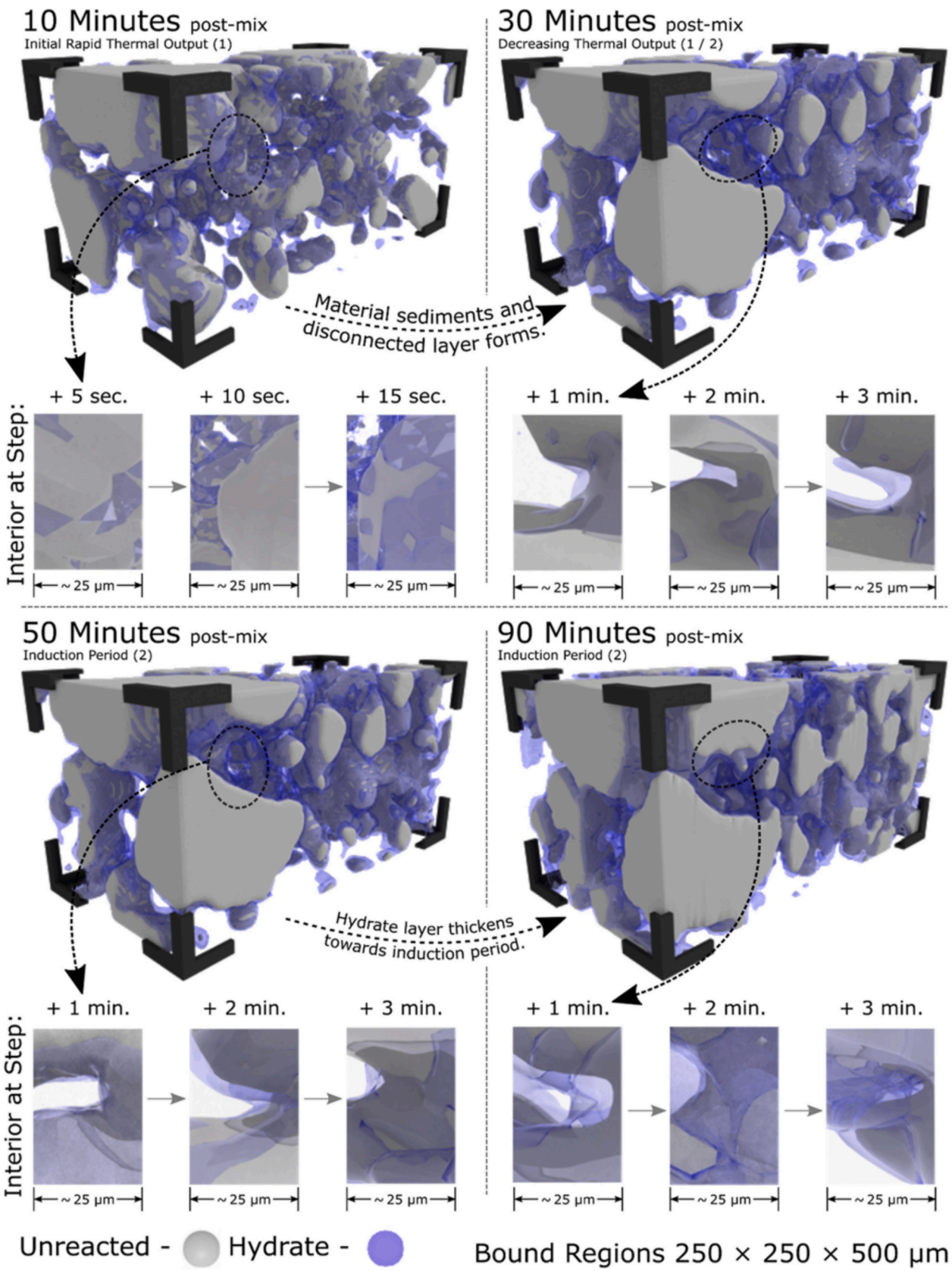


Fig. 6. 3D reconstructions from ph−µCT of a PC paste as a function of hydration time in the very early period of hydration. Reproduced from [56], published under a Creative Commons CC-BY 4.0 licence.

(capillary) porosity evolution. It is noted that a perspective article from one of the authors has very recently published in this topic [10] and therefore, this emerging field is only briefly elaborated here.

In order to have the required spatial resolution and contrast between the coexisting components, 4D X-ray nanoimaging is based on those synchrotron techniques leveraging the coherent properties of synchrotron radiation, see Fig. 1. In particular HX−nCT may yield the fastest data and nf−PXnCT higher spatial resolution. The five strict requirements necessary for obtaining relevant results [10], when investigating early-age cement hydration, are: (i) to analyse pastes with w/b ~ 0.30–0.50, which are the values used in field applications, restricting the growth of hydrates in confined spaces; (ii) to measure sufficiently large volumes, i.e. more than 150 μm for the diameter of the capillaries, to study cement hydration with the particle sizes of commercial samples (further grinding the samples should not be an option); (iii) good contrast between the components to be able to distinguish between different hydrates, and to measure the C-S-H gel densification with time; (iv) fast acquisition time, ~100 min or faster, to study the acceleration period; and (iv) best possible spatial resolution, ideally ~100 nm, to measure the required nanofeatures discussed just above.

It is noted that 3D nanoimaging of cementitious systems is not difficult and there are several examples with spatial resolution better than 100–150 nm [94–96]. However, to move from 3D to 4D nanoimaging is very challenging as data acquisition has to be relatively fast to match the kinetics of reaction of the cementitious systems being investigated. Here, we summarise the most important findings of the recent 4D nanoimaging studies of a PC hydrating paste [97]. Fig. 7 shows selected plane views of the same region at 19, 47 and 93 h after water mixing. The transition from the acceleration to the deceleration stages took place at 14 h, instead of the standard ~10 h for a neat PC 52.5 R, because the use of a superplasticiser to densely fill the 0.2 mm capillary, which is the widest that can currently be nanoimaged by nf−PXnCT. Nanoimaging data were taken in the deceleration stage of cement hydration because the overall acquisition time, larger than 3 h, was too slow to collect data in the acceleration stage. Many nanofeatures were derived in this study; only the most relevant are highlighted here.

At 19 h, the hydrating PC still has plenty of capillary water, electron density 0.33 e^{-} $Å^{-3}$, and a C-S-H gel shell surrounded every alite grain [97] with a water-filled gap of ~500 nm. This gel shell had an average mass density of 1.51 cm^{-3} and an average thickness of ~450 nm. These C-S-H gel shells densify with time and at 47 h the average mass density has already risen to 1.71 g cm^{-3}. The spatial resolution of this study, ~250 nm, did not permit study of the growth rate of C-S-H gel needles in the pore solution. Segmentation measurements and electron density line profiles, see Fig. 7, enabled determination of the average alite spatial dissolution rate from 19 to 47 h, which was ~25 nm/h [97]. During the same period of time, the average etch-pit growth rate was almost double this value, ~40 nm/h [97]. This clearly reflects the importance of defects in the dissolution of alite [98]. Because every alite particle with an initial size smaller than 3 μm was fully dissolved at 19 h, it could be indirectly determined that alite spatial dissolution rate during this period was ~100 nm/h [97]. During the same period and under some assumptions (to be confirmed), it was deduced the alite spatial dissolution rate was ~33 nm/h, for particles bigger than ~10 μm [97]. Therefore, the initial alite spatial dissolution rates seem to be strongly dependent upon the alite particle size. Fig. 7 also shows that C_4AF regions, visible as the brightest regions intergrown with C_3S particles, slowed down alite hydration because the hydration fronts stop as soon as the C_4AF region is exposed. This also justifies the acceleration effect of alkanolamines which contribute to the dissolution of ferrite at early ages, by exposing new alite surfaces [97,99] when there is still plenty of capillary water that favours diffusion and reactivity.

3.4. In-situ rheology and X-ray radiography studies

The very high intensity of synchrotron beams, and the use of sufficiently fast two-dimensional detector systems, opens the opportunity to conduct experiments for better understanding the flow of cementitious materials in the fresh state. Time-lapse radiography has been demonstrated on both laboratory and synchrotron-based X-ray sources for various complex fluids and granular flows [100,101]. The fact that cementitious pastes are optically opaque, corrosive, and change relatively rapidly with time, and are granular pastes that need sufficiently large volumes to obtain representative results, mean that synchrotron sources are particularly valuable in examining cements; the use of laboratory X-ray sources is beyond the scope of this review. Numerous studies have used synchrotron (and neutron) radiographic techniques to investigate the transport of moisture or ions in hardened cements, where X-ray based imaging is particularly valuable in conjunction with heavy tracer ions (Cs^{+} or I^{-}), and neutron imaging is particularly sensitive to the spatial distribution of water within the sample. However, the study of fresh cement pastes by time-resolved 2D and 3D imaging techniques is less common, and forms the focus of this subsection.

As an example of the value that can be obtained from this technique, Sanderson [102] used X-ray radiographic imaging to observe the flow of cement paste into canisters filled with simulant radioactive waste (chopped stainless steel tubes) to ensure the design of cementitious blends that satisfactorily infilled the void space within the canisters. Fig. 8 shows time series of radiographic data collected during filling of canisters of lateral dimensions 76 × 76 mm with cement pastes, one with satisfactory fluidity, see Fig. 8a, and one with insufficient fluidity, see Fig. 8b. In each case, the cement paste was mixed and poured into an external reservoir, and then pumped into the canisters using a peristaltic pump, to simulate the operation of an industrial waste encapsulation plant. The industrial process being simulated here uses a 500 L drum filled with waste [103]; the canisters used for these experiments were designed to give sufficient volume to accommodate the full-sized waste simulant sections, and for each canister to hold enough simulant waste to give realistic flow paths of the cement around and within the tubes for comparison with the full-scale drums. Radiographic imaging through this size of steel canister, filled with a cement paste, requires a high-energy and high-intensity synchrotron X-ray source; in this case, a 124 keV beam energy was used at the JEEP BL of DLS [102].

The information about cement flow paths and infilling that is made available by this in-situ analysis is not easily obtained through other methods; post-hardening sectioning of canisters to examine infill patterns, or tomographic scanning of filled canisters, are possible but give only a single time-point rather than the time-resolved information shown here. This work provides important support for the scale-up and validation of cement formulations based on new cementitious powder sources for use in encapsulation of radioactive wastes; this is valuable because powder supplies can change on relatively short notice [104] and it is essential to ensure successful infilling of the void space within the waste-containing drums to enable them to eventually be disposed safely.

It is also notable that recent advances in fast acquisition of tomographic data can give direct 3D insight into flow processes, including the "Tomoscopy" approach which is based on a SR BL [105]. The pioneering work of Link et al. [106] has demonstrated the ability to directly observe shear banding and shear zones, see Fig. 9, within a cement paste sample using a specialised rheometer installed on the TOMCAT BL of the SLS (PSI). The application of this technique to cementitious materials is clearly in its infancy – and the technique itself is very much cutting-edge science even in application to less-complex materials – but there is evidently a strong possibility to obtain new insight into cement behaviour in 3D under flow conditions or the application of shear.

Considering the behaviour of cement pastes in the fresh state at a micron length scale, it has also been possible to identify the movement (settlement) of individual particles in the time between mixing and setting, using time-lapse in-situ μCT [85]. This is important for the ability to monitor the reactions of specific particles (or microstructural regions) during the process of setting, because the difference in density between the particles and fluid within cementitious pastes means that

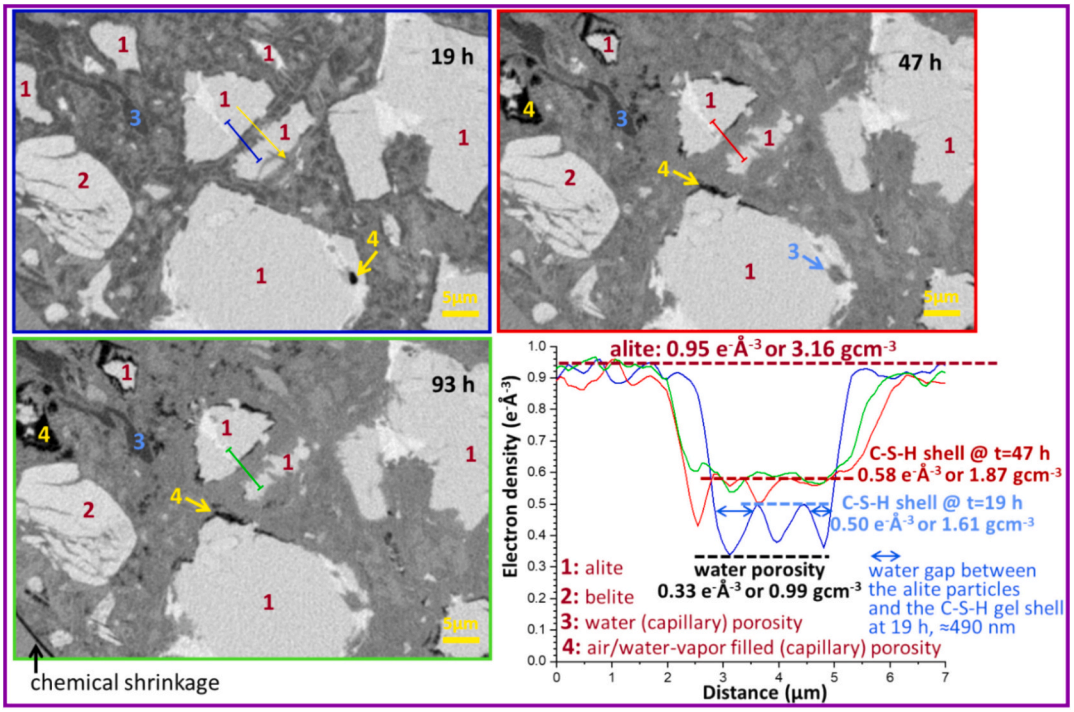


Fig. 7. 4D nf−PXnCT nanoimaging investigation of a PC paste, w/c ~ 0.40, showing the alite spatial dissolution and C-S-H gel shell densification with time. Electron density profiles are shown in the bottom-right panel which correspond to the lines in the other panels (19 h: blue, 47 h: red, 93 h: green). The C-S-H gel shell mass densities are also given which highlights the densification between 19 and 47 h. Capillary porosity (electron density ~ 0.33 $e^{-}Å^{-3}$) is easily differentiated from water-vapor filled porosity (electron density = 0 $e^{-}Å^{-3}$). Adapted with permission from reference [97]. Published under a Creative Commons CC-BY licence. (For interpretation of the references to colour in this figure legend, the reader is referred to the web version of this article.)

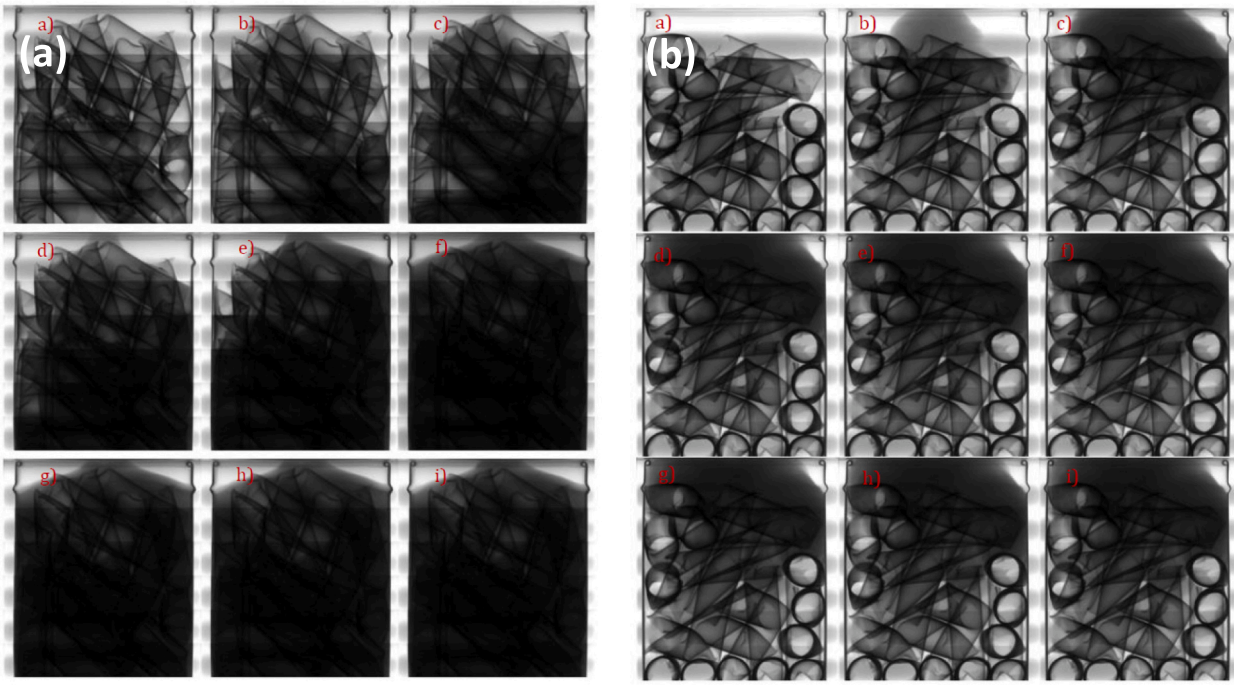


Fig. 8. Time-series of X-ray radiographs showing the filling of void spaces within canisters of simulated radioactive waste (chopped stainless steel tubes) by PC-BFS blends containing either a gap-graded (a) or a fine (b) slag powder. Sample dimensions are 76 × 76 × 100 mm; data collection for each scan (stitched together from six overlapping strips of 25 mm height) was completed within 25 s, and the time interval between successive images displayed (labelled a-f in red lettering, progressing from top left to bottom right in each composite image) is 150 s. Data were collected using the JEEP BL of DLS. From [102], used by permission of R.A. Sanderson. (For interpretation of the references to colour in this figure legend, the reader is referred to the web version of this article.)

particles can move within the sample during analysis, up to the time at which setting occurs. This also means that a fast scan acquisition time is essential for high-resolution in-situ tomography of fluid pastes, because any particle movement during the time taken for a single scan (rotation)

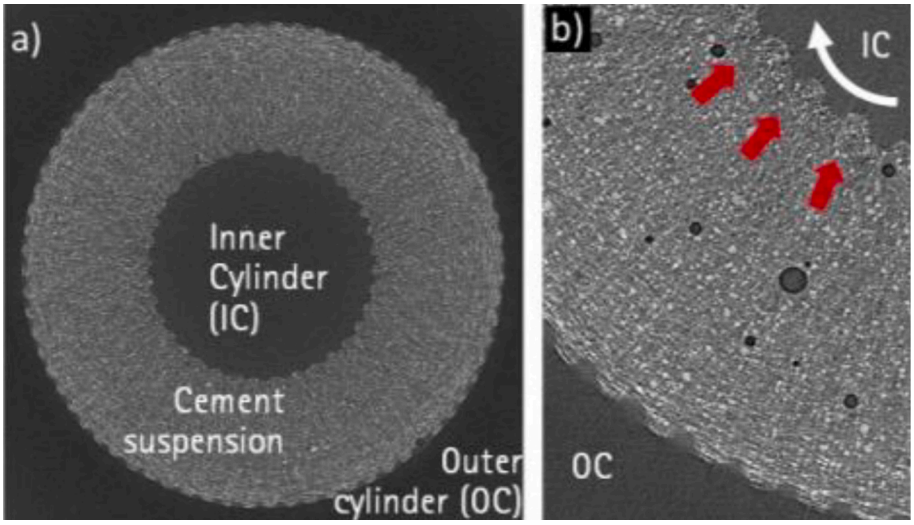


Fig. 9. Slices taken from in-situ tomographic reconstruction of a cement paste during shearing within a concentric-cylinder rheometer with a shear gap (from inner to outer cylinder) of 2.55 mm, imaged using the TOMCAT BL at the SLS (PSI). (a) Unsheared paste sample within the instrument geometry; (b) shear banding (red arrows) and concentrated shear zone, imaged within a sample sheared at $\dot{\gamma} = 0.01\ s^{-1}$ for 10 s. From [106], published under a Creative Commons CC-BY 4.0 licence. (For interpretation of the references to colour in this figure legend, the reader is referred to the web version of this article.)

of the sample can compromise the quality, i.e. partial blurring, of the tomographic reconstruction.

4. Selected synchrotron radiation-based techniques for analysis of hardened cement pastes

As previously discussed, cement hydration is a complex, time-dependent set of processes involving multiple interconnected reactions with different kinetics. Although early hydration has been addressed in Section 3, it is important to note that several slower processes, such as the pozzolanic reaction, and porosity development/refinement also play critical roles in the long-term evolution of the systems. These processes significantly influence microstructural development, and consequently the mechanical properties and durability performance of hardened mortars and concretes. Moreover, understanding the long-term stability of hydration products is essential, and in this area SXRPD offers valuable insights into their evolution over extended curing periods.

4.1. Diffraction and scattering to study cementitious structures at later age

4.1.1. SXRPD analysis of mature cements and cement hydrates

The experimental procedure for the characterisation of systems at late ages generally follows the methodology described in Section 3.1. Typically, the specimens are prepared ex-situ, i.e. in the home laboratory, and subsequently transported to the synchrotron facility for data acquisition. This approach was employed in the previously discussed study involving C_3S with different particle sizes [55], which were investigated both in-situ (at early ages) and ex-situ (at later hydration ages) in pastes prepared in advance at appropriate times, for data acquisition on a unique date when beamtime was allocated. Under these conditions, proper sealing of the capillaries is critical not only to prevent water loss but also to avoid/minimise carbonation. To ensure airtight conditions, capillaries could be sealed using a polymer-based adhesive, such as UV-curable glue, which provides both chemical resistance and mechanical stability during transport and measurement.

In this context, a new experimental facility was implemented at I11 BL of DLS to enable long-term SXRPD experiments. This setup is specifically tailored for investigating slow-reacting systems, such as pozzolanic reactions. It features an additional experimental hutch installed in series with the main I11 BL, allowing multiple sample environments to operate in parallel. Each sample environment is scheduled to receive periodic X-ray beam exposure, enabling the collection of time-lapse diffraction data from several specimens simultaneously over extended durations [107]. Profiting from this facility, Vasconcelos et al. [108] reported an 18-month study on the hydration behaviour of the CEBAMA reference low-pH cement, formulated for geological disposal of radioactive wastes. The results revealed the persistence of unreacted clinker phases (alite and belite), in line with the inherently slow hydration kinetics of low-pH binders and the low w/s ratio of 0.25 that was used. Additionally, the progressive consumption of portlandite confirmed the occurrence of ongoing pozzolanic reactions, because of the presence of SCMs (in this case, silica fume and BFS).

The early and medium age hydration of magnesium potassium phosphate cements blended with FA or BFS, to be potentially used for the encapsulation of reactive metals such as uranium, have also been studied at this facility [109]. Struvite-K ($MgKPO_4{\cdot}6H_2O$) was the main crystalline product, which crystallised earlier in MKPC-FA blends than in blends with BFS.

While the long-term in-situ capabilities of the I11 BL allow the continuous monitoring of slow-reacting systems, alternative ex-situ methodologies are often employed when such extended access is not feasible. Here, it is clarified that long term in-situ SXRPD analyses mean studying the same specimen with time, meanwhile ex-situ SXRPD analyses mean investigating samples of the same cement paste but prepared at predefined times to match the required date, i.e. hydration age. Therefore, in this second approach, variability is larger because the 'same' paste is prepared several times and SXRPD data are collected usually in a single (i.e. awarded) beamtime. In such cases, the hydration is stopped at the specific hydration times using either solvent exchange or mechanical grinding. The hydration arresting step usually alters the content of labile phases such as ettringite [110], although this is not always fully destroyed even when a vacuum-oven drying step is applied [111]. The hydration-arrested pastes are then loaded into capillaries and sealed until SXRPD measurements are performed. This approach has been employed to investigate the hydration behaviour of C_3S blended with different SCMs, including silica fume [21] and FA [112], using SXRPD combined with PDF analysis. While both studies utilized SXRPD to elucidate hydration mechanisms and phase evolution, the presence of FA was found to extend the induction period of C_3S hydration but ultimately resulted in a higher degree of hydration at later ages [112]. In contrast, the study involving silica fume enabled a more detailed local structure analysis of the C-S-H with the overall Ca/Si ratio of the blends

[21].

Another important application of SXRPD is in conjunction with a specialised cell that can generate exceptionally high pressures (in the GPa range), for example a diamond anvil cell, to determine the elastic properties of cement hydrate phases (and related minerals) via the relationship between applied pressure and the variations of the measured lattice parameters. Such an approach has provided valuable insight into the intrinsic elastic properties of phases such as ordered and disordered C-(A)-S-H [113,114], and the portlandite [115], AFm [116], AFt [117,118], and hydrogarnet [116] phases relevant to PC, several of the key crystalline hydrate products of calcium aluminate cement [119,120], and also phases such as artinite [121] and struvite-K [122], which are essential constituents of some types of magnesium-based cements. It is noted that the second study for AFt was carried out by synchrotron single crystal diffraction at high pressures.

To finish this subsection, two very different works are selected to highlight the diversity of studies that can be tacked. On the one hand, high-resolution SXRPD is still being used for a better analysis of anhydrous PCs. A recent investigation [123] studied six industrial clinkers. One sample had a high amount of M1 alite polymorph. This allowed the development of a better structural description for this polymorph, which was validated by bond valence sum analysis. On the other hand, hydration can be followed by accelerated carbonation and the resulting phase assemblages elucidated. Total scattering SXRPD data (see also Section 4.1.4 for more details of this approach) were collected in BL04-MSPD of ALBA synchrotron and the data were analysed by the Rietveld method and by the PDF approach [124]. Alite-, belite- and ye'elimite-containing pastes were studied before and after accelerated carbonation under controlled relative humidity. The presence and amounts of the different crystalline calcium carbonates (calcite, aragonite and vaterite) were determined and the presence of additional amorphous calcium carbonate was also firmly established [124].

4.1.2. *μXRD for spatially-resolved assessment of crystals in cement microstructures*

Microscopically resolved X-ray diffraction (μXRD) is a valuable technique by which the spatial arrangement of crystalline phases within a cementitious microstructure – with or without the presence of aggregates – can be assessed. This technique can be applied using thin-section samples in transmission mode, or polished surfaces scanned in reflection mode. Valuable insight has been gained through the application of μXRD to cementitious samples containing high levels of SCM substitution [125,126], or interacting with materials such as clay-rocks [127] or steel [128,129].

The ability to investigate the crystallographic details of phases within complex microstructures, including within cracks in cement monoliths [130] or within ASR-affected aggregate grains [131], can also bring significant new insight. Differential water uptake between different ASR products under wetting-drying conditions [132] could be specifically identified through monitoring of the basal spacings of the various layered products present in the identifiable ASR-damaged parts of a field-exposed concrete cube, along with differences in crystallinity between the various measured products. These results aided in identifying that the swelling due to moisture uptake in crystalline ASR products is not likely to be the main factor controlling ASR-induced expansion, providing a significant contribution to the ongoing search for fundamental insight into this complex and important concrete degradation phenomenon.

The μXRD analysis of C-A-S-H and its partial crystallisation to Al-tobermorite in aged (decades-old) [15] and ancient (Roman-era [133,134]) structures has also proven highly instructive to researchers seeking to understand the mechanisms controlling durability and long-term mechanical performance of concretes, as exemplified in Fig. 10. These data, together with information about the relative crystallite orientations, were used to infer that the Al-tobermorite had formed via a mechanism of dissolution-reprecipitation within the concrete as it aged.

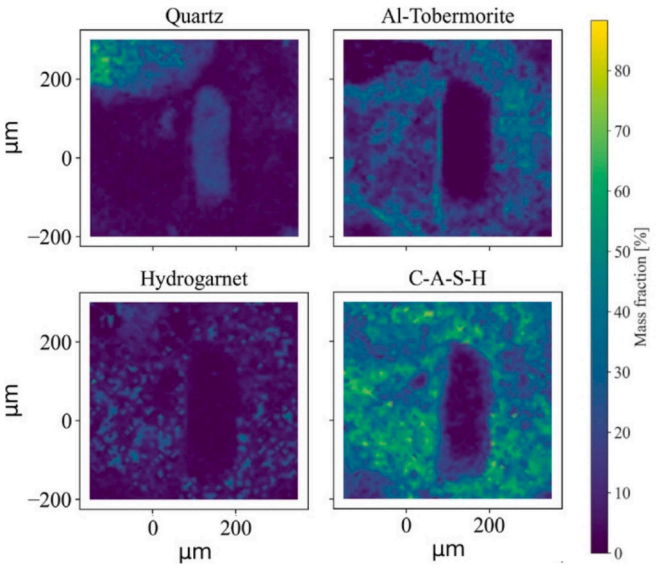


Fig. 10. μXRD data showing the relationship between more-ordered (Al-tobermorite) and less-ordered (C-A-S-H) regions within the microstructure of the cement paste around a sandstone fine aggregate grain, in a concrete taken from a nuclear reactor structure which had been in service at around 40 °C for 16.5 years. Adapted from [15], with permission from John Wiley and Sons.

4.1.3. *SAXS and WAXS applied to cements*

Small-angle and wide-angle scattering techniques can provide complementary information about the nature of particulates and pores within cementitious materials. Probably the most important application of synchrotron-based SAXS to cements, in combination with its neutron-based counterpart SANS, was in the seminal study of Allen et al. [19] which resolved long-standing uncertainty about the intrinsic water content and mass density of C-S-H. This study yielded a representative formula of $(CaO)_{1.70}(SiO_2)(H_2O)_{1.80}$ for the 'solid fraction' of C-S-H synthesised at a C/S ratio representative of PC hydration products (i.e. gel pore water excluded). The differences in sensitivity of X-ray and neutron radiation to different elements/isotopes, particularly the hydrogen present in water, can be used to provide a sensitive and precise probe of the nature of hydrous particles such as those which dominate cementitious phase assemblages. Li et al. [135] also extracted SAXS data from ptychographic scans of synthetic C-S-H and C-A-S-H particles to define the fundamental thickness of the platelet-shaped units that they could identify, with both Al-free and Al-containing hydrates seen to form with a fundamental thickness of 6–7 nm, within the "crumpled foil"-like microstructure that was observable. They also used SR-based WAXS to define the basal spacings of these products, which fall in an angle (and *d*-spacing) range that is not always possible to access on a laboratory diffractometer.

4.1.4. *Total scattering and pair distribution functions*

When an X-ray (or neutron) scattering dataset is collected up to sufficiently high momentum transfer (i.e. high diffraction angle), calculating its sine Fourier transform yields the PDF, which is a means of representing the correlations between positions of different atoms within the structure of a material which may be significantly disordered or nano-particulate [20,136]. The mathematical details of this technique, with a specific view towards applications in cement science, are outlined concisely but clearly in the review of Meral et al. [137]. The use of the total scattering pattern – both within and outside the Bragg peaks corresponding to crystalline phases [138] – provides the opportunity to simultaneously probe ordered and disordered phases in a cementitious microstructure. As a key example of this, Skinner et al. [139] used a total scattering technique to separate the contributions of disordered C-S-H from coexisting C_3S and CH within a hydrated C_3S paste sample, and

demonstrated effectively that synthetic C-S-H produced from CaO and amorphous silica has a very similar nanostructure to that which is produced from C_3S hydration. Both samples were able to be accurately modelled as a size-broadened (nanoparticulate) 11 Å tobermorite with short-range but not long-range ordering. It is noted that there is growing evidence, from this technique, that points towards a heterogeneous nature of C-S-H gel at the nanostructure for Ca/Si ratios higher than about 1.4. For these gels, there could be two intimately-mixed nanometric phases: tobermorite-like and nanoportlandite-like [21,55,140].

PDF analysis has also been extensively applied to the study of alkali-activated and geopolymer cements, where the disordered nature of the binding phases means that the ability of the PDF technique to probe nanostructural details is important. This technique came to prominence in cements research in the early 2000s, particularly through the work of Bell et al. [141,142], who developed a methodology whereby the room-

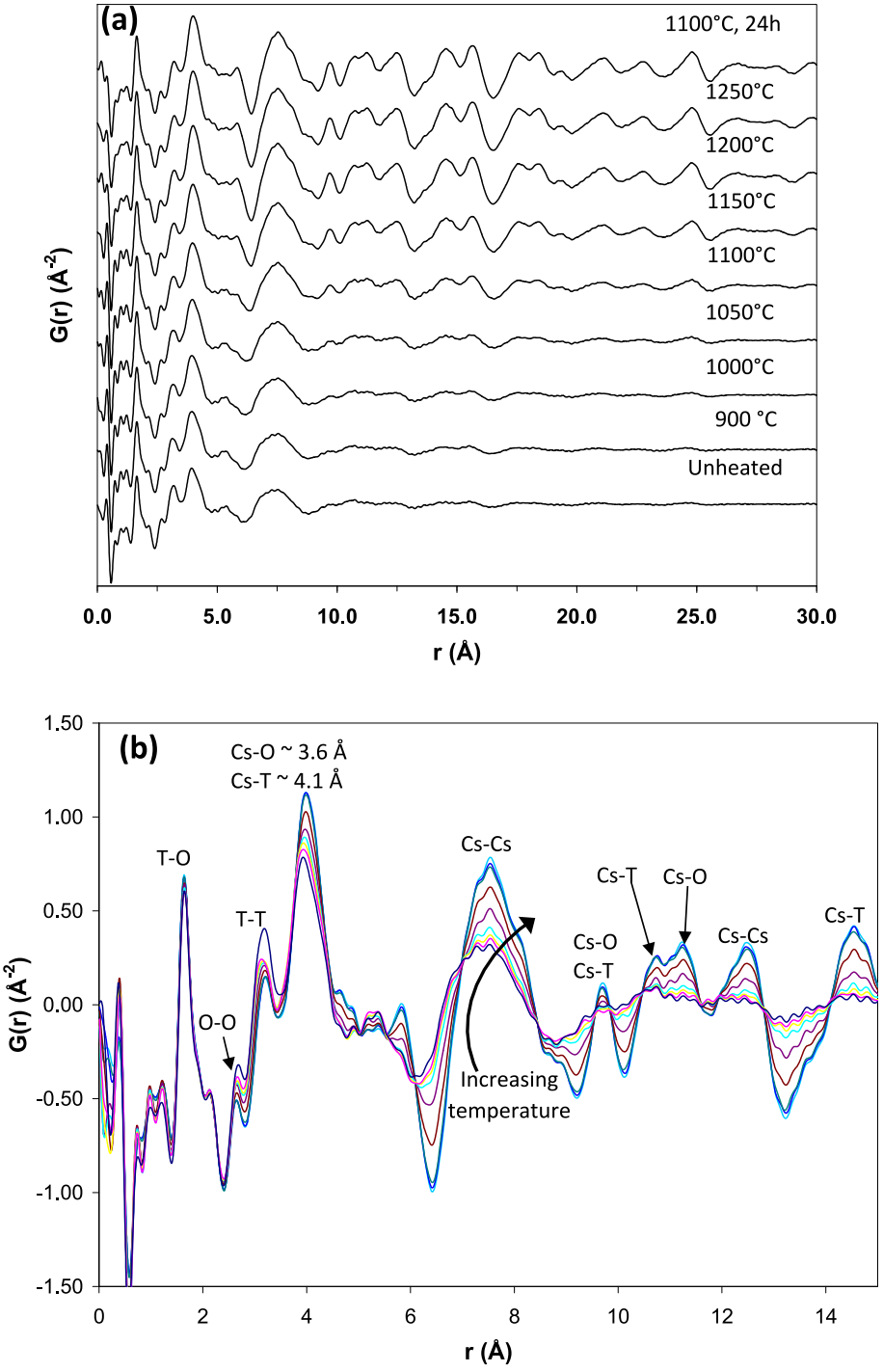


Fig. 11. (a) X-ray PDFs of $CsAlSi_2O_6$ geopolymers heated to various temperatures (as marked), with no soak time except for the 1100 °C, 24 h dataset. Data were collected at APS (Argonne, USA) BL 11ID-B using an X-ray energy of 90.3 keV, measuring up to a momentum transfer Q $\left(=\frac{4\pi\sin\theta}{\lambda}\right)$ of 27 $Å^{-1}$, and corrected and converted to PDF form as described in [142]. (b) Enlarged view of the low-*r* section of (a) with the datasets overlaid on each other, showing the peak assignments according to the crystalline structure of pollucite (the cesium-containing member of the leucite group). Data from [142], re-plotted for inclusion in this review.

temperature structure of a stoichiometrically-designed geopolymer could be interpreted by comparison to a crystalline counterpart produced by heating to 1200 °C. This approach yielded key insights into the nanostructure of the geopolymer gel – which up to that time had largely been treated as being "amorphous" without access to further structural details – as being related to a zeolitic structure on a length scale of up to ~10 Å (exemplified in Fig. 11 for a cesium aluminosilicate geopolymer synthesised to match the composition of pollucite), but lacking the long-range order that would enable it to show crystallinity in a conventional diffraction experiment.

PDF analysis has also provided interesting new insight into the process of formation of metakaolin by calcination of kaolinite [143,144], of the formation of $Al(OH)_3$ gel within calcium aluminate cement hydration products [145], and of the formation of different $CaCO_3$ polymorphs during carbonation of C-S-H [146]. The application of the PDF technique to the analysis of total scattering data collected from C-S-H paste under applied mechanical load [147] has also enabled researchers to relate elastic properties to nanostructural differences in silicate chain length and interlayer water content, and to define contributions to deformation mechanisms at length scales down to atomic resolution.

4.2. Synchrotron spectroscopic techniques for chemically-resolved imaging

The unique and tailorable characteristics of synchrotron radiation, across the full energy range from infrared to hard X-rays, offer opportunities for the application of many different spectroscopic techniques that are relevant to cementitious materials. While it is not feasible to provide a comprehensive overview of all techniques within the scope of this review, the following discussion highlights several methods that are prominently featured in recent literature. The high brilliance, collimation, and tunability of the energy range (monochromatic, pink, or white beams) are particularly valuable in spectroscopic analysis of cements; the body of published work in cement science to date does not appear to make use of the ability to polarise SR, or to generate and use very short pulses, but these are potential opportunities for future innovation [5]. The sections that follow will give a brief overview of some of the published applications of synchrotron-based spectroscopy to cement science, moving from longer to shorter wavelengths of the incident beam, and aiming to provide the reader with some insight into available opportunities rather than aiming for exhaustive coverage of the literature.

4.2.1. Infrared studies

Synchrotron infrared BLs, with photon energies on the order of hundreds of meV, offer high photon flux for rapid data collection, and the collimated beams from the synchrotron source can bring high spatial resolution [148]. Infrared microscopy is also possible (and in other fields of materials science, applied more or less routinely [149]) with laboratory sources, and this has the advantage of a relatively more accessible instrument, not requiring BL access via competitive proposal procedures, but tends to be rather slower in data collection. The spatial resolution of infrared-based microscopic analysis is to some degree restricted by the wavelength of the incident light, which limits the degree to which the spot size can be reduced via conventional optics.[1]

The application of synchrotron infrared microscopy to cements was pioneered by Hajimohammadi et al. [150], who applied hierarchical clustering techniques to distinguish and analyse the spatially-heterogeneous gels that formed within alkali-activated cements produced from FA and geothermal silica. This enables some of the most challenging materials analytical questions in cement science – related to the analysis of multiple amorphous (or highly disordered) phases within a single sample [5] – to be directly addressed. By measuring an infrared spectrum at each point on the polished surface of a sample, with a spatial resolution on the order of 5–10 μm, it is possible to identify differences in chemical structure (bonding and connectivity) with microstructural specificity, which cannot easily be achieved by other approaches - see for instance [151,152]. This technique could have a relevant impact in the study of carbonation of pastes and mortars but it has not yet been exploited in this context, to the best of the authors' knowledge.

4.2.2. UV/Vis studies

The application of synchrotron-based UV–visible spectroscopy (with an energy of a few eV) to cement science is relatively uncommon, with the exception of studies of luminescence in doped anhydrous calcium aluminate phases ($C_{12}A_7$ or C_3A) in the context of their use in optical applications [153,154]. However, the relationship of this work to the more general field of cement science is largely coincidental. Laboratory-based UV–visible spectroscopy is useful for determination of various organic and inorganic constituents in cements, but it is unclear whether the use of synchrotron radiation is necessary in this specific context, to meet any shortcomings in the capabilities of the currently-available analytical tools.

4.2.3. Soft/tender X-ray studies

Cements and their hydration products contain large quantities of low-Z elements in important – and structurally complex – roles. In particular, elements such as Na, Mg, Al, and Si have characteristic X-ray K-edge energies in the range 1–2 keV, characteristic of the soft X-ray range and often requiring vacuum conditions for spectroscopic analysis on BLs, while P, S, Cl, K, and Ca all have K-edges between 2 and 6 keV [155]. The exact distinction between "soft" and "tender" X-ray regimes is not particularly well defined in the literature, and so these energy ranges will be grouped together in the discussion here. The important commonality, in a practical sense, is that the presence of air in the beam-path can interfere significantly with data collection, and so experiments are often conducted under vacuum or helium environments.

XAS, including both EXAFS and XANES techniques, experiments in this energy range can provide important information about the coordination environments of both major and minor elements in cementitious hydrates. For example, Fig. 12a shows a database of Si K-edge X-ray absorption spectra for different hydrous calcium silicate minerals collected by Li et al. [156], who also compared the K-edge peak energy with various structural features including Ca/Si ratio, mean Q^n silicate connectivity, and Si—O bond length, and determined that the most evident relationship was with mean Ca—Si connectivity, Fig. 12b. There is at most a very weak dependence of the Si K-edge spectra on Al substitution into the tobermorite-like C-A-S-H structure, which is quite distinct from observations via other spectroscopic techniques e.g. infrared or nuclear magnetic resonance spectroscopy. Yan et al. [157] also found that the Al K-edge XANES spectra are relatively insensitive to Al/Si substitution within C-A-S-H phases, but provided a very sensitive probe for the presence of intimately intermixed secondary phases that were difficult to quantify by other methods.

Mg K-edge XANES has also been shown to be valuable in distinguishing and interpreting the structures of M-S-H phases, including analysis in combination with ab initio simulation of the spectra to aid in correlating spectral features with specific aspects of the magnesium silicate nanostructure [158,159], and also the structural role of Mg in N-(M)-A-S-H gels [160].

This work in bulk XAS analysis can also be extended into spatially-resolved analysis, in particular through the use of XAS as the spectroscopic underpinning of STXM [161], which has been applied extensively

[1] It should be mentioned that laboratory-based near-field probe techniques, which use (for example) the tip of an atomic force microscopy probe to conduct infrared spectroscopy with a spatial resolution well below the wavelength of the incident light [282] have been applied to cements at ~20 nm spatial resolution [283]. Although it is possible to use this technique with synchrotron radiation [284,285], this does not yet appear to have been demonstrated/used for cementitious materials.

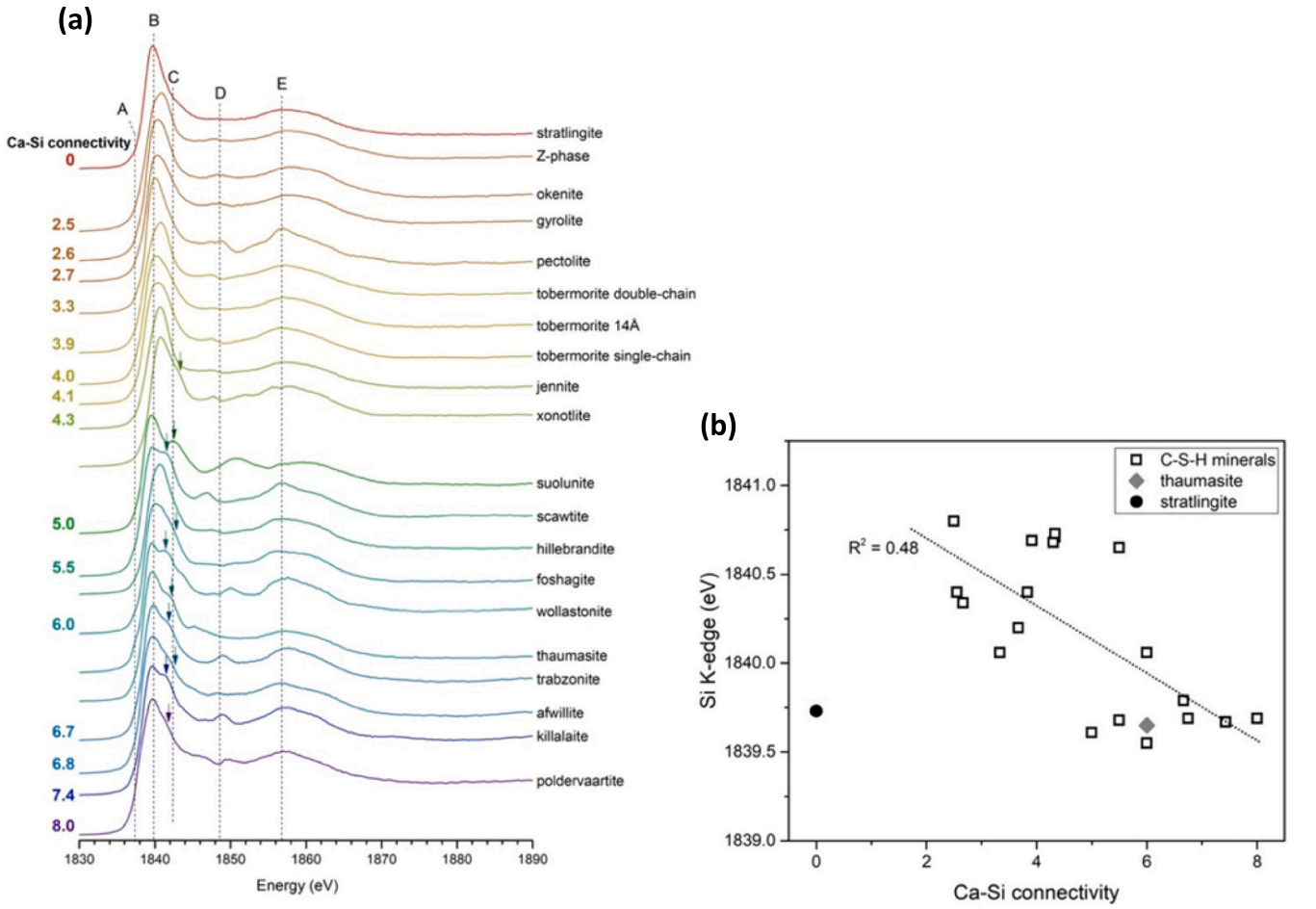


Fig. 12. Si K-edge XANES spectra for selected hydrous calcium silicate phases: (a) experimental spectra plotted in order of average Ca—Si connectivity; (b) correlation between Ca—Si connectivity and Si K-edge energy (marked as peak B in the spectra in (a)). Other marked peaks in (a) are the pre-edge peak A, and multiple scattering peaks C and D, and the Si 1s-3d electron transition peak E. Reproduced from [156], with permission from Elsevier B.V.

to cements by the research team led by Monteiro [162]. This technique combines soft X-ray transmission microscopy, which provides nanoscale-resolved absorption contrast images of cementitious microstructures and nanostructures [163], with the collection of an XAS spectrum at each point in the 2D sample. This provides unique access to details of atomic coordination environments in cementitious materials as a function of location within the micro- and nanostructure. For example, the conversion process between hydrates in calcium aluminate cement was assessed by STXM on a 15 nm spatial resolution [164] to determine the details of solid-state and through-solution reaction processes involved in this important aspect of the chemistry of alternative cements.

Fig. 13 shows an example of the application of STXM to the analysis of FA particles [165], where the spectra measured at each point within the scan region have been clustered into three representative groups, which are colour-coded in Fig. 13a and c, and then correspondingly mapped in Fig. 13b and d to show the chemical heterogeneity and phase separation of the various glasses present within the FA particles.

The use of STXM in the soft/tender X-ray regime has also given useful insight into other complex cementitious systems, such as hydrous magnesium carbonates [166] and limestone-calcined clay cements [8]. Micro-XANES spectra collected in this energy range using fluorescence mode detection (rather than in transmission, as in STXM) have provided essential insight into the spatial distribution of different sulfoaluminate phases [167], alkali-silica reaction products [168], and chloride binding [169]. It is expected that further advances in BL and instrument capabilities in future will provide additional opportunities for innovative time-lapse and spatially-resolved spectroscopic analysis of cements in this energy range.

4.2.4. *Hard X-ray studies*

Spectroscopic experiments in the hard X-ray regime, above approximately 6 keV, often probe the interaction of guest elements with cements; EXAFS analysis of the coordination of numerous heavier metal cations in contact with cement paste or C-S-H has particularly given insight into the likely binding of radionuclides or toxic contaminants that are immobilised in cements for environmental protection purposes [170], and the influence of additional species such as organic ligands on these binding environments [171]. The K-edges of important light transition metals [172,173], and metalloids [174], and the L-edges of actinides [175,176], are commonly investigated with the intention of better understanding the host environments of these elements in cements. Synchrotron-based facilities which offer laboratories for the handling and analysis of samples containing radionuclides have in particular contributed significantly to the understanding of the chemistry and interactions of technetium in cementitious environments [177–179]. As was noted above for the case of soft/tender X-rays, spatially resolved XAS analysis in the hard X-ray regime can provide micron-resolution [180,181] spectroscopic information about the chemistry of specific phases within a cementitious microstructure.

Fe is a significant constituent of many cements, being introduced particularly via the ferrite phase in PC, and also from iron-containing glasses in FAs and fayalitic slags that are used as SCMs or in alkali-activated cements [182,183]. It is also supplied to cementitious

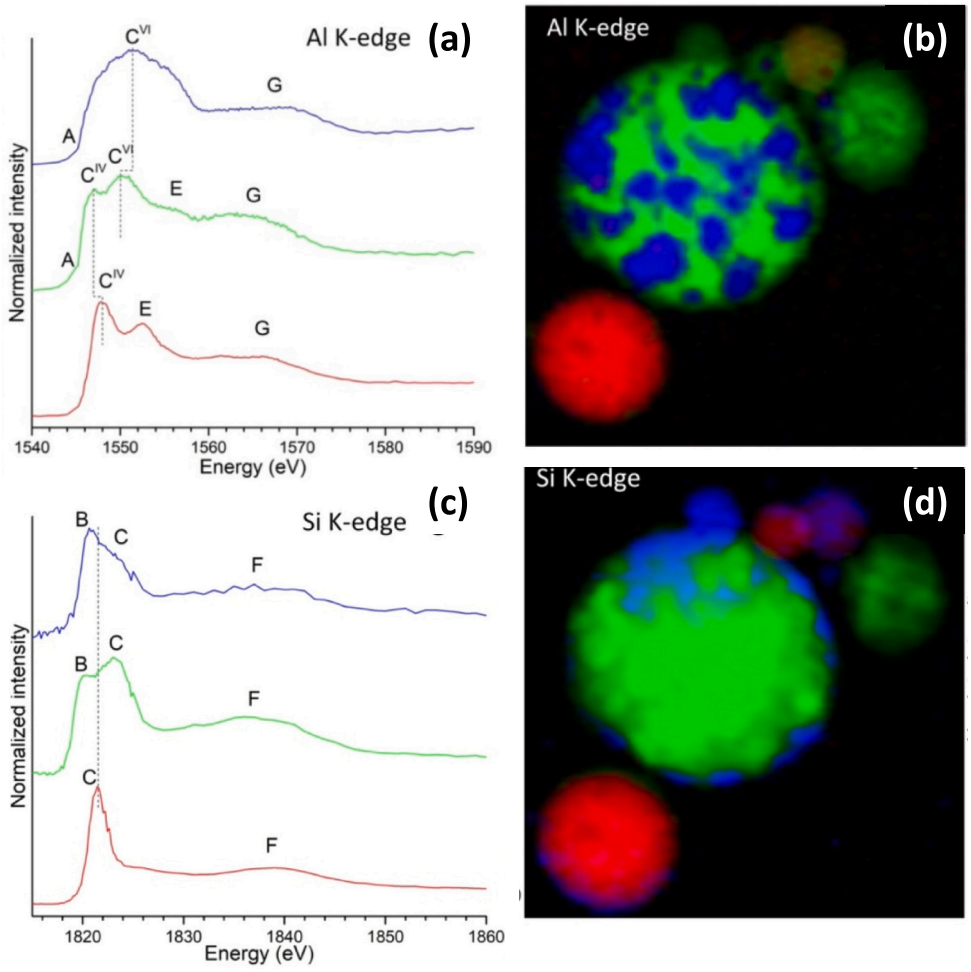


Fig. 13. XANES spectra (a; c) mathematically clustered from the recorded spectra collected at the Al and Si K-edges for samples of FA, at each point, and categorised into three representative spectra per element; and (b; d) maps showing the regions in the sample in which the recorded spectra fall into each of the colour-coded clusters. The field of view is 7.9 × 7.9 μm in each image. Adapted from [165], with permission from Elsevier B.V.

systems via corrosion processes at the steel-concrete interface in reinforced concretes [184], and thus the influence of redox states (which can readily be probed by EXAFS) on its interactions with cementitious hydrates in the very long term need to be considered in detail for important engineering applications. Fe(II) has been found to interact only relatively weakly with C-S-H [173], while the combination of EXAFS and ^{29}Si MAS NMR spectroscopy has shown that Fe(III) in octahedral coordination can participate in the interlayer of high-Ca/Si ratio C-S-H phases [185], see Fig. 14. EXAFS data were also central to the identification that Fe—Al siliceous hydrogarnets are a dominant Fe-containing hydrate in longer-term aged cement pastes [186], confirming the formation of a solid solution phase under realistic cement hydration conditions.

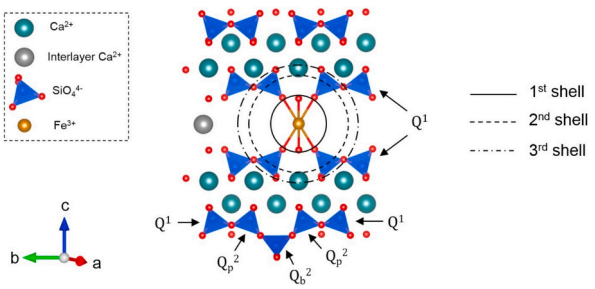


Fig. 14. Coordination of Fe^{3+} in C-S-H with Ca/Si = 1.2–1.5, as deduced from EXAFS spectroscopy at the Fe K-edge and corresponding determination of the occupancy of the first three shells around the Fe site (as circled), together with information from ^{29}Si MAS-NMR regarding silicon coordination environments. Reproduced from [185], with permission from Elsevier B.V.

Spatially resolved XRF mapping based on hard X-ray synchrotron sources has also been applied, both at the micron scale and at the nanoscale, to the study of cementitious materials. Micron-scale resolved XRF provides a useful complement to the more-commonly applied electron-based techniques (EDX and EPMA), offering high sensitivity to trace elements. Nanoprobe-based fluorescence mapping, using a step size of a few tens of nanometres, has given useful insight into the environments of minor transition metal constituents in fly ash-based [187] and slag-based [188] alkali-activated cements. This technique can also be coupled with nanometre-resolved X-ray tomographic approaches [189,190] or microdiffraction [191] to provide insight into the spatial arrangement of the main cementitious hydrate phases at a nanoscopic level.

The opportunity to generate a white (polychromatic) hard X-ray beam from a bending magnet or wiggler-based synchrotron source brings the opportunity to study materials by EDXRD, which is included in this section of this review because it is technically a spectroscopic technique, distinguishing Bragg-diffracted radiation as a function of its energy using a detector at a fixed angle. The white-beam sources are typically of high intensity and so enable time-lapse analysis of processes taking place on a length scale of seconds to minutes, which is very relevant to cementitious materials. The study of cements by the EDXRD

technique was one of the early case studies used in its development [192,193], and it has since been applied also to the study of geopolymer formation through the use of the potential to study a relatively thick, sealed sample in transmission mode, distinguishing the contributions from multiple amorphous phases to quantify the conversion from metakaolin to a hardened binder [194,195]. Spatially-resolved EDXRD has provided useful insight into carbonation [196] and sulfate attack [197] on cm-sized samples of cement paste; the extension of this technique to three dimensions (termed TEDDI) is discussed in Section 4.3.1 as an example of diffraction tomography, and has also provided interesting results for cements.

4.3. SR−μCT for microstructure characterisation

Synchrotron-based μCT – defined here as analysis at a spatial resolution of 0.5 μm or lower (i.e. larger numerical values), to distinguish this from the nanotomography regime at finer spatial resolution – has been used in various ways and with various aims in the study of cement pastes, mortars and concretes. It should be mentioned that voxel size and spatial resolution are related but not necessarily in a proportional way. As a rule of thumb, it can be considered that about three voxels are needed to be able to distinguish fine details, however the relationship between voxel size and spatial resolution, and the definition of spatial resolution and the ways to determine it [198], are quite complex matters and they will not be treated in this work. Moreover, SR–μCT data can be obtained in a number of experimental configurations, including absorption/phase-based techniques and diffraction/scattering-based ones, see Section 2. Here, we will limit the discussion to these two types of CTs.

4.3.1. X-ray diffraction/scattering computed tomography (XDS−CT)

X-ray diffraction/scattering computed tomography (XDS–CT) is a non-destructive class of synchrotron-based chemical imaging techniques enabling reconstructions of sample cross-sections with spatially resolved chemical information. Such techniques include X-ray diffraction micro–computed tomography (XRD−μCT), small angle X-ray scattering computed tomography (SAXS–CT), pair distribution function computed tomography (PDF–CT), and multimodal techniques offering even greater chemical insight of specific materials. A recent review [199] provides a brief history of these techniques, as well as a description of their principles and advances in data processing. Here, only XRD–μCT will be discussed.

Seminal work on XRD−μCT [200,201] demonstrated the potential of this technique to spatially detect scattering patterns of amorphous and crystalline phases with similar atomic densities and compositions. The XRD−μCT technique involves acquiring radial diffraction profiles in transmission with a 2D detector, while translating and rotating a sample illuminated by a pencil beam. The reconstruction yields the variation of the intensity of any diffraction region of interest in 3D in the horizontal plane. This enables researchers to capture structural information such as lattice parameters, structure refinement, texture and grain size, which can be determined in an arbitrarily defined part of the sample down to the voxel size. Equally, XRD−μCT can be combined with fluorescence and absorption to enable multi-modal tomography analysis of specimens, providing detailed structural and chemical information of the analysed material.

There are a limited number of studies applying XRD−μCT for the analysis in cementitious materials. Some studies have only reported 2D cross-section images of tested specimens along with the averaged X-ray diffraction pattern, so that features of PC [202], as well as alterations occurring in cementitious materials due to carbonation exposure and immersion in hot water [203], were identified. Other studies have centred on evaluating specific Bragg reflections of clinker phases (e.g. C_3S, C_2S [204] as well as hydrated products (e.g. mainly AFt [204] and C-S-H [202,203]) to identify the correlations between spatial distribution of selected clinker phases/unreacted PC particles, preferential sites for phases formation, and porosity distribution. Tomographic reconstructions of the diffraction data were also employed for investigating the water uptake during the alkali-silica-reaction [132].

Voltolini et al. [203] reported time-lapse XRD−μCT results for PC hydration, and highlighted that the time required for data collection was a constraint at the time of conducting the experiments. As cement hydration progressed, it was challenging to capture the structural feature changes taking place, to enable reliable quantification of the results for direct comparison with other techniques (e.g. isothermal calorimetry). In a later study by the same authors [205], they applied this technique (ex-situ) to evaluate the growth of C-S-H in PC from 7 h to 7 days of curing. This revealed that, in the absence of a superplasticiser, C-S-H growth occurs in the proximity of anhydrous PC phases. The inclusion of a superplasticiser led instead to formation of C-S-H in the available free (i.e. capillary pore) space.

The time-resolved spatial distribution of crystalline phases forming in ternary cements produced with PC, FA and BFS has also been evaluated via this technique, as well as formation of carbonates due to CO_2 exposure of the specimens [206]. The results were consistent with what has been reported for similar mixes applying laboratory techniques, with the added value that neither sample pre-conditioning nor destruction of the specimens was required.

More recent studies applied XRD−μCT to evaluate the influence of the activator type and CO_2 exposure in the microstructure features of alkali-activated cements [207,208]. X-ray diffraction patterns as a function of the sample thickness (see Fig. 15), as well as 3D reconstructions showing the spatial distribution of C-(A)-S-H, Mg—Al LDH, and AFt were reported [207] (see Fig. 16). These studies provided unique and novel insight into the interaction of different hydration products with CO_2, particularly demonstrating that Mg—Al LDH formed in these systems can act as a CO_2 sink. Also, the XRD−μCT results were correlated with those obtained from μCT, enabling identifying changes in pore structure occurring in the samples as a function of phase changes due to their reaction with CO_2.

TEDDI is another synchrotron-based technique that enables collection of spatially resolved X-ray diffraction and fluorescence information simultaneously of sizable specimens, making it suitable for evaluating chemical processes inducing microstructure changes. A limited number of studies have reported the use of TEDDI applied to cementitious materials. Early studies centred on the analysis of aged concrete specimens (24 years old), revealing the microcrystalline phases present in the paste within a large sampling volume, and the distribution of such phases on a sub-millimetre scale [209]. Gonzales-Saborido et al. [210] developed a configuration for applying TEDDI for the in-situ monitoring of changes induced by CO_2 exposure in cementitious materials by evaluating the spatial distribution of the carbonatable phases (e.g. portlandite and C-S-H) in 3D (see Fig. 17).

4.3.2. X-ray absorption/phase contrast computed tomography (μCT)

With improvements in laboratory-based μCT instrumentation in recent years, the advantages of SR are now particularly evident when the samples to be studied are either large, complex, or otherwise inconvenient to study in a laboratory context. For the early-age properties discussed in Section 3, it was essential to reach high time resolution to distinguish rapid evolution of the material, but the ability to collect data very rapidly from a synchrotron source is less critical at later ages. Both synchrotron and laboratory-based X-ray microtomographic approaches to cement characterisation were recently reviewed [31], and the reader is referred to that publication for more detailed discussion of some of the topics mentioned in this subsection.

Initial synchrotron X-ray tomographic investigations of cement paste samples provided valuable new insight into the 3D geometry and connectivity of the pore network on a length scale (voxel size) of 1–5 μm, particularly in the early 2000s when this length scale was not so readily accessible on laboratory instruments as is now the case [211,212]. It should be noted that hydrated cement contains important pores on

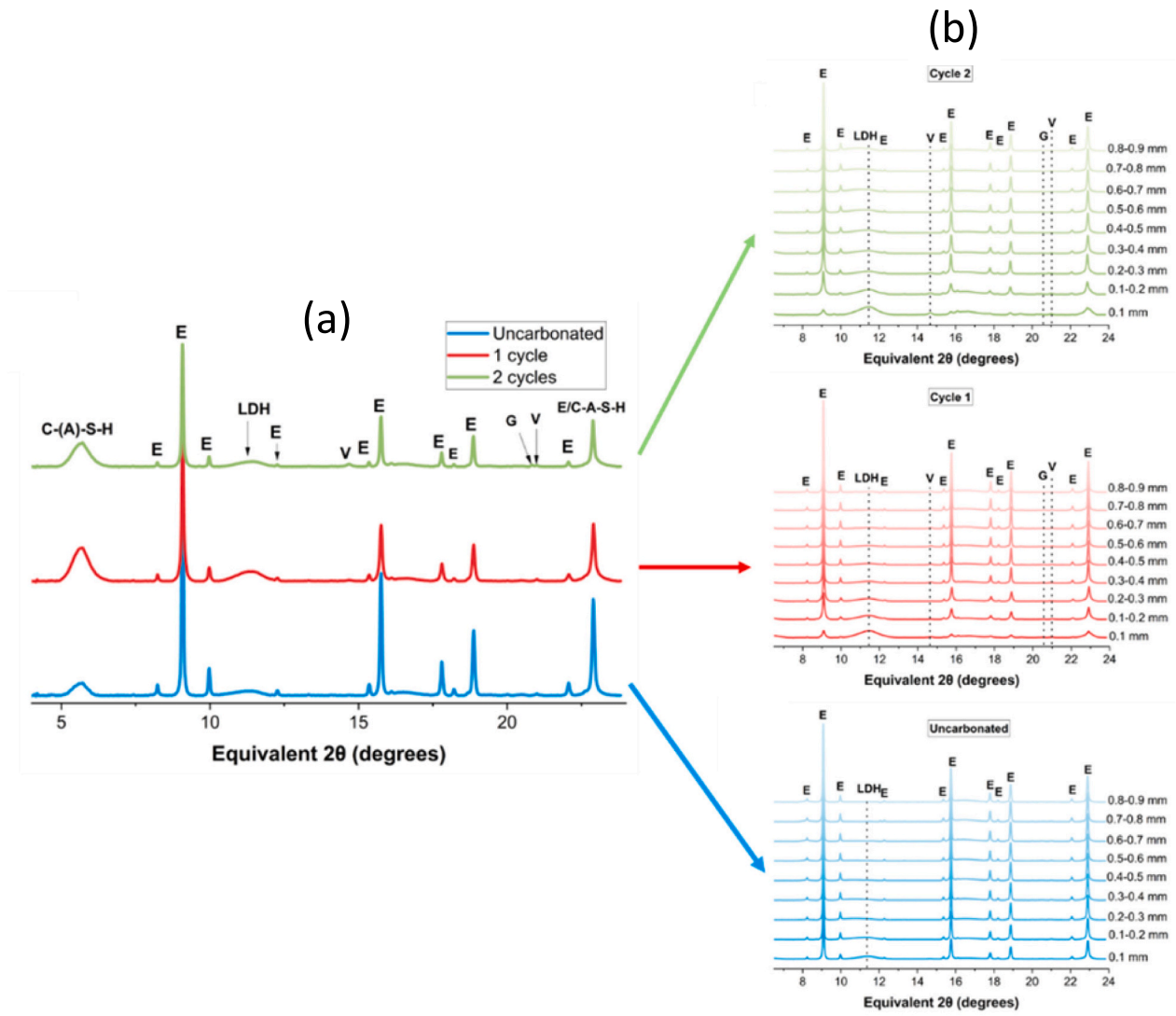


Fig. 15. Cu-Kα equivalent XRD patterns of: (a) cumulative XRD patterns for entire specimens before and after carbonation; and (b) each layer (depths as marked) from the surface to the core of a sodium sulfate activated slag cement paste. C-(A)-S-H: aluminium-substituted calcium silicate hydrate, E: ettringite; LDH: Mg-Al-CO_3-LDH; G: gypsum; V: vaterite. Adapted from [207], published under the terms of the Creative Commons CC-BY licence.

length scales far below what is accessible via microtomographic techniques, including (but by no means limited to) the length scales discussed in Section 3 in the context of nanotomography. However, once this limitation of microtomography is understood and taken into account when discussing data and comparing different samples [30], there is certainly valuable information to be gained from synchrotron-based examination of cementitious materials at this length scale. For example, Leite and Monteiro [213] provided new insight into the distribution of larger pores near the interface between recycled aggregate and newly cast concrete, and Chung et al. [29] used a multi-resolution synchrotron/laboratory approach to assess pore structures in macroporous cementitious foams.

Synchrotron tomographic analysis of concrete under load was pioneered by Landis et al. [214], where the ability to image damage and fracture patterns in 3D was shown to bring new engineering insight. Since that time, such an approach has been applied to various cementitious materials, notably including Roman concrete samples from the Pompeii site [215], whose partially ductile fracture modes were identified by those authors as one of the factors underlying the excellent durability of these ancient concretes. As an example of the type of information that can be obtained through this experimental approach, Fig. 18 shows the absorption-contrast tomographic reconstruction of a sample of ultra-high-performance concrete which was subjected by Homel et al. [216] to stepwise compressive loading, and imaged before (steps 3 and 4 in Fig. 18) and after (steps 5 and 6) failure. The tomograms are coloured according to the phases that were identified to contribute to the microstructure in each region via a thresholding approach, and the results were used as experimental validation for a mesoscale model that connected the fracture behaviour of the overall material to the characteristics and distribution of the individual phases that comprise it [216]. It should be noted that there is still ongoing discussions about the best method to use for component segmentation in synchrotron tomograms of cementitious materials [217], including the suggestion that the addition of high-Z contrast agents can aid in segmentation of different hydrate products, due e.g. to the selective binding of iodide into the AFm phase [218], which enables AFm to be better distinguished from C-S-H. This will be elaborated in Section 5 where the impact of AI in segmentation is treated.

Promentilla et al. [32,219] developed a methodology whereby reconstructed synchrotron μCT data were used to conduct random walker-based simulations of mass transport through a connected pore network; this provided information about the tortuosity (and therefore resistance to diffusional transport) of the pore structure as a function of the age of PC pastes [220]. Sugiyama et al. [221] also used the same

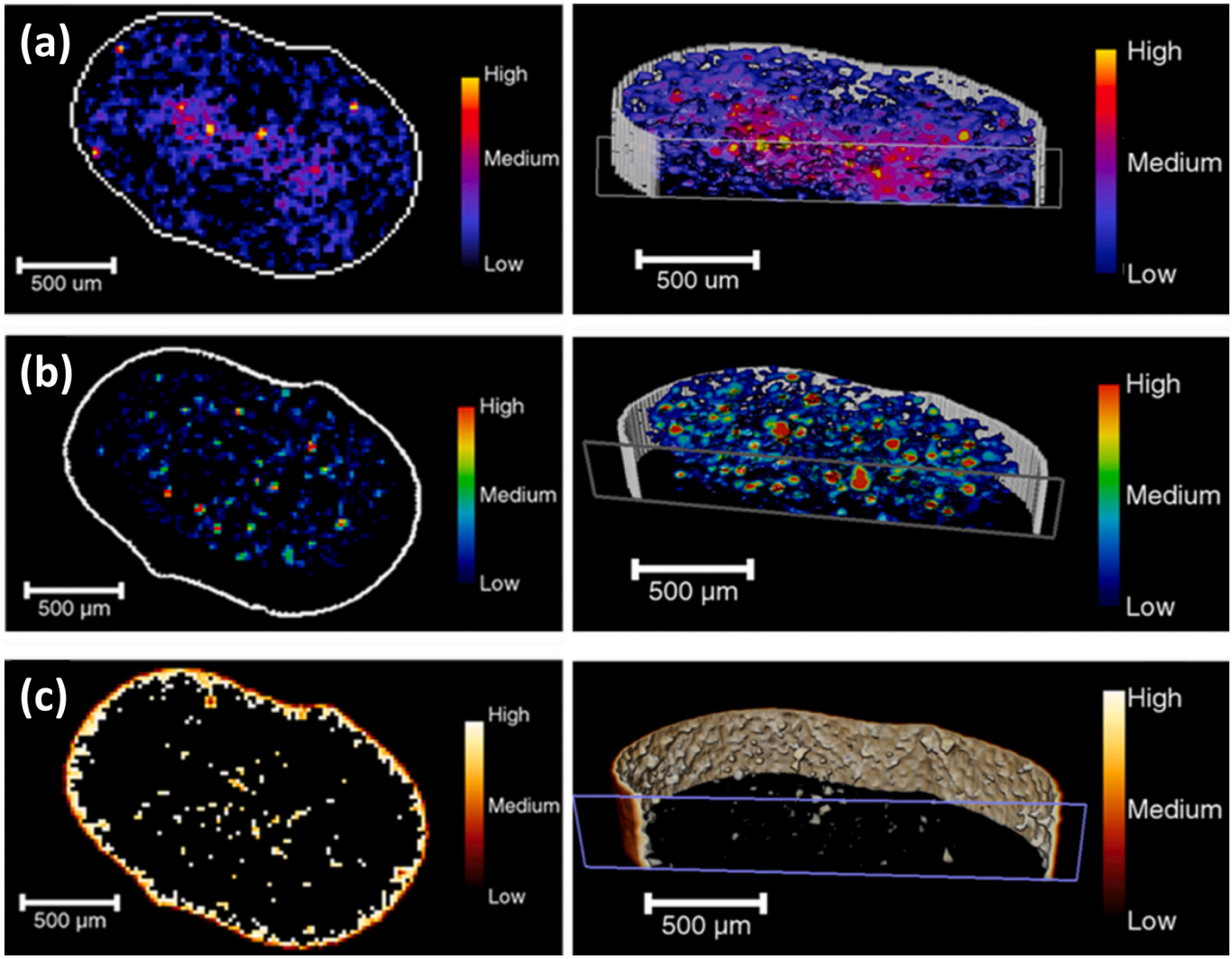


Fig. 16. Cross-section (left) and corresponding 3D spatial distribution (right) images obtained by XRD–µCT showing the distribution of (a) C-(A)-S-H gel, (b) ettringite, and (c) Mg—Al layered double hydroxide, in a carbonated sodium sulfate-activated slag paste. Reproduced from [207], published under the terms of the Creative Commons CC-BY licence.

methodology to demonstrate the changes in pore structure upon decalcification of a PC paste via leaching.

Provis et al. [222] later adapted this procedure to the analysis of alkali-activated cement pastes based on a blend of FA and BFS, and developed new insight into the effects of both time and gel chemistry on the pore structure of these pastes, where a calcium-rich gel provided pore-filling character while the calcium-poor alkali-aluminosilicate did not. Vigor et al. [223] also applied this methodology (i.e. absorption contrast) to the reconstruction of their tomographic data for high volume slag-PC blends, with pore structures as shown in Fig. 19. They identified that the porosity consistently decreased, and tortuosity increase, as the samples (with 90% or 75% replacement of PC by BFS) were cured from 1 to 360 days. Although the sample with 90% PC replacement had much higher porosity at 1 day, and initially developed its microstructure much more slowly, it eventually reached a notably higher tortuosity than the 75%-slag sample at 360 days, indicating the successful progress of the latent hydraulic reaction of this component even at such high replacement levels [223].

The larger sample sizes made accessible by synchrotron-based techniques also mean that it is possible to use phase-contrast (propagation based) µCT to analyse ASR at the micron-scale, in mortars with realistic aggregates [224]. A related work used SR absorption-contrast µCT to study the influence of fibre reinforcement on the progress of ASR [225]. Damage within and around aggregate particles is identifiable by this technique, and the correlation between tomographic and microdiffraction scans showing formation of ASR products provides important insight into the mineralogical evolution of the aggregate and cement at and near the affected interface [224].

The analysis of the encapsulation of wastes – both organic [226] and metallic [227,228] – in cement is another area in which SR absorption-based µCT has been successfully employed. Particularly in cases where the waste is potentially hazardous (e.g. metallic uranium in [228]), the use of non-destructive analysis with a highly penetrating (high-energy) X-ray source is very valuable in providing insight into microstructural details that would otherwise be very difficult to access.

To end this subsection, it must be noted that SR phase-contrast propagation-based µCT is still not widely adopted in cementitious materials research. Two notable exceptions are the 3D µCT analysis of LC^3 [229] and belite cement [230] binders. In these cases, the phases were retrieved by the Paganin algorithm [33] which has the additional advantage of being able to process images frame-by-frame. The data were taken on the TOMCAT BL of SLS (PSI) by using monochromatic X-rays, E = 15 keV, and a sample-to-detector distance of 5.5 mm. The Paganin phase-retrieval increased the contrast without introducing very significant edge artefacts; see Fig. 22 for a comparison between the attenuation and Paganin reconstructions. The calcite particles, an

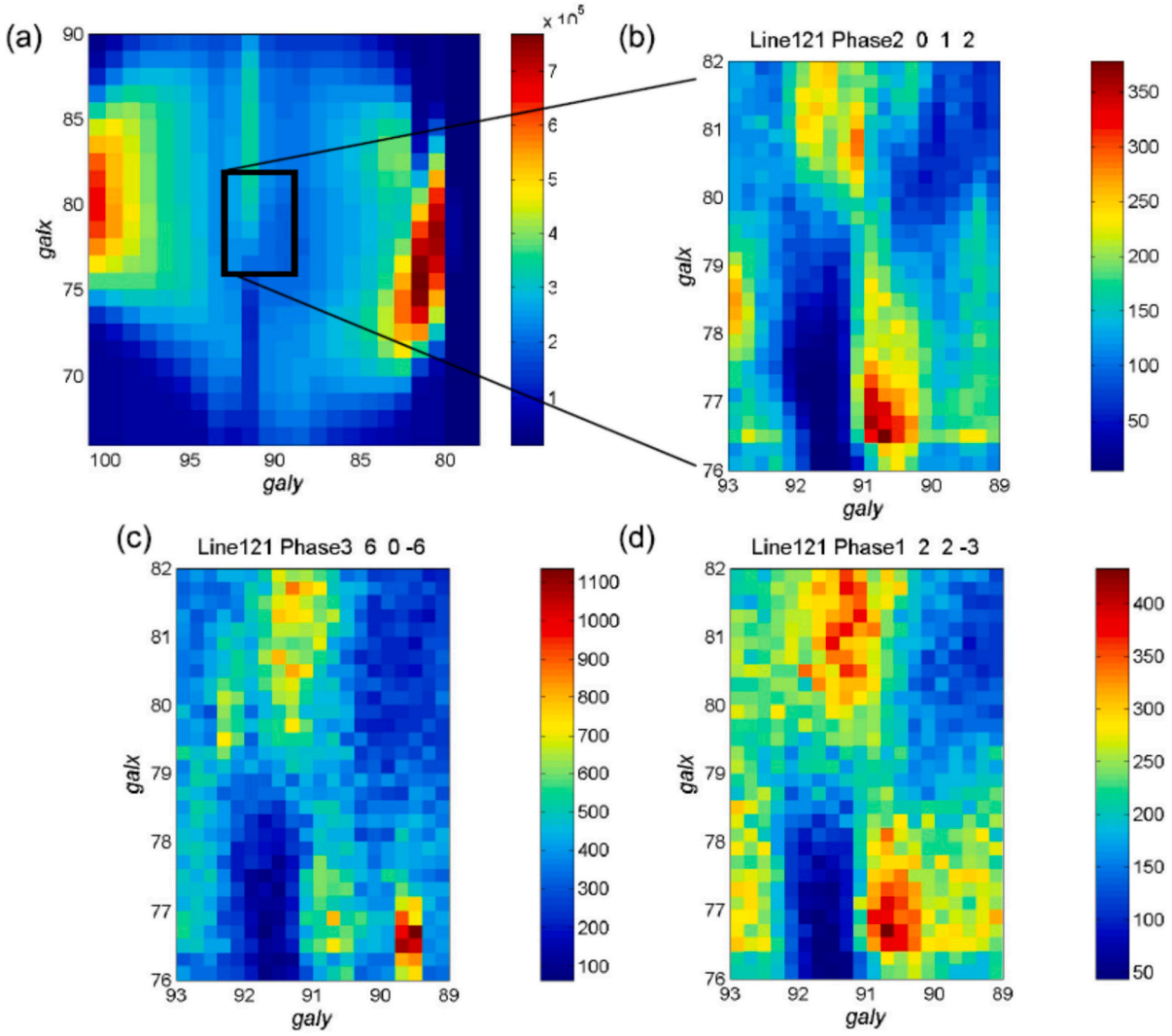


Fig. 17. Example of TEDDI 2D images showing (a) the distribution of total diffracted intensity; and enlarged regions showing the distribution of: (b) the 012 reflection of portlandite; (c) the 22$\underline{3}$ reflection of C_2S; and (d) the 60$\underline{6}$ reflection of C-S-H. Reproduced from [210], with permission from the authors.

important component of LC^3 binders, are easily identified in the Paganin reconstructed datasets, see Fig. 20. Moreover, the variation in pore connectivity with hydration time was studied for this type of low-carbon cements.

Moreover, and as was detailed in Section 2, multi-modal synchrotron imaging [34,35] is so far not commonly used for studying cementitious materials. This is likely due to the poor spatial resolution of early experimental setups, and the difficulties in data processing requiring significant knowledge in physics, computer science, as well as cement chemistry. However, this may change in the near future because of: (i) the additional information that can be gained from the phase-contrast and dark-field contrast channels of information; (ii) the recent improvements in spatial resolution; (iii) the larger availability of these approaches at many synchrotron facilities; and (iv) the emergence of easy-to-use advanced data analysis approaches, as it will be discussed in Section 5. As an example, Fig. 21 shows a SR–μCT (grating interferometry setup) study of a concrete sample of 50 mm height and 10 mm diameter [34]. The data were taken at ID19 BL of the ESRF with monochromatic X-rays, E = 53 keV, and two gratings (i.e. phase and absorption). It can be readily seen that enhanced information is derived from the three channels of information, which are extracted in the single tomographic experiment. It is expected that the use of AI tools, see Section 5, will allow researchers to profit from this plethora of information by integrating the different features in a unique model that could be expanded to 4D studies. To the best of the authors' knowledge, this type of work has not still been undertaken for cementitious materials.

5. General remarks

5.1. Beyond synchrotron radiation studies of cement hydration: material's response to controlled exposure environments

The techniques reviewed here can be used beyond hydration studies to evaluate the phase alterations and microstructure evolutions of cementitious materials when exposed to different environments. In this context, it is important to differentiate between studies aiming to investigate the impact of aggressive environments in the durability performance, and those where materials are exposed to specific environments (e.g. CO_2) for understanding mechanism and efficiency of processes such as mineralising CO_2 into cementitious systems.

Regarding to durability studies, the use of SR techniques has been somehow overlooked, with some notable exceptions. Evaluating the durability performance of cementitious materials via time-lapse analytical techniques is not always feasible or suitable, as the deterioration mechanisms are driven by slow chemical reactions between the

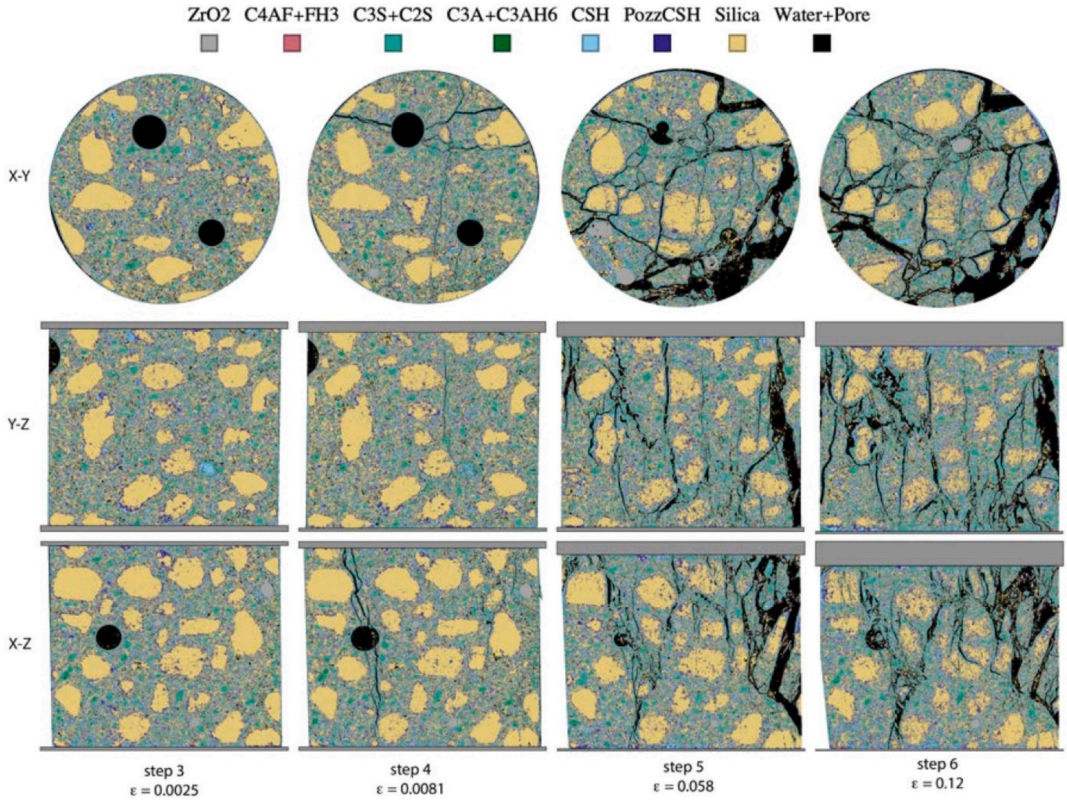


Fig. 18. Reconstructed SR μCT data for a specimen of ultra-high-performance concrete under compressive load applied in the Z direction as labelled: 125 MPa at step 3; 200 MPa at step 4; 85 MPa at step 5 (after failure at 220 MPa during loading); 50 MPa at step 6. Phases identified by distinct colours were identified by a thresholding segmentation approach. The ZrO_2 present is believed to be an impurity from ball milling in the preparation of precursor powders. Nominal sample size is 1.54 mm diameter, 1.47 mm height, cut as a prism from a larger specimen then honed to cylindrical shape using a manual diamond lathe. The sample was contained in a low-density polymeric foam during testing to prevent loss or ejection of fragments. Image from [216], published under a Creative Commons CC-BY-NC-ND licence.

hardened cement and specific species, enabled by the movement of potentially harmful substances (e.g. sulfates, CO_2, chlorides) into the material. Therefore, microstructural changes often occur on time scales that cannot be captured in a few hours or days, which is usually the practical limit of continuous availability of both laboratory and synchrotron analytical equipment. Nevertheless, accelerated tests are often adopted for material selection purposes, and to infer how degradation mechanisms are likely to proceed. Understanding the type and extent of microstructural alterations that a cementitious material can undergo upon exposure to an aggressive environment, enables identification and selection of strategies to extend their service life, as well as the development of more accurate models for service life prediction.

Firstly, and related to sulfate exposure, there were several studies evaluating the consequences of sulfate attack on cementitious phase assemblages and microstructures using μXRD. As the sulfate ingress takes place after hardening, and in a directional manner, the sample preparation is key; the material is normally processed as a thin slab and the spatial arrangement of the resulting crystalline components can be mapped by μXRD [231,232]. This methodology can also be applied to many other cementitious systems. Moreover, these processes could also be monitored by SR−μCT as in [233]. Secondly, and related to chloride exposure/attack, similar approaches can be undertaken as exemplified in [234,235]. The authors are not aware of published XRD−μCT studies after sulfate or chloride exposure.

Related to the exposure of cementitious systems to CO_2, i.e. carbonation, the situation is far more complex as there are many ways for these chemical reactions to take place. In this context, it must be distinguished whether carbonation takes place in loose powders or in hardened bulk specimens. This distinction is key as the CO_2 diffusion is quite different. Loose powders can be carbonated to produce enhanced pozzolanic materials as in recycled concrete fines [236] or to enhance the reactivity of hydrating cementitious materials [237] prior to the hardening step. In both cases, the main objective is to utilise, i.e. mineralise, CO_2 as one of the levers for reducing the carbon footprint of cementitious materials. In this case, a key technique is SXRPD (including total scattering) to analyse the resulting materials and the hydration reactions in the corresponding hydrating systems. To the best of the authors' knowledge, in-situ SR investigations of carbonation of loose powders have not been reported, although there are recent reports using laboratory XRPD [238,239]. This type of in-situ investigations can be carried out with higher accuracy and faster time resolution using SXRPD, even under moderate CO_2 pressures.

Carbonation of bulk cementitious specimens could also be studied by SR techniques. Here, it is possible to distinguish natural carbonation, which is of key relevance for durability studies but where spatially-resolved SR data must be collected in long time intervals (likely months), from accelerated carbonation. The latter approach uses enriched CO_2 atmospheres implying shorter time intervals, but still time intervals of days to weeks are needed. It is noteworthy that a recent review focused on characterisation techniques gathered studies using laboratory μCT but not synchrotron μCT [240]. Most of the current (laboratory) μCT studies [241,242] have focused on cementitious pastes and synchrotron μCT has been scarcely used [243]. SR-μCT may allow investigators not only to study the carbonation of pastes with higher spatial resolution, but importantly, to study more relevant mortar samples, as kinetic effects are dominant and depend upon the microstructure of the specimens, as well as upon the experimental conditions (e.g. temperature, relative humidity, CO_2 concentration, etc.). In any

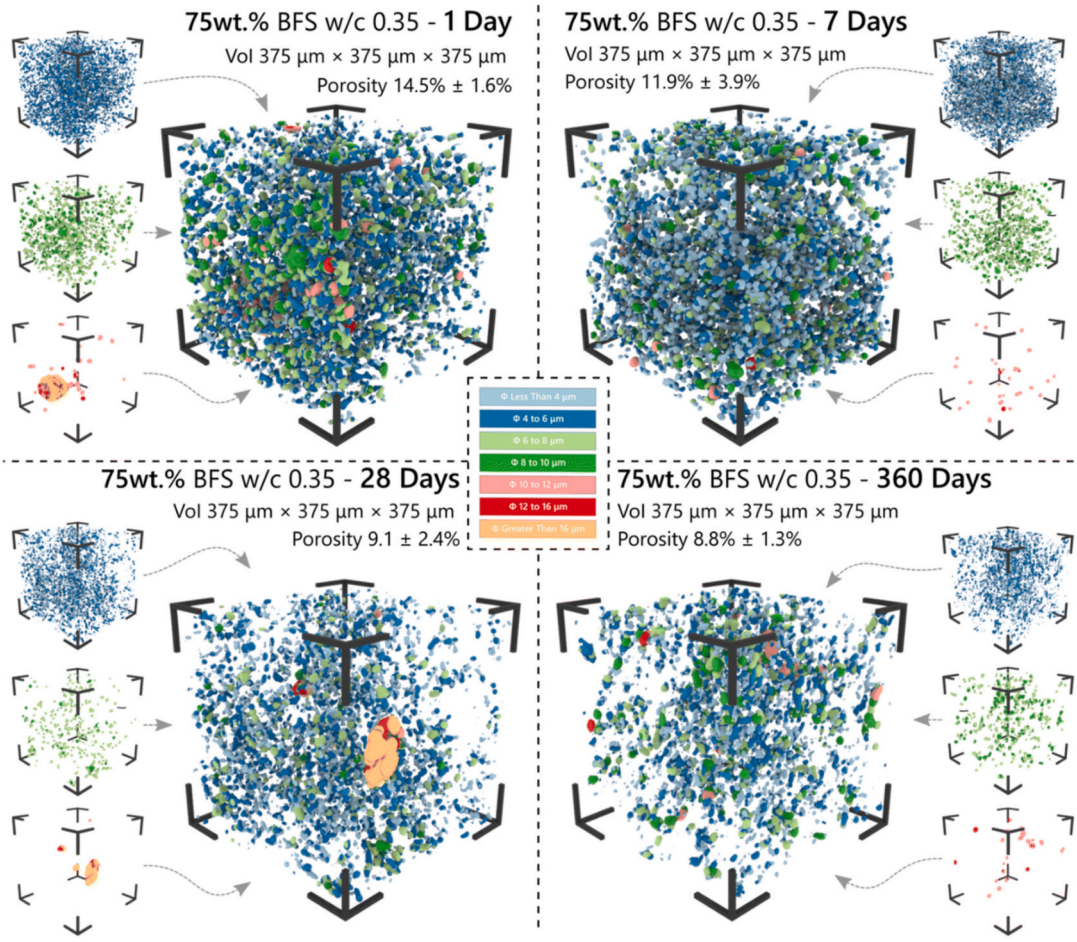


Fig. 19. Reconstructions of the pore structure of a PC-25%-BFS-75% paste as a function of curing duration (as marked on each image), with pores classified and coloured according to their effective diameter in the reconstructed microstructure. Image from [223], published under a Creative Commons CC-BY licence.

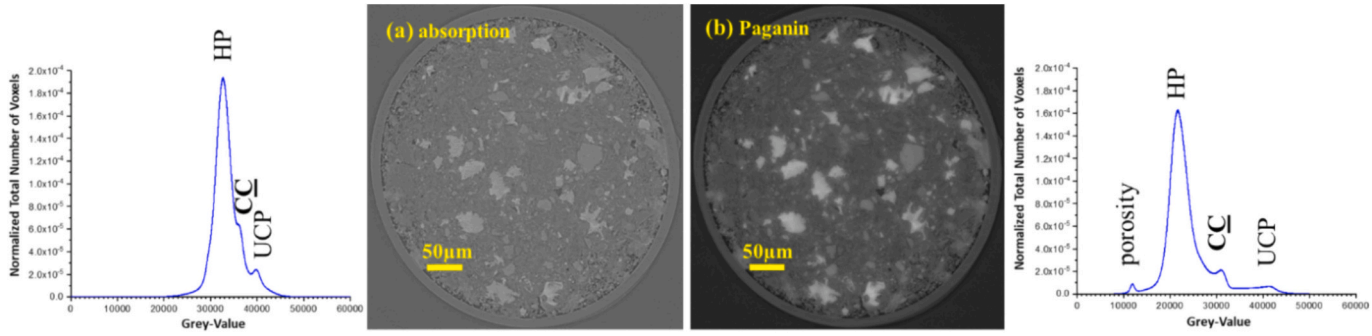


Fig. 20. Synchrotron µCT orthoslices (a) attenuation- (b) Paganin-reconstructions for a LC^3 binder after 60 hydration days. The histograms (blue) show the increase of contrast in (b), i.e. limestone (CC) is shown as a shoulder in the absorption trace but resolved in the Paganin one (HP: hydrated product, UCP: unhydrated cement particles), adapted from [229], published under the Creative Commons CC-BY-NC-ND. (For interpretation of the references to colour in this figure legend, the reader is referred to the web version of this article.)

case and to minimise variability, the same specimens should be non-destructively investigated as a function of the CO_2 exposure time, implying the need for beamtime access in the relevant time-scales, i.e. days to weeks. It should be noted that the benefit of week-to-month access is starting to be acknowledged, and therefore allowed by synchrotrons [244]. It is also noted that XRD−µCT is starting to be used to study the (accelerated) carbonation processes of cementitious pastes [207,208,245]. To end this subsection, it is underlined that to the best of the authors' knowledge, SR−µCT in-situ studies of CO_2 mineralisation, i.e. curing, under the mild pressures (1–4 bars) of possible interest for the precast concrete industry, have still not been reported.

To determine moisture/water movement in cementitious specimens, techniques such as neutron tomography have been extensively used [246]. As water has a very low X-ray attenuation coefficient, attempts to track water movement using synchrotron SR−µCT (or its two-dimensional counterpart, radiography) often require the use of substances to enhance its contrast; for example, NaCl in the reinforced mortar sample imaged in Fig. 22 [247]. Successful outcomes have also been reported when using solutions of CsCl in the study of paste specimens [248,249], whose results are comparable to those obtained when

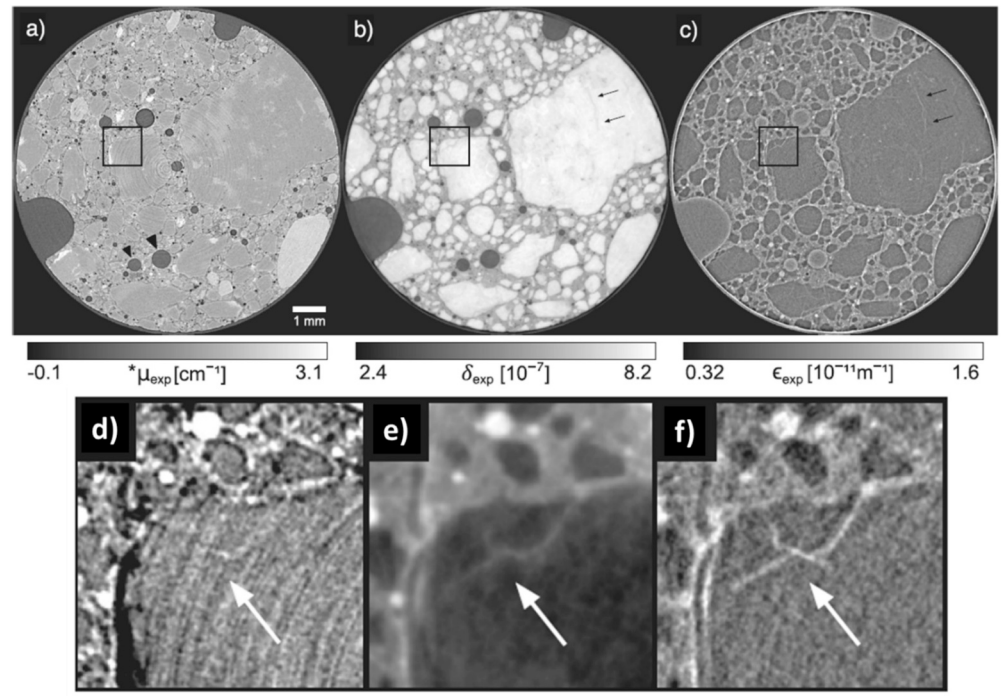


Fig. 21. (a) Attenuation-contrast, (b), phase-contrast, and (c) dark-field-contrast orthoslices from a SR-μCT (grating interferometry experimental setup) study of a concrete sample. The corresponding enlarged views of the highlighted regions are shown in the bottom panels. The CNR between the cement paste and the aggregates is very much enhanced in the phase-contrast channel. The cracks are more visible, i.e. better CNR, in the dark-field-contrast channel. The spatial resolution is higher in the attenuation-contrast channel. CNR values are given in the original publication. Adapted from [34], reproduced with permission from AIP Publishing.PL.

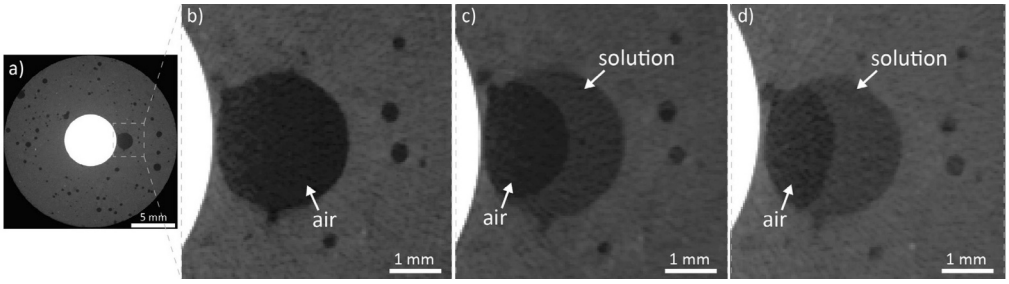


Fig. 22. Synchrotron X-ray CT cross-sections of a cylindrical mortar specimen (containing a 6 mm smooth carbon steel rebar) undergoing moisture ingress, showing how the water progressively penetrates the voids: a) the full specimen after 28 days of hydration; b) magnified view of an interfacial air void in this specimen; c) magnified interfacial air void after 8 weeks of immersion in 3.5 wt% NaCl solution, showing partial filling of the void space; d) the same partially-filled air void after 12 weeks of immersion. Reproduced from [247], published under a Creative Commons CC-BY licence.

applying neutron techniques, even when using laboratory X-ray μCT equipment. These types of studies are of great relevance for cementitious materials research as neutron source facilities are very limited, while X-ray μCT facilities (both synchrotron and laboratory) are relatively more widely available.

There are very few studies applying time-lapse μCT aimed at identifying alteration of cementitious materials when exposed to CO_2 rich environments. Chavez Panduro et al. [250] used laboratory– and SR–μCT to determine the alteration of Class G well-cements by CO_2-brine solutions (1% NaCl) under high pressure conditions, to elucidate its integrity in conditions relevant to CO_2 storage reservoirs. A dedicated pressure cell compatible with a laboratory μCT instrument was designed, so that the exposure pressure could be controlled while simultaneously exposing the hardened cement to CO_2 and the brine solution. This study presented novel insight into the kinetics of precipitation of calcium carbonate, see Fig. 23, which depending on the exposure conditions achieved (e.g. prevalence of carbonate vs. bicarbonate precipitation) can lead to self-healing of cavities/leakage paths in the cement when in contact with a CO_2-rich brine solution. This is dependent on the defect aperture size. In another study by those same authors [251] the HADES triaxial deformation apparatus at ESRF [252] was used to evaluate the microstructure alterations of a Class G cement exposed to CO_2 at high pressure (280 bar) and temperature (80 °C), which are conditions relevant to CO_2 storage. This study revealed novel insight into the precipitation and dissolution of $CaCO_3$ in leakage pathways, to understand how a reservoir might fail in the case of leakage. For example, at reduced CO_2 flow rates formation of the carbonated zone is promoted, leading to precipitation of $CaCO_3$ in large cavities. Conversely, at a high CO_2 flow rate in a leakage path, the formation of a weak and porous silica layer was identified in the carbonated cement.

5.2. *Discussion on well-established X-ray synchrotron techniques*

In this section, some comments are made referred to well established synchrotron techniques such as powder diffraction and micro-computed tomography. Concerning SXRPD, data collection and data analysis are considered to be robust. In most cases, cement paste within capillaries

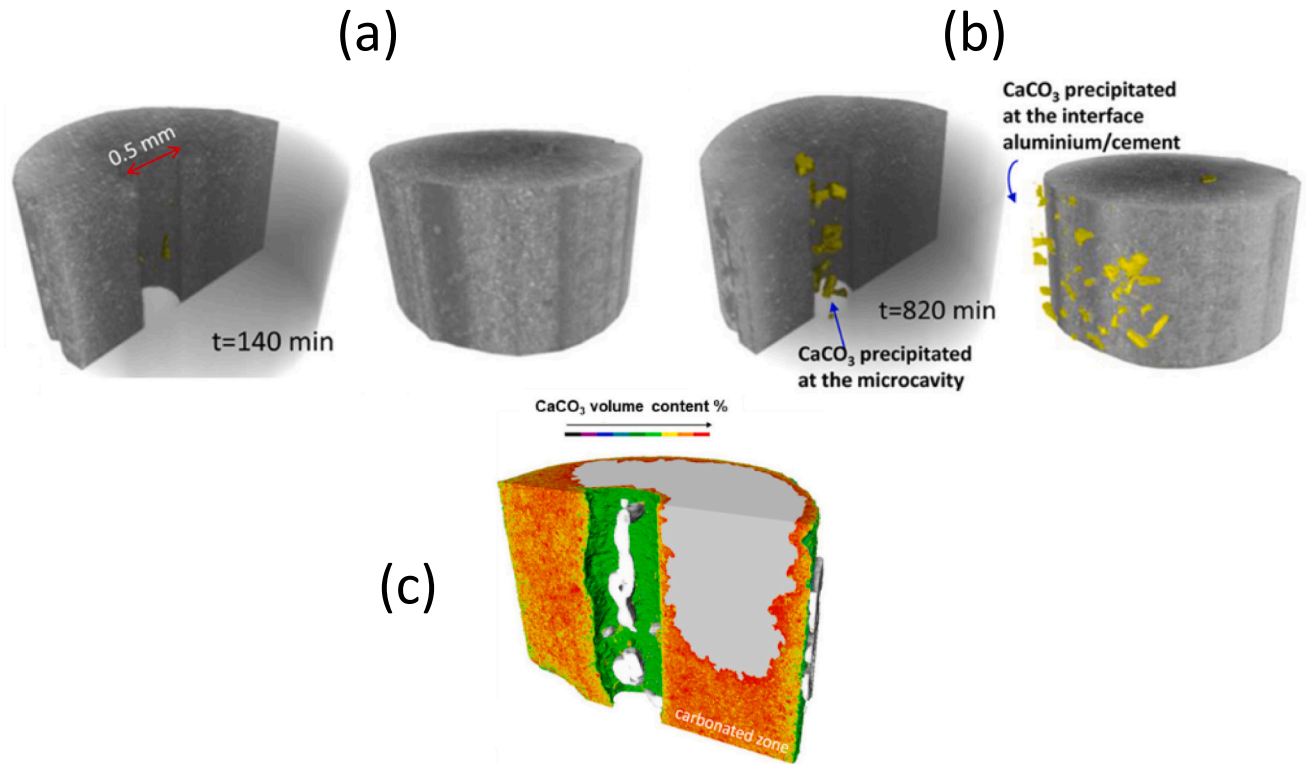


Fig. 23. 3D lab−μCT reconstructions of a cement sample with $CaCO_3$ precipitation (shown in yellow) after (a) 140 and (a) 820 min of CO_2 exposure. (c) 3D SR−μCT map showing distribution of $CaCO_3$ volume in the sample. Adapted from [250], with permission from American Chemical Society. (For interpretation of the references to colour in this figure legend, the reader is referred to the web version of this article.)

are being investigated, and thus sample conditioning is not required. Data analysis by the Rietveld method is relatively robust and most of the important crystal structures are known, although further improvements in the crystallographic description of solid solutions in cement hydrate phase assemblages are still important. For time-lapse studies (e.g. hydration, temperature, CO_2-curing, and others), sequential analyses could (and wherever possible, should) be done with the 'fundamental parameter approach', where the minimum number of variables are optimised/varied. This procedure can be carried out with software such as TOPAS [253] and GSAS-II [254,255], and it yields more robust results.

The most important developments that will enable the widespread use of this technique are related to the extensive knowledge gained of the influence of different experimental setups on the results collected, enabling the development of novel setups to resolve more complex scientific questions. For instance, new cells may allow in-situ studies of carbonation of cementitious materials under variable exposure conditions (e.g. CO_2 partial pressures, relative humidities, and/or temperature). Moreover, the possibility to select high X-ray energies enables the collection of SXRPD data for thick samples, e.g. 2 mm or more. In turn, this will allow collection of patterns for mortars, or at least mortars with sand sieved up to a largest particle size of 0.5–0.8 mm. Collecting SXRPD data for mortars, instead of pastes, will permit investigation of the possible differences in phase assemblages due to the differences in microstructures induced by the presence of sand. This is particularly important when kinetics effects are dominant. To the best of the authors' knowledge, such systematic studies are not yet available, but it is expected that they will be very informative.

Other relevant experimental developments could be computer-controlled mixing and injection of the cement pastes into the sample holders, using pastes with w/b ratios close to 0.40–0.50 and very homogeneous mixing. This would allow accurate measurement of the amount of AFt formed during the first minutes, and moreover, new and important research could be carried out such as collecting data series dealing with delayed (for different times) SP addition. Here, the main challenge could be to have highly-reproducible and intense mixing.

Concerning μCT data collection, X-ray microimaging is becoming well-established for parallel beams, and using both attenuation-based and propagation-based phase-contrast imaging with phases retrieved by the Paganin algorithm. From the data collection point of view, and working with parallel synchrotron beams, the relationship between the FoV and the obtained resolution is straightforward for the most commonly employed optic setups and detectors. For the μCT detectors usually employed at microimaging BLs, the physical pixel size is 6.5 μm and they have an area of approximately 2000 × 2000 pixels. To attain the highest possible spatial resolution, a 20× microscope is used which results in a voxel size of 0.375 μm for imaging a sample of ~0.6 mm of horizontal size (i.e. diameter). The use of a microscope of 40× or 50× reduces the FoV proportionally, which leads to difficulties in reproducible sample preparation, and it does not result in proportional improvements in spatial resolution because other effects start to dominate, such as those related to the thickness of the scintillator (which must be used to transform the X-ray photons to visible ones). Here, detector improvements are key as smaller (physical) pixel sizes will result in higher spatial resolution and larger detectors, i.e. 4000 × 4000 pixels, directly translate to bigger FoVs. However, in this last case, data processing and analysis issues (see Section 5.3) will be exacerbated as the sizes of the data sets will be much larger.

Concerning μCT data analysis, X-ray microimaging cannot yet be considered mature, even after twenty years of usage. Data analysis of tomographic experiments is problem-dependent as it is quite different to determine clinker-phase spatial dissolution rates or (micro)crack propagation studies, to mention just two cases. Because cementitious materials are very heterogeneous, the best possible spatial resolution is necessary for determining the tiniest details. Moreover, to have sufficient contrast between the components is key for a successful

classification (i.e. segmentation) of the different components. This is the reason why phase-contrast microimaging is gaining momentum, as the contrast between components is enhanced. Around 2020, most segmentation investigation relied on global thresholding methods (with slight variations in how borders were determined), and in some cases, morphological features, such as watershed segmentation, were also used. A game-changer event has been the appearance of widely available (and easy-to-use) AI approaches for tomographic data analysis, such as those present in the ImageJ [256], IPSDK [257] and Dragonfly [258] software, to mention just three, which will be discussed in more detail in the following section.

5.3. Opportunities and required efforts concerning data processing and analysis, including the role of AI

In this section we focus on SR X-ray imaging techniques which can be demanding from data processing and data analysis perspectives. Diffraction and spectroscopic techniques, without spatially-resolved features, are relatively easy to handle and they are not discussed here. However, it is acknowledged that AI is starting to be adopted for analysis of large XRPD datasets, and the reader is referred to [259–261] for further information on the topic.

Regarding SR microimaging CT, in simple terms, data are collected in 2D detectors in a suitable experimental configuration to yield the CTs with the required contrast mechanism (i.e. single crystal diffraction, powder diffraction, pair distribution function, attenuation-contrast, phase-contrast, coherent diffraction, just to name a few). After data acquisition, for the processing of tomographic data, mathematical algorithms are applied to reconstruct the 3D distribution of the resulting features from the measured data. Data processing, automated in some cases by "big data" scientific computing approaches [262], is carried out at the synchrotron facilities, and the results are therefore reconstructed virtual volumes. In some cases, postprocessing could be needed, such as filtering or denoising. Then, the users take to their home institutions the 3D stack of reconstructed images to conduct the appropriate data analysis. Data transfer can be an issue for very large datasets (dozens to hundreds of TBs) which are generated in, for example, time-lapse studies of evolution of materials properties in three spatial dimensions. Synchrotron facilities are starting to develop online data analysis tools, in order to avoid data transfer, and the analyses could be carried out by remote access. However, this is still in its infancy.

For the simplest case of SR abs−μCT, a grey level histogram can be used to segment the 3D stack of images for distinguishing specific components or features which can then be quantified [263]. The grey levels or thresholding at which specific components can be identified can vary significantly depending on the person conducting the segmentation, spatial resolution of the data collected, and the intrinsic properties of the material evaluated (e.g. similar grey values can correspond to different components with similar densities [264]). Therefore, harmonised protocols for data processing/analysis are needed so that quantitative results derived from different studies can be compared.

As a starting point to create more confidence in the data resulting from these analyses, and demonstrate its value for understanding cementitious materials, agreement about methods for segmenting/thresholding images to assigning specific grey level values to given phases, is required. Deboodt et al. [217] investigated the impact of applying different image pre-processing and segmentation algorithms in quantifying synthesised hydration cementitious products. It was reported that histogram based, global thresholding, algorithms can accurately quantify phases when adequate contrast is observed in the reconstructed image volume; however, more accurate results for quantification of binary mixtures of AFm and C-S-H were achieved when applying a statistical global thresholding algorithm, compared with a Gaussian histogram deconstruction approach. This study highlighted how even when data are evaluated by the same operator, adopting different approaches to its analysis can yield to different results.

In this context, SR μCT datasets, particularly those of multiscale/multimodal experiments, can be difficult to process without the assistance of computational tools such as ML approaches and algorithms. Some early examples dealing with the implementation of ML algorithms and data analytics methods for systematic and quantitative analyses of microimaging have been reviewed [8]. Here, we elaborate on this matter as this is a fast-growing field that will importantly impact the data analysis of CTs in their different modalities. Two of the approaches that are being most widely adopted for tomographic data analysis include trainable WEKA segmentation (TWS) [265], as implemented for example in the Fiji distribution of ImageJ [256] and the Watershed segmentation (WS) algorithm used in AVIZO® [266].

In the TWS plugin of Fiji, it is possible to manually label pixels and assign them to different phases/components. The trained pixels are then used to conduct the classification/segmentation of phases from the dataset being analysed [267]. TWS also uses different image filters which can be selected for advanced data processing, including reducing noise, extraction of image texture, and others [265]. Related user-friendly approaches can be carried out for AI training and data analysis using software including IPSDK [257] and Dragonfly [258]; a full comparison of these techniques is beyond the scope of the present review. It is noted that it is not straightforward to start the use of the AI modules of these programs. Thus, the interested readers are referred to the web and YouTube tutorials [268–270]. After this, the AI approach, which is field- and in some cases even sample- dependent, can be consulted in scientific publications. Some examples are [208,245,271,272].

In principle, the WS method involves the conversion of an image to a topological landscape where the height of each point reflects the pixel value at that point [273]. The segmentation requires an initial identification of how many components are expected to be present and distinguishable in the sample analysed, and then creation of specific boundaries between the different phases by finding the lines of highest gradients via a small cubic kernel or an edge detection filter. Then, seed points for the distinguished phases are identified by thresholding [267]. In the case of the software AVIZO [266], the image stack is imported into the software, a filter for reducing noise can be applied, and the watershed wizard can be used to define the watershed lines and seed points for the different phases.

These brief summaries describe current examples of the use of AI/ML for analysis of tomographic data for cementitious systems [93,207,274,275]. Other automated processing approaches for multimodal CT techniques have been developed (e.g. [276]), but they are not yet so prominent in the analysis of cements and so they will not be discussed in this review.

Concerning the accuracy of tomographic analyses, it is important to note that at present, it is unlikely that two users would determine the same microstructural distribution for the phases/components, when analysing exactly the same dataset. Most importantly, phase estimates do not typically come with error bars, and data collected under (slightly) different conditions can lead to different quantification of components and pore structure features. Clearly, efforts are needed to provide simple approach(es) for obtaining *robust quantifications with associated uncertainties*. The segmentation model should assign a probability to each pixel or voxel, allowing the uncertainty in segmentation to be quantified. Automated and robust workflows are essential when analysing sequences that could include tens of datasets (or more), gathered over time. Any effort in this direction is most welcome and will have a broad impact beyond cement sciences.

To finish this section, the data deluge issue, already faced by synchrotrons, should be mentioned [277]. Data deluge is a situation where more data are produced than can be successfully and efficiently managed (i.e. processed, analysed, stored, and possibly re-used). As an example, already in 2017, the TOMCAT microimaging BL of SLS (PSI) was producing 7.7 GB/s, or several tens of TB of data per day [278]; the BL16U2 fast imaging BL at SSRF (Shanghai, China) produces up to 480

TB/d [279], and the B7 hard X-ray microscope BL at HEPS (Beijing, China) is expected to average 250 TB/d [280]. This issue is most problematic for very fast acquisitions, and so is not totally applicable to cementitious systems, where the kinetics are relatively slow. However, imaging large volumes at high resolution will also produce an enormous amount of data, particularly if coupled to 4D studies. This is already the case of BM18, the BL for hierarchical ph−μCT at the ESRF [281]. This BL can image samples with thicknesses up to 300 mm, which is relevant for mortars and (especially) concretes. In fact, reference [281] shows the microimaging study of a standard concrete cylinder (320 × 160 mm, vertical-horizontal) provided by Dr. Olivier Plé (LOCIE, Chambery). The full cylinder was scanned at a voxel size of 34.66 μm, with a high-resolution local CT at 4.26 μm in its centre. The corresponding scientific paper is still not published, but some images can be seen in [281]. Cement scientists motivated to contribute to multiscale 4D imaging of cementitious materials should be aware of this data deluge challenge, and to have resources to face it.

5.4. Concluding remarks: future research needs, opportunities and perspectives

Synchrotron radiation techniques, when compared to laboratory ones, can provide:

(i) much higher spatial and angular resolutions;
(ii) lower limits of detection and quantification, both in real space (i.e. imaging) and in reciprocal space (i.e. diffraction and scattering);
(iii) better contrast between components in microimaging;
(iv) chemical speciation selectively through spectroscopy;
(v) much faster data acquisition times; and
(vi) the capability to design in-situ experiments with much lower errors/bias (e.g. hydration, carbonation, temperature-dependence, pressure-dependence, and combinations of these, just to mention the most important ones).

Hence, using SR for analysis of cementitious materials offers unique advantages, particularly considering the challenges posed by the development of more complex cement formulations and more demanding application scenarios. However, there are also trade-offs related to the use of SR techniques, such as limited observation times, and the need to submit proposals that if awarded, lead to measurements that are carried out between 9 and 12 months after the initial planning. It is acknowledged that data collection, processing and analysis for some of the techniques discussed in this review are not trivial. However, with the rapid advances in computing capacity, and development of tools such as ML and AI, it will be possible to distil relevant and novel scientific information data in a very rapid, reliable, and efficient manner.

Below we detail, in bullet point format, a selection of unique findings based on the use of synchrotron techniques.

- Related to micro- and meso- structures: Non-destructive high spatial resolution in-situ tomographic analysis of different processes (under chemical –H_2O– gradient [i.e. hydration], under chemical –CO_2– gradient [i.e. carbonation], under chemical –other species– gradient (i.e. Cl^-/SO_4^{2-}), under mechanical loads, under heating, pressure, and combinations), giving unique access to datasets with both spatial and time resolution for a mechanistic understanding of these processes. The novel and fundamental understanding gained by applying high spatial resolution X-ray imaging techniques has a tremendous practical impact for accelerated materials design and selection for given performance characteristics.
- Related to disordered materials: Identifying the composition and local structure of poorly crystalline reaction products forming in cementitious materials during hydration processes, or when exposed to an aggressive environment. Such understanding could not be achieved by conventional laboratory techniques, and it is underpinning the development of fundamental theories that explain the hydration and degradation processes of cementitious materials as a function of their intrinsic properties.
- Related to the chemical environments of selected elements: Spectroscopic analysis requiring precise tuning of incident X-ray energy – particularly XAS, which has provided insight into chemical environments and bonding states of numerous elements (major and minor) in cementitious materials in a way that would not be possible otherwise.
- Related to the elastic properties of individual phases in cement pastes: High-pressure SR-based measurements of the elastic properties of cementitious phases have contributed enormously to our fundamental understanding of material properties at the microscale.

Specialised equipment (often solely available in synchrotrons) as well as trained personnel for data collecting and processing are required. Nevertheless, as fundamental and advanced materials science approaches continue to be applied for understanding cementitious materials, particularly in terms of their formation and their responses when exposed to different environments, a broader widespread uptake of these techniques is occurring. In most cases, robust pipelines for data acquisition and data processing are established at synchrotrons. However, it is also true that synchrotrons do not always have the manpower to provide continuous support for data processing and analysis for non-specialist users. Although specialised training courses focused on the application of X-ray techniques for advanced-quantitative analysis do exist, those are not usually focused on cementitious materials. Therefore, there is an urgent need to increase the efforts to equip the next generation of cement materials scientists with the knowledge and ability to continue advancing the utilisation of these valuable tools. This will enable the research community to answer the key fundamental questions that remain unresolved, and to design and create the next generation of cementitious materials for service of society and the planet.

CRediT authorship contribution statement

Miguel A.G. Aranda: Writing – review & editing, Writing – original draft, Investigation, Conceptualization. **Angeles G. De la Torre:** Writing – review & editing, Writing – original draft, Investigation, Conceptualization. **Susan A. Bernal:** Writing – review & editing, Writing – original draft, Investigation, Conceptualization. **John L. Provis:** Writing – review & editing, Writing – original draft, Investigation, Conceptualization.

Declaration of Generative AI and AI-assisted technologies in the writing process

AI software has not been used to write or edit this work.

Declaration of competing interest

S.A. Bernal and J.L. Provis are members of the board of Editors of *Cement and Concrete Research*. The authors declare no other competing interest.

Acknowledgements

The authors are grateful to Rebecca Sanderson (UKNNL) for giving permission for the use of her data in Section 4.2, and to Brant Walkley (U. Sheffield) for his input into the collection and interpretation of those data. The authors would also like to express our gratitude to the many colleagues (in our research groups and at the facilities) who have collaborated and supported our beamline-based experiments in numerous synchrotrons worldwide, and whose input into scientific discussions over many years has provided much of the insight that we

have attempted to distil into this paper. The participation of S.A. Bernal in this study was funded by the UK Engineering and Physical Sciences Research Council (EPSRC), grant EP/W021811/1. M.A.G. Aranda acknowledges partial funding by the European Union-ERC (acronym: syn4cem, grant agreement: 101139298). Views and opinions expressed are however those of the author(s) only and do not necessarily reflect those of the European Union or the European Research Council. Neither the European Union nor the granting authority can be held responsible for them. Funding for open access charge: Universidad de Malaga/CBUA.

Data availability

No data was used for the research described in the article.

References

[1] P. Willmott, An Introduction to Synchrotron Radiation: Techniques and Applications, second edi, Wiley, 2019.
[2] S. Mobilio, F. Boscherini, C. Meneguini, Synchrotron Radiation Basics, Methods and Applications, 1st ed., Springer, 2015.
[3] A.S. Schlachter, A.L. Robinson, A. Bienenstock, D. Mills, G. Shenoy, H. Winick, Synchrotron Radiation, McGraw Hill, 2021, https://doi.org/10.1036/1097-8542.675200.
[4] L. Bertrand, M. Cotte, M. Stampanoni, M. Thoury, F. Marone, S. Schöder, Development and trends in synchrotron studies of ancient and historical materials, Phys. Rep. 519 (2012) 51–96, https://doi.org/10.1016/J.PHYSREP.2012.03.003.
[5] M.A.G. Aranda, Recent studies of cements and concretes by synchrotron radiation crystallographic and cognate methods, Crystallogr. Rev. 22 (2016) 150–196, https://doi.org/10.1080/0889311X.2015.1070260.
[6] L. Mino, E. Borfecchia, J. Segura-Ruiz, C. Giannini, G. Martinez-Criado, C. Lamberti, Materials characterization by synchrotron x-ray microprobes and nanoprobes, Rev. Mod. Phys. 90 (2018) 25007, https://doi.org/10.1103/RevModPhys.90.025007.
[7] P.J.M. Monteiro, G. Geng, D. Marchon, J. Li, P. Alapati, K.E. Kurtis, M.J.A. Qomi, Advances in characterizing and understanding the microstructure of cementitious materials, Cem. Concr. Res. 124 (2019) 105806, https://doi.org/10.1016/j.cemconres.2019.105806.
[8] E. Qoku, K. Xu, J. Li, P.J.M. Monteiro, K.E. Kurtis, Advances in imaging, scattering, spectroscopy, and machine learning-aided approaches for multiscale characterization of cementitious systems, Cem. Concr. Res. 174 (2023) 107335, https://doi.org/10.1016/j.cemconres.2023.107335.
[9] Z. Zhang, Y. Yan, G. Geng, A review of micro-resolved crystochemical and mechanical probes for sustainable cement-based material studies, Npj Mater. Sustain. 3 (2025) 1, https://doi.org/10.1038/s44296-024-00044-6.
[10] M.A.G. Aranda, 4D synchrotron X-ray nanoimaging for early age cement curing: where are we and where should we go? Acc. Mater. Res. 6 (2025) 814–827, https://doi.org/10.1021/ACCOUNTSMR.5C00018.
[11] C. Naber, S. Stegmeyer, D. Jansen, F. Goetz-Neunhoeffer, J. Neubauer, The PONKCS method applied for time resolved XRD quantification of supplementary cementitious material reactivity in hydrating mixtures with ordinary Portland cement, Construct. Build Mater. 214 (2019) 449–457, https://doi.org/10.1016/J.CONBUILDMAT.2019.04.157.
[12] N.V.Y. Scarlett, I.C. Madsen, Quantification of phases with partial or no known crystal structures, Powder Diffract. 21 (2006) 278–284, https://doi.org/10.1154/1.2362855.
[13] S. Shirani, A. Cuesta, A.G. De la Torre, I. Santacruz, A. Morales-Cantero, I. Koufany, C. Redondo-Soto, I.R. Salcedo, L. León-Reina, M.A.G. Aranda, Mix and measure - combining in situ X-ray powder diffraction and microtomography for accurate hydrating cement studies, Cem. Concr. Res. 175 (2024) 107370, https://doi.org/10.1016/J.CEMCONRES.2023.107370.
[14] J. Fernandez-Sanchez, A. Cuesta, S. Shirani, C. Redondo-Soto, A.G. De la Torre, I. Santacruz, I.R. Salcedo, L. Leon-Reina, M.A.G. Aranda, Mix and measure II: joint high-energy laboratory powder diffraction and microtomography for cement hydration studies, J. Appl. Cryst. 57 (2024) 1067–1084, https://doi.org/10.1107/s1600576724004527.
[15] A. Aili, I. Maruyama, G. Geng, S. Umeki, K. Sumitani, S. Sawada, S. Ueda, Y. Umeki, Micro X-ray diffraction and elemental study on Al-tobermorite formation in aged modern concrete, J. Am. Ceram. Soc. 105 (2022) 6924–6937, https://doi.org/10.1111/jace.18624.
[16] M.C. Dalconi, G. Artioli, N. Masciocchi, C. Giacobbe, F. Castiglioni, G. Ferrari, The crystal structure of a new calcium aluminate phase containing formate, Cem. Concr. Res. 146 (2021) 106490, https://doi.org/10.1016/J.CEMCONRES.2021.106490.
[17] N. Krautwurst, L. Nicoleau, M. Dietzsch, I. Lieberwirth, C. Labbez, A. Fernandez-Martinez, A.E.S. Van Driessche, B. Barton, S. Leukel, W. Tremel, Two-step nucleation process of calcium silicate hydrate, the nanobrick of cement, Chem. Mater. 30 (2018) 2895–2904, https://doi.org/10.1021/ACS.CHEMMATER.7B04245.
[18] S. Im, H. Jee, M. Kanematsu, S. Morooka, H. Choe, N. Yuhei, A. Machida, A. Tominaga, B. Jeon, S. Bae, Multi-scale synchrotron X-ray scattering studies on thermo-induced changes in structural and mechanical properties of CSH/PCE composites, Construct. Build Mater. 459 (2025) 139742, https://doi.org/10.1016/J.CONBUILDMAT.2024.139742.
[19] A.J. Allen, J.J. Thomas, H.M. Jennings, Composition and density of nanoscale calcium–silicate–hydrate in cement, Nat. Mater. 6 (2007) 311–316, https://doi.org/10.1038/nmat1871.
[20] S.J.L. Billinge, The rise of the X-ray atomic pair distribution function method: a series of fortunate events, Philos. Trans. R. Soc. A 377 (2019) 20180413, https://doi.org/10.1098/RSTA.2018.0413.
[21] A. Cuesta, I. Santacruz, A.G. De la Torre, M. Dapiaggi, J.D. Zea-Garcia, M.A. G. Aranda, Local structure and Ca/Si ratio in C-S-H gels from hydration of blends of tricalcium silicate and silica fume, Cem. Concr. Res. 143 (2021) 106405, https://doi.org/10.1016/j.cemconres.2021.106405.
[22] K. Gong, C.E. White, Time-dependent phase quantification and local structure analysis of hydroxide-activated slag via X-ray total scattering and molecular modeling, Cem. Concr. Res. 151 (2022) 106642, https://doi.org/10.1016/J.CEMCONRES.2021.106642.
[23] G. Kim, S. Im, H. Jee, H. Suh, S. Cho, M. Kanematsu, S. Morooka, T. Koyama, Y. Nishio, A. Machida, J. Kim, S. Bae, Effect of magnesium silicate hydrate (M-S-H) formation on the local atomic arrangements and mechanical properties of calcium silicate hydrate (C-S-H): in situ X-ray scattering study, Cem. Concr. Res. 159 (2022) 106869, https://doi.org/10.1016/J.CEMCONRES.2022.106869.
[24] C. Giannini, V. Holy, L. De Caro, L. Mino, C. Lamberti, Watching nanomaterials with X-ray eyes: probing different length scales by combining scattering with spectroscopy, Prog. Mater. Sci. 112 (2020) 100667, https://doi.org/10.1016/J.PMATSCI.2020.100667.
[25] F. Pfeiffer, X-ray ptychography, Nat. Photonics 12 (2018) 9–17, https://doi.org/10.1038/s41566-017-0072-5.
[26] M. Guizar-Sicairos, P. Thibault, Ptychography: a solution to the phase problem, Phys. Today 74 (2021) 42, https://doi.org/10.1063/PT.3.4835.
[27] P.J. Withers, C. Bouman, S. Carmignato, V. Cnudde, D. Grimaldi, C.K. Hagen, E. Maire, M. Manley, A. Du Plessis, S.R. Stock, X-ray computed tomography, Nat. Rev. Methods Prim. 1 (2021) 1–21, https://doi.org/10.1038/s43586-021-00015-4.
[28] L. Quenot, S. Bohic, E. Brun, X-ray phase contrast imaging from synchrotron to conventional sources: a review of the existing techniques for biological applications, Appl. Sci. 12 (2022) 9539, https://doi.org/10.3390/APP12199539.
[29] S.Y. Chung, J.S. Kim, D. Stephan, T.-S. Han, Overview of the use of micro-computed tomography (micro-CT) to investigate the relation between the material characteristics and properties of cement-based materials, Construct. Build Mater. 229 (2019) 116843, https://doi.org/10.1016/j.conbuildmat.2019.116843.
[30] A. du Plessis, W.P. Boshoff, A review of X-ray computed tomography of concrete and asphalt construction materials, Constr. Build. Mater. 199 (2019) 637–651, https://doi.org/10.1016/j.conbuildmat.2018.12.049.
[31] S. Brisard, M. Serdar, P.J.M. Monteiro, Multiscale X-ray tomography of cementitious materials: a review, Cem. Concr. Res. 128 (2020) 105824, https://doi.org/10.1016/j.cemconres.2019.105824.
[32] T. Sugiyama, M.A.B. Promentilla, Advancing concrete durability research through X-ray computed tomography, J. Adv. Concrete Technol. 19 (2021) 730–755, https://doi.org/10.3151/jact.19.730.
[33] D. Paganin, S.C. Mayo, T.E. Gureyev, P.R. Miller, S.W. Wilkins, Simultaneous phase and amplitude extraction from a single defocused image of a homogeneous object, J. Microsc. 206 (2002) 33–40, https://doi.org/10.1046/j.1365-2818.2002.01010.x.
[34] A. Sarapata, M. Ruiz-Yaniz, I. Zanette, A. Rack, F. Pfeiffer, J. Herzen, Multi-contrast 3D X-ray imaging of porous and composite materials, Appl. Phys. Lett. 106 (2015) 15–19, https://doi.org/10.1063/1.4918617.
[35] F. Prade, K. Fischer, D. Heinz, P. Meyer, J. Mohr, F. Pfeiffer, Time resolved X-ray dark-field tomography revealing water transport in a fresh cement sample, Sci. Rep. 6 (2016) 29108, https://doi.org/10.1038/srep29108.
[36] S. Savatović, M.-C. Zdora, F. De Marco, C. Bikis, M. Olbinado, A. Rack, B. Müller, P. Thibault, I. Zanette, Multi-resolution X-ray phase-contrast and dark-field tomography of human cerebellum with near-field speckles, Biomed. Opt. Express 15 (2024) 142, https://doi.org/10.1364/boe.502664.
[37] M.M. Thakur, N.A. Henningsson, J. Engqvist, P.O. Autran, J.P. Wright, R. C. Hurley, On mesoscale modeling of concrete: role of heterogeneities on local stresses, strains, and representative volume element, Cem. Concr. Res. 163 (2023) 107031, https://doi.org/10.1016/J.CEMCONRES.2022.107031.
[38] R.C. Hurley, D.C. Pagan, E.B. Herbold, C. Zhai, Examining the micromechanics of cementitious composites using in-situ X-ray measurements, Int. J. Solids Struct. 267 (2023) 112162, https://doi.org/10.1016/J.IJSOLSTR.2023.112162.
[39] M.M. Thakur, N.A. Henningsson, J. Engqvist, P.O. Autran, J.P. Wright, R. C. Hurley, Grain-scale stress heterogeneity in concrete from in-situ X-ray measurements, Cem. Concr. Res. 190 (2025) 107789, https://doi.org/10.1016/J.CEMCONRES.2025.107789.
[40] X. Liu, W. Lin, B. Chen, F. Zhang, P. Zhao, A. Parsons, C. Rau, I. Robinson, Coherent diffraction study of calcite crystallization during the hydration of tricalcium silicate, Mater. Des. 157 (2018) 251–257, https://doi.org/10.1016/J.MATDES.2018.07.031.
[41] X. Liu, M.A.G. Aranda, B. Chen, P. Wang, R. Harder, I. Robinson, In situ Bragg coherent diffraction imaging study of a cement phase microcrystal during hydration, Cryst. Growth Des. 15 (2015) 3087–3091, https://doi.org/10.1021/cg5013389.

[42] Light sources of the world – Lightsources.org. https://lightsources.org/lightsources-of-the-world/, 2025. (Accessed 15 May 2025).
[43] WayForLight. https://www.wayforlight.eu/, 2025. (Accessed 28 May 2025).
[44] E. John, B. Lothenbach, Cement hydration mechanisms through time – a review, J. Mater. Sci. 58 (2023) 9805–9833, https://doi.org/10.1007/S10853-023-08651-9.
[45] K.L. Scrivener, A. Ouzia, P. Juilland, A. Kunhi Mohamed, Advances in understanding cement hydration mechanisms, Cem. Concr. Res. 124 (2019) 105823, https://doi.org/10.1016/j.cemconres.2019.105823.
[46] A. Takeuchi, Advances in multiscale/multimodal X-ray tomography, Synchrotron Radiat. News. 37 (2024) 2–3, https://doi.org/10.1080/08940886.2024.2414705.
[47] D.P. Bentz, E.J. Garboczi, C.J. Haecker, O.M. Jensen, Effects of cement particle size distribution on performance properties of Portland cement-based materials, Cem. Concr. Res. 29 (1999) 1663–1671, https://doi.org/10.1016/S0008-8846(99)00163-5.
[48] F. Fauth, I. Peral, C. Popescu, M. Knapp, The New Material Science Powder Diffraction Beamline at ALBA Synchrotron, Cambridge University Press, 2013, https://doi.org/10.1017/S0885715613000900.
[49] F. Fauth, R. Boer, F. Gil-Ortiz, C. Popescu, O. Vallcorba, I. Peral, D. Fullà, J. Benach, J. Juanhuix, The crystallography stations at the Alba synchrotron, Eur. Phys. J. Plus 130 (8) (2015) 1–13, https://doi.org/10.1140/EPJP/I2015-15160-Y.
[50] A.S. Brand, S.B. Feldman, P.E. Stutzman, A.V. Ievlev, M. Lorenz, D.C. Pagan, S. Nair, J.M. Gorham, J.W. Bullard, Dissolution and initial hydration behavior of tricalcium aluminate in low activity sulfate solutions, Cem. Concr. Res. 130 (2020) 105989, https://doi.org/10.1016/J.CEMCONRES.2020.105989.
[51] S.J. Gurgul, G. Seng, G.R. Williams, A kinetic and mechanistic study into the transformation of calcium sulfate hemihydrate to dihydrate, J. Synchrotron Radiat. 26 (2019) 774–784, https://doi.org/10.1107/S1600577519001929.
[52] M.C. Schlegel, A. Sarfraz, U. Müller, U. Panne, F. Emmerling, First seconds in a building's life—in situ synchrotron X-ray diffraction study of cement hydration on the millisecond timescale, Angew. Chemie Int. Ed. 51 (2012) 4993–4996, https://doi.org/10.1002/ANIE.201200993.
[53] M. Merlini, G. Artioli, T. Cerulli, F. Cella, A. Bravo, Tricalcium aluminate hydration in additivated systems. A crystallographic study by SR-XRPD, Cem. Concr. Res. 38 (2008) 477–486, https://doi.org/10.1016/J.CEMCONRES.2007.11.011.
[54] A. Cuesta, G. Alvarez-Pinazo, S.G. Sanfélix, I. Peral, M.A.G. Aranda, A.G. De la Torre, Hydration mechanisms of two polymorphs of synthetic ye'elimite, Cem. Concr. Res. 63 (2014) 127–136, https://doi.org/10.1016/j.cemconres.2014.05.010.
[55] A. Cuesta, J.D. Zea-Garcia, D. Londono-Zuluaga, A.G. De la Torre, I. Santacruz, O. Vallcorba, M. Dapiaggi, S.G. Sanfélix, M.A.G. Aranda, Multiscale understanding of tricalcium silicate hydration reactions, Sci. Rep. 8 (2018) 8544, https://doi.org/10.1038/s41598-018-26943-y.
[56] J.E. Vigor, S.A. Bernal, X. Xiao, J.L. Provis, Time-resolved 3D characterisation of early-age microstructural development of Portland cement, J. Mater. Sci. 57 (2022) 4952–4969, https://doi.org/10.1007/s10853-022-06952-z.
[57] S. Kawaguchi, M. Takemoto, K. Osaka, E. Nishibori, C. Moriyoshi, Y. Kubota, Y. Kuroiwa, K. Sugimoto, High-throughput powder diffraction measurement system consisting of multiple MYTHEN detectors at beamline BL02B2 of SPring-8, Rev. Sci. Instrum. 88 (2017) 85111, https://doi.org/10.1063/1.4999454/964798.
[58] M. Andrä, A. Bergamaschi, F. Baruffaldi, M. Brückner, M. Carulla, N. Casati, A. Cervellino, R. Dinapoli, E. Fröjdh, D. Greiffenberg, S. Hasanaj, J. Heymes, V. Hinger, P. Kozlowski, C. Lopez Cuenca, D. Meister, D. Mezza, K. Moustakas, A. Mozzanica, K. Paton, C. Ruder, V. Scagnoli, G. Smolentsev, B. Schmitt, D. Thattil, X. Xie, J. Zhang, MYTHEN III: advancements in single photon counting detectors for synchrotron powder diffraction experiments, J. Synchrotron Radiat. 32 (2025) 365–377, https://doi.org/10.1107/S1600577525000438.
[59] E. Fröjdh, A. Bergamaschi, B. Schmitt, Single-photon counting detectors for diffraction-limited light sources, Front. Phys. 12 (2024) 1304896, https://doi.org/10.3389/FPHY.2024.1304896.
[60] A.P. Hammersley, S.O. Svensson, M. Hanfland, A.N. Fitch, D. Häusermann, Two-dimensional detector software: from real detector to idealised image or two-theta scan, High Press. Res. 14 (1996) 235–248, https://doi.org/10.1080/08957959608201408.
[61] D.E. Boyce, J.V. Bernier, heXRD: Modular, Open Source Software for the Analysis of High Energy X-Ray Diffraction Data, 2013, https://doi.org/10.2172/1062217.
[62] M. Basham, J. Filik, M.T. Wharmby, P.C.Y. Chang, B. El Kassaby, M. Gerring, J. Aishima, K. Levik, B.C.A. Pulford, I. Sikharulidze, D. Sneddon, M. Webber, S. S. Dhesi, F. Maccherozzi, O. Svensson, S. Brockhauser, G. Náray, A.W. Ashton, Data Analysis WorkbeNch (DAWN), J. Synchrotron Radiat. 22 (2015) 853–858, https://doi.org/10.1107/S1600577515002283.
[63] A. Morales-Cantero, A. Cuesta, I. Santacruz, M.A.G. Aranda, A.G. De la Torre, Phase-selective degree of hydration at setting: an in situ synchrotron diffraction study, Construct. Build Mater. 328 (2022) 127117, https://doi.org/10.1016/J.CONBUILDMAT.2022.127117.
[64] J.W. Bullard, H.M. Jennings, R.A. Livingston, A. Nonat, G.W. Scherer, J. S. Schweitzer, K.L. Scrivener, J.J. Thomas, Mechanisms of cement hydration, Cem. Concr. Res. 41 (2011) 1208–1223, https://doi.org/10.1016/j.cemconres.2010.09.011.
[65] E. Qoku, D. Reuschle, T. Fitzgibbons, A.P. Wilkinson, K.E. Kurtis, HEMC modifications to tricalcium silicate hydration: changes in kinetics and nanostructure examined by time-resolved high energy X-ray scattering, Cem. Concr. Res. 195 (2025) 107915, https://doi.org/10.1016/J.CEMCONRES.2025.107915.
[66] J.S. Andrade Neto, I.C. Carvalho, P.J.M. Monteiro, P.R. de Matos, A.P. Kirchheim, Unveiling the key factors for clinker reactivity and cement performance: a physic-chemical and performance investigation of 40 industrial clinkers, Cem. Concr. Res. 187 (2025) 107717, https://doi.org/10.1016/J.CEMCONRES.2024.107717.
[67] J.S. Andrade Neto, I.C. Carvalho, H.A. Santana, P. Matos, A.P. Kirchheim, The role of clinker mineralogy in cement properties: an analysis using statistical mixture design, Cem. Concr. Res. 201 (2026) 108102, https://doi.org/10.1016/J.CEMCONRES.2025.108102.
[68] J.E. Vigor, Photons and Subatomic Particles. What Can These Tell Us About Cements, Moisture, and Nuclear Waste? University of Sheffield, 2019 (Diessertation Thesis).
[69] G. Alvarez-Pinazo, A. Cuesta, M. García-Maté, I. Santacruz, E.R. Losilla, S. G. Sanfélix, F. Fauth, M.A.G. Aranda, A.G. De La Torre, In-situ early-age hydration study of sulfobelite cements by synchrotron powder diffraction, Cem. Concr. Res. 56 (2014) 12–19, https://doi.org/10.1016/j.cemconres.2013.10.009.
[70] R. Pérez-Bravo, A. Morales-Cantero, A. Cuesta, M.A.G. Aranda, I. Santacruz, A. G. De la Torre, Early hydration of belite-ye'elimite-ferrite cements: role of admixtures, Construct. Build Mater. 371 (2023) 130765, https://doi.org/10.1016/j.conbuildmat.2023.130765.
[71] J.D. Zea-Garcia, S.G. Sanfelix, O. Vallcorba, M.A.G. Aranda, I. Santacruz, A.G. De la Torre, Hydration activation of alite-belite-ye'elimite cements by doping with boron, ACS Sustain. Chem. Eng. 8 (2020) 3583–3590, https://doi.org/10.1021/acssuschemeng.9b05975.
[72] A.G. De la Torre, S. Bruque, M.A.G. Aranda, Rietveld quantitative amorphous content analysis, J. Appl. Cryst. 34 (2001) 196–202, https://doi.org/10.1107/S0021889801002485.
[73] A. Morales-Cantero, A. Cuesta, A.G. De la Torre, I. Santacruz, O. Mazanec, P. Borralleras, K.S. Weldert, D. Gastaldi, F. Canonico, M.A.G. Aranda, C-S-H seeding activation of Portland and Belite cements: an enlightening in situ synchrotron powder diffraction study, Cem. Concr. Res. 161 (2022) 106946, https://doi.org/10.1016/j.cemconres.2022.106946.
[74] A. Morales-Cantero, A. Cuesta, A.G. De la Torre, O. Mazanec, P. Borralleras, K. S. Weldert, D. Gastaldi, F. Canonico, M.A.G. Aranda, Portland and belite cement hydration acceleration by C-S-H seeds with variable w/c ratios, Materials (Basel) 15 (2022) 3553, https://doi.org/10.3390/MA15103553.
[75] A. Morales-Cantero, A.G. De la Torre, A. Cuesta, I. Santacruz, O. Mazanec, A. Dalla-Libera, P. Borralleras, M.A.G. Aranda, In situ synchrotron powder diffraction study of LC3 cement activation at very early ages by C-S-H nucleation seeding, Cem. Concr. Res. 178 (2024) 107463, https://doi.org/10.1016/j.cemconres.2024.107463.
[76] E. Fraga, J.D. Zea-Garcia, A. Yáñez, A.G. De la Torre, A. Cuesta, R. Valcárcel-Fernández, F. Farré-París, M. Malfois, M.A.G. Aranda, High-pressure and -temperature spinning capillary cell for in situ synchrotron X-ray powder diffraction, J. Synchrotron Radiat. 26 (2019) 1238–1244, https://doi.org/10.1107/S1600577519005150.
[77] K. Kupwade-Patil, P.J. Boul, D.K. Rasner, S.H. Lapidus, J.B. Leao, K.D. Johnson, C.J. Thaemlitz, O. Büyüköztürk, In situ investigation of phosphonate retarder interaction in oil well cements at elevated temperature and pressure conditions, J. Am. Ceram. Soc. 103 (2020) 6400–6413, https://doi.org/10.1111/JACE.17373.
[78] E. Fraga, A. Cuesta, J.D. Zea-Garcia, A.G. De la Torre, A. Yáñez-Casal, M.A. G. Aranda, Rietveld quantitative phase analysis of oil well cement: in situ hydration study at 150 bars and 150 °C, Materials (Basel) 12 (2019) 1897, https://doi.org/10.3390/ma12121897.
[79] A. Morales-Cantero, A.G. De la Torre, A. Cuesta, E. Fraga-Lopez, S. Shirani, M.A. G. Aranda, Belite hydration at high temperature and pressure by in situ synchrotron powder diffraction, Construct. Build Mater. 262 (2020) 120825, https://doi.org/10.1016/j.conbuildmat.2020.120825.
[80] Z. Yang, W. Ren, R. Sharma, S. McDonald, M. Mostafavi, Y. Vertyagina, T. J. Marrow, In-situ X-ray computed tomography characterisation of 3D fracture evolution and image-based numerical homogenisation of concrete, Cem. Concr. Compos. 75 (2017) 74–83, https://doi.org/10.1016/j.cemconcomp.2016.10.001.
[81] S. Jiang, L. Shen, F. Guillard, I. Einav, Characterisation of fracture evolution of a single cemented brittle grain using in-situ X-ray computed tomography, Int. J. Rock Mech. Min. Sci. 145 (2021) 104835, https://doi.org/10.1016/J.IJRMMS.2021.104835.
[82] Z.J. Yang, A. Qsymah, Y.Z. Peng, L. Margetts, R. Sharma, 4D characterisation of damage and fracture mechanisms of ultra high performance fibre reinforced concrete by in-situ micro X-ray computed tomography tests, Cem. Concr. Compos. 106 (2020) 103473, https://doi.org/10.1016/J.CEMCONCOMP.2019.103473.
[83] Y. Kawabata, D. Takano, K. Takahashi, M. Iwanami, In situ observation for the influence of hydraulic pressure on internal damage of cement-based materials, Mater. Des. 216 (2022) 110556, https://doi.org/10.1016/J.MATDES.2022.110556.
[84] Z.J. Yang, B.B. Li, J.Y. Wu, X-ray computed tomography images based phase-field modeling of mesoscopic failure in concrete, Eng. Fract. Mech. 208 (2019) 151–170, https://doi.org/10.1016/J.ENGFRACMECH.2019.01.005.
[85] J.E. Vigor, S.A. Bernal, X. Xiao, J.L. Provis, Automated correction for the movement of suspended particulate in microtomographic data, Chem. Eng. Sci. 223 (2020) 115736, https://doi.org/10.1016/j.ces.2020.115736.
[86] M. Parisatto, M.C. Dalconi, L. Valentini, G. Artioli, A. Rack, R. Tucoulou, G. Cruciani, G. Ferrari, Examining microstructural evolution of Portland cements by in-situ synchrotron micro-tomography, J. Mater. Sci. 50 (2015) 1805–1817, https://doi.org/10.1007/s10853-014-8743-9.

[87] M. Moradian, Q. Hu, M. Aboustait, B. Robertson, M.T. Ley, J.C. Hanan, X. Xiao, Direct in-situ observation of early age void evolution in sustainable cement paste containing fly ash or limestone, Compos. Part B Eng. 175 (2019) 107099, https://doi.org/10.1016/J.COMPOSITESB.2019.107099.
[88] M. Moradian, Q. Hu, M. Aboustait, M.T. Ley, J.C. Hanan, X. Xiao, G.W. Scherer, Z. Zhang, Direct observation of void evolution during cement hydration, Mater. Des. 136 (2017) 137–149, https://doi.org/10.1016/j.matdes.2017.09.056.
[89] K. Liu, X. Cheng, Y. Ma, X. Gao, Y. Yu, C. Zhang, X. Guo, J. Zhuang, Visualization and quantification of pore structure of oil-well cement slurry in liquid-solid transition stage using high-resolution computed tomography, Cem. Concr. Compos. 111 (2020) 103633, https://doi.org/10.1016/j.cemconcomp.2020.103633.
[90] M. Poirier, S. Blotevogel, C. Noiriel, A. Bonnin, J. Kaknics, M. Olbinado, L. Steger, C. Patapy, M. Cyr, Synchrotron X-ray micro-tomography investigation of the early hydration of blended cements: a case study on CaCl2-accelerated slag-based blended cements, Construct. Build Mater. 321 (2022) 126412, https://doi.org/10.1016/J.CONBUILDMAT.2022.126412.
[91] M. La Bella, R. Besselink, J.P. Wright, A.E.S. Van Driessche, A. Fernandez-Martinez, C. Giacobbe, Hierarchical synchrotron diffraction and imaging study of the calcium sulfate hemihydrate–gypsum transformation, J. Appl. Cryst. 56 (2023) 660–672, https://doi.org/10.1107/S1600576723002881.
[92] A.S. Madathiparambil, F. Mirzaei, K.R. Tekseth, B. Cordonnier, N. Agofack, P. Cerasi, F. Renard, B. Chattopadhyay, D.W. Breiby, Mechanical response of cement and shale admixtures under cyclic triaxial loading monitored by in-situ synchrotron micro-computed tomography, Cem. Concr. Res. 186 (2024) 107682, https://doi.org/10.1016/J.CEMCONRES.2024.107682.
[93] K. Xu, Q. Jin, J. Li, D.M. Ushizima, V.C. Li, K.E. Kurtis, P.J.M. Monteiro, In-situ microtomography image segmentation for characterizing strain-hardening cementitious composites under tension using machine learning, Cem. Concr. Res. 169 (2023) 107164, https://doi.org/10.1016/J.CEMCONRES.2023.107164.
[94] A. Cuesta, A.G. De la Torre, I. Santacruz, P. Trtik, J.C. Da Silva, A. Diaz, M. Holler, M.A.G. Aranda, Chemistry and mass density of aluminum hydroxide gel in eco-cements by ptychographic X-ray computed tomography, J. Phys. Chem. C 121 (2017) 3044–3054, https://doi.org/10.1021/acs.jpcc.6b10048.
[95] A. Cuesta, A.G. De la Torre, I. Santacruz, A. Diaz, P. Trtik, M. Holler, B. Lothenbach, M.A.G. Aranda, Quantitative disentanglement of nanocrystalline phases in cement pastes by synchrotron ptychographic X-ray tomography, IUCrJ 6 (2019) 473–491, https://doi.org/10.1107/S2052252519003774.
[96] S. Shirani, A. Cuesta, A.G. De la Torre, A. Diaz, P. Trtik, M. Holler, M.A.G. Aranda, Calcium aluminate cement conversion analysed by ptychographic nanotomography, Cem. Concr. Res. 137 (2020) 106201, https://doi.org/10.1016/j.cemconres.2020.106201.
[97] S. Shirani, A. Cuesta, A. Morales-Cantero, I. Santacruz, A. Diaz, P. Trtik, M. Holler, A. Rack, B. Lukic, E. Brun, I.R. Salcedo, M.A.G. Aranda, 4D nanoimaging of early age cement hydration, Nat. Commun. 14 (2023) 2652, https://doi.org/10.1038/s41467-023-38380-1.
[98] Q. Zheng, C. Liang, J. Jiang, H. Mao, K.C. Bustillo, C. Song, J.A. Reimer, P.J. M. Monteiro, H. Zheng, S. Li, Atomic-scale identification of defects in alite, Cem. Concr. Res. 176 (2024) 107391, https://doi.org/10.1016/J.CEMCONRES.2023.107391.
[99] E. Gartner, D. Myers, Influence of tertiary alkanolamines on Portland cement hydration, J. Am. Ceram. Soc. 76 (1993) 1521–1530, https://doi.org/10.1111/j.1151-2916.1993.tb03934.x.
[100] A. Kastengren, C.F. Powell, Synchrotron x-ray techniques for fluid dynamics, Exp. Fluids 55 (2014) 1–15, https://doi.org/10.1007/S00348-014-1686-8.
[101] M. Gholami, A. Rashedi, N. Lenoir, D. Hautemayou, G. Ovarlez, S. Hormozi, Time-resolved 2D concentration maps in flowing suspensions using X-ray, J. Rheol. (N. Y. N. Y) 62 (2018) 955–974, https://doi.org/10.1122/1.4994063.
[102] R.A. Sanderson, Optimising Blends of Blast Furnace Slag for the Immobilisation of Nuclear Waste, University of Sheffield, 2019. https://etheses.whiterose.ac.uk/id/eprint/23519/ (accessed May 16, 2025).
[103] G.G. Howarth, W. Heafield, A. Elsden, Intermediate-level waste encapsulation, in: Waste Manag, 1986, pp. 497–500, in: https://archivedproceedings.econference.io/wmsym/1986/V3/91.pdf.
[104] M. Angus, I. Godfrey, M. Hayes, S. Foster, Managing change in the supply of cement powders for radioactive waste encapsulation – twenty years of operational experience, in: Waste Manag, 2010, in: https://archivedproceedings.econference.io/wmsym/2010/pdfs/10122.pdf.
[105] F. García-Moreno, P. Hans Kamm, T. Robert Neu, F. Bülk, M. Andreas Noack, M. Wegener, N. von der Eltz, C. Matthias Schlepütz, M. Stampanoni, J.F. Banhart García-Moreno, P.H. Kamm, T.R. Neu, J. Banhart, F. García-Moreno, F. Bülk, M.A. Noack, M. Wegener, N. von der Eltz, C.M. Schlepütz, M. Stampanoni, Tomoscopy: time-resolved tomography for dynamic processes in materials, Adv. Mater. 33 (2021) 2104659, https://doi.org/10.1002/ADMA.202104659.
[106] J. Link, B. Strybny, T. Divoux, T. Sowoidnich, M. Coenen, S. Gstöhl, C. M. Schlepütz, M. Zuber, S. Hellmann, C. Rößler, J. Lützenkirchen, F. Heberling, S. Manneville, T. Schäfer, H.-M. Ludwig, M. Haist, Mechanisms of thixotropy in cement suspensions considering influences from shear history and hydration, Ce/Papers 6 (2023) 698–704, https://doi.org/10.1002/CEPA.2810.
[107] C.A. Murray, J. Potter, S.J. Day, A.R. Baker, S.P. Thompson, J. Kelly, C.G. Morris, S. Yang, C.C. Tang, New synchrotron powder diffraction facility for long-duration experiments, J. Appl. Cryst. 50 (2017) 172–183, https://doi.org/10.1107/S1600576716019750.
[108] R.G.W. Vasconcelos, B. Walkley, S. Day, C.C. Tang, H. Paraskevoulakos, L. J. Gardner, C.L. Corkhill, 18-month hydration of a low-pH cement for geological disposal of radioactive waste: the Cebama reference cement, Appl. Geochemistry 116 (2020) 104536, https://doi.org/10.1016/J.APGEOCHEM.2020.104536.
[109] L.J. Gardner, C.L. Corkhill, S.A. Walling, J.E. Vigor, C.A. Murray, C.C. Tang, J. L. Provis, N.C. Hyatt, Early age hydration and application of blended magnesium potassium phosphate cements for reduced corrosion of reactive metals, Cem. Concr. Res. 143 (2021) 106375, https://doi.org/10.1016/J.CEMCONRES.2021.106375.
[110] A. Mezhov, D. Kulisch, A. Goncharov, S. Zhutovsky, A comparative study of factors influencing hydration stoppage of hardened cement paste, Sustainability 15 (2023) 1080, https://doi.org/10.3390/su15021080.
[111] J. Stroh, B. Meng, F. Emmerling, Monitoring of sulphate attack on hardened cement paste studied by synchrotron XRD, Solid State Sci. 48 (2015) 278–285, https://doi.org/10.1016/J.SOLIDSTATESCIENCES.2015.08.006.
[112] S. Bae, R. Taylor, D. Kilcoyne, J. Moon, P.J.M. Monteiro, Effects of incorporating high-volume fly ash into tricalcium silicate on the degree of silicate polymerization and aluminum substitution for silicon in calcium silicate hydrate, Materials (Basel) 10 (2017) 131, https://doi.org/10.3390/MA10020131.
[113] M. Polisi, M.G. Vezzalini, E. Bonaccorsi, C. Biagioni, R. Arletti, High pressure behaviour of tobermorite supergroup minerals: an in situ synchrotron X-ray powder diffraction study, Cem. Concr. Res. 138 (2020) 106249, https://doi.org/10.1016/J.CEMCONRES.2020.106249.
[114] J. Li, W. Zhang, K. Garbev, G. Beuchle, P.J.M. Monteiro, Influences of cross-linking and Al incorporation on the intrinsic mechanical properties of tobermorite, Cem. Concr. Res. 136 (2020) 106170, https://doi.org/10.1016/J.CEMCONRES.2020.106170.
[115] J.J. Biernacki, C.J. Parnham, T.R. Watkins, C.R. Hubbard, J. Bai, Phase-resolved strain measurements in hydrated ordinary Portland cement using synchrotron X-rays, J. Am. Ceram. Soc. 89 (2006) 2853–2859, https://doi.org/10.1111/j.1551-2916.2006.01118.x.
[116] J.H. Moon, J.E. Oh, M. Balonis, F.P. Glasser, S.M. Clark, P.J.M. Monteiro, Pressure induced reactions amongst calcium aluminate hydrate phases, Cem. Concr. Res. 41 (2011) 571–578, https://doi.org/10.1016/J.CEMCONRES.2011.02.004.
[117] S.M. Clark, B. Colas, M. Kunz, S. Speziale, P.J.M. Monteiro, Effect of pressure on the crystal structure of ettringite, Cem. Concr. Res. 38 (2008) 19–26, https://doi.org/10.1016/J.CEMCONRES.2007.08.029.
[118] D. Comboni, G.D. Gatta, P. Lotti, M. Merlini, M. Hanfland, Anisotropic compressional behavior of ettringite, Cem. Concr. Res. 120 (2019) 46–51, https://doi.org/10.1016/J.CEMCONRES.2019.03.012.
[119] A. Cuesta, P. Rejmak, A. Ayuela, A.G. De la Torre, I. Santacruz, L. Fernandez Carrasco, C. Popescu, M.A.G. Aranda, Experimental and theoretical high pressure study of calcium hydroxyaluminate phases, Cem. Concr. Res. 97 (2017) 1–10, https://doi.org/10.1016/J.CEMCONRES.2017.03.011.
[120] G. Geng, J. Li, Y. Zhou, L. Liu, J. Yan, M. Kunz, P.J.M. Monteiro, A high-pressure X-ray diffraction study of the crystalline phases in calcium aluminate cement paste, Cem. Concr. Res. 108 (2018) 38–45, https://doi.org/10.1016/J.CEMCONRES.2018.03.004.
[121] R. Yang, J. Li, Probing the intrinsic mechanical properties of artinite using high-pressure X-ray diffraction for reactive MgO cement, Cem. Concr. Res. 194 (2025) 107894, https://doi.org/10.1016/J.CEMCONRES.2025.107894.
[122] J. Li, W. Zhang, P.J.M. Monteiro, Mechanical properties of struvite-K: a high-pressure X-ray diffraction study, Cem. Concr. Res. 136 (2020) 106171, https://doi.org/10.1016/J.CEMCONRES.2020.106171.
[123] W.V. Fernandes, S.M. Torres, C.A. Kirk, A.F. Leal, M.R. Lima Filho, D. Diniz, Incorporation of minor constituents into Portland cement tricalcium silicate: bond valence assessment of the alite M1 polymorph crystal structure using synchrotron XRPD data, Cem. Concr. Res. 136 (2020) 106125, https://doi.org/10.1016/J.CEMCONRES.2020.106125.
[124] A. Cuesta, A.G. De la Torre, M.A.G. Aranda, X-ray total scattering study of phases formed from cement phases carbonation, Minerals 11 (2021) 519, https://doi.org/10.3390/MIN11050519.
[125] S. Bae, C. Meral, J.E. Oh, J. Moon, M. Kunz, P.J.M. Monteiro, Characterization of morphology and hydration products of high-volume fly ash paste by monochromatic scanning x-ray micro-diffraction (μ-SXRD), Cem. Concr. Res. 59 (2014) 155–164, https://doi.org/10.1016/J.CEMCONRES.2014.03.001.
[126] A. Mancini, B. Lothenbach, G. Geng, D. Grolimund, D.F. Sanchez, S.C. Fakra, R. Dähn, B. Wehrli, E. Wieland, Iron speciation in blast furnace slag cements, Cem. Concr. Res. 140 (2021) 106287, https://doi.org/10.1016/J.CEMCONRES.2020.106287.
[127] R. Dähn, D. Popov, P. Schaub, P. Pattison, D. Grolimund, U. Mäder, A. Jenni, E. Wieland, X-ray micro-diffraction studies of heterogeneous interfaces between cementitious materials and geological formations, Phys. Chem. Earth, Parts A/B/C 70–71 (2014) 96–103, https://doi.org/10.1016/J.PCE.2013.10.010.
[128] S. Grousset, F. Kergourlay, D. Neff, E. Foy, J.L. Gallias, S. Reguer, P. Dillmann, A. Noumowé, In situ monitoring of corrosion processes by coupled micro-XRF/micro-XRD mapping to understand the degradation mechanisms of reinforcing bars in hydraulic binders from historic monuments, J. Anal. At. Spectrom 30 (2015) 721–729, https://doi.org/10.1039/C4JA00370E.
[129] M. Serdar, C. Meral, M. Kunz, D. Bjegovic, H.R. Wenk, P.J.M. Monteiro, Spatial distribution of crystalline corrosion products formed during corrosion of stainless steel in concrete, Cem. Concr. Res. 71 (2015) 93–105, https://doi.org/10.1016/J.CEMCONRES.2015.02.004.
[130] H.R. Wenk, P.J.M. Monteiro, M. Kunz, K. Chen, N. Tamura, L. Lutterotti, J. Del Arroz, Preferred orientation of ettringite in concrete fractures, J. Appl. Cryst. 42 (2009) 429–432, https://doi.org/10.1107/S0021889809015349.
[131] R. Dähn, A. Arakcheeva, P. Schaub, P. Pattison, G. Chapuis, D. Grolimund, E. Wieland, A. Leemann, Application of micro X-ray diffraction to investigate the

reaction products formed by the alkali–silica reaction in concrete structures, Cem. Concr. Res. 79 (2016) 49–56, https://doi.org/10.1016/J.CEMCONRES.2015.07.012.
[132] G. Geng, S. Barbotin, M. Shakoorioskooie, Z. Shi, A. Leemann, D.F. Sanchez, D. Grolimund, E. Wieland, R. Dähn, An in-situ 3D micro-XRD investigation of water uptake by alkali-silica-reaction (ASR) product, Cem. Concr. Res. 141 (2021) 106331, https://doi.org/10.1016/J.CEMCONRES.2020.106331.
[133] M.D. Jackson, E.N. Landis, P.F. Brune, M. Vitti, H. Chen, Q. Li, M. Kunz, H. R. Wenk, P.J.M. Monteiro, A.R. Ingraffea, Mechanical resilience and cementitious processes in Imperial Roman architectural mortar, Proc. Natl. Acad. Sci. U. S. A. 111 (2014) 18484–18489, https://doi.org/10.1073/PNAS.1417456111.
[134] M.D. Jackson, H. Chen, J.G. Peterson, C. Meral Akgul, B. Richards, Synchrotron X-ray microdiffraction studies of the mortars of ancient Roman concretes, in: Synchrotron Radiation, Cult. Heritage, Biominer, John Wiley & Sons, Ltd, 2024, pp. 203–231, https://doi.org/10.1002/9781394332458.CH7.
[135] J. Li, G. Geng, R. Myers, Y.S. Yu, D. Shapiro, C. Carraro, R. Maboudian, P.J. M. Monteiro, The chemistry and structure of calcium (alumino) silicate hydrate: a study by XANES, ptychographic imaging, and wide- and small-angle scattering, Cem. Concr. Res. 115 (2019) 367–378, https://doi.org/10.1016/J.CEMCONRES.2018.09.008.
[136] S.J.L. Billinge, M.G. Kanatzidis, Beyond crystallography: the study of disorder, nanocrystallinity and crystallographically challenged materials with pair distribution functions, Chem. Commun. (2004) 749, https://doi.org/10.1039/b309577k.
[137] C. Meral, C.J. Benmore, P.J.M. Monteiro, The study of disorder and nanocrystallinity in C–S–H, supplementary cementitious materials and geopolymers using pair distribution function analysis, Cem. Concr. Res. 41 (2011) 696–710, https://doi.org/10.1016/J.CEMCONRES.2011.03.027.
[138] T. Egami, S.J.L. Billinge, Underneath the Bragg Peaks: Structural Analysis of Complex Materials, 2nd ed., Elsevier Science, Pergamon, 2012.
[139] L.B. Skinner, S.R. Chae, C.J. Benmore, H.R. Wenk, P.J.M. Monteiro, Nanostructure of calcium silicate hydrates in cements, Phys. Rev. Lett. 104 (2010) 195502, https://doi.org/10.1103/PhysRevLett.104.195502.
[140] S. Grangeon, A. Fernandez-Martinez, A. Baronnet, N. Marty, A. Poulain, E. Elkaïm, C. Roosz, S. Gaboreau, P. Henocq, F. Claret, Quantitative X-ray pair distribution function analysis of nanocrystalline calcium silicate hydrates: a contribution to the understanding of cement chemistry, J. Appl. Cryst. 50 (2017) 14–21, https://doi.org/10.1107/S1600576716017404.
[141] J.L. Bell, P. Sarin, P.E. Driemeyer, R.P. Haggerty, P.J. Chupas, W.M. Kriven, X-ray pair distribution function analysis of a metakaolin-based, KAlSi2O6·5.5H2O inorganic polymer (geopolymer), J. Mater. Chem. 18 (2008) 5974–5981, https://doi.org/10.1039/B808157C.
[142] J.L. Bell, P. Sarin, J.L. Provis, R.P. Haggerty, P.E. Driemeyer, P.J. Chupas, J.S. J. Van Deventer, W.M. Kriven, Atomic structure of a cesium aluminosilicate geopolymer: a pair distribution function study, Chem. Mater. 20 (2008) 4768–4776, https://doi.org/10.1021/CM703369S.
[143] C.E. White, J.L. Provis, T. Proffen, D.P. Riley, J.S.J. Van Deventer, Density functional modeling of the local structure of kaolinite subjected to thermal dehydroxylation, J. Phys. Chem. A 114 (2010) 4988–4996, https://doi.org/10.1021/jp911108d.
[144] C.E. White, J.L. Provis, T. Proffen, D.P. Riley, J.S.J. Van Deventer, Combining density functional theory (DFT) and pair distribution function (PDF) analysis to solve the structure of metastable materials: the case of metakaolin, Phys. Chem. Chem. Phys. 12 (2010) 3239–3245, https://doi.org/10.1039/b922993k.
[145] A. Cuesta, R. Ichikawa, D. Londono-Zuluaga, A.G. De la Torre, I. Santacruz, X. Turrillas, M.A.G. Aranda, Aluminum hydroxide gel characterization within a calcium aluminate cement paste by combined Pair Distribution Function and Rietveld analyses, Cem. Concr. Res. 96 (2017) 1–12, https://doi.org/10.1016/j.cemconres.2017.02.025.
[146] A.E. Morandeau, C.E. White, In situ X-ray pair distribution function analysis of accelerated carbonation of a synthetic calcium–silicate–hydrate gel, J. Mater. Chem. A 3 (2015) 8597–8605, https://doi.org/10.1039/C5TA00348B.
[147] S. Bae, H. Jee, H. Suh, M. Kanematsu, A. Shiro, A. Machida, T. Watanuki, T. Shobu, S. Morooka, G. Geng, H. Suzuki, Analysis of atomistic structural deformation characteristics of calcium silicate hydrate in 53-year-old tricalcium silicate paste using atomic pair distribution function, Construct. Build Mater. 237 (2020) 117714, https://doi.org/10.1016/j.conbuildmat.2019.117714.
[148] J.A. Reffner, P.A. Martoglio, G.P. Williams, Fourier transform infrared microscopical analysis with synchrotron radiation: the microscope optics and system performance (invited), Rev. Sci. Instrum. 66 (1995) 1298–1302, https://doi.org/10.1063/1.1145958.
[149] D.L. Wetzel, S.M. LeVine, Imaging molecular chemistry with infrared microscopy, Science 285 (1999) 1224–1225, https://doi.org/10.1126/SCIENCE.285.5431.1224.
[150] A. Hajimohammadi, J.L. Provis, J.S.J. Van Deventer, Effect of alumina release rate on the mechanism of geopolymer gel formation, Chem. Mater. 22 (2010) 5199–5208, https://doi.org/10.1021/CM101151N.
[151] A. Hajimohammadi, T. Ngo, J.L. Provis, T. Kim, J. Vongsvivut, High strength/density ratio in a syntactic foam made from one-part mix geopolymer and cenospheres, Compos. Part B Eng. 173 (2019) 106908, https://doi.org/10.1016/J.COMPOSITESB.2019.106908.
[152] D.A. Geddes, B. Walkley, T. Matsuda, J.L. Provis, Multi-year cementitious hydrate product formation in non-Portland high performance concretes, Cement 18 (2024) 100111, https://doi.org/10.1016/J.CEMENT.2024.100111.
[153] E. Tõldsepp, T. Avarmaa, V. Denks, E. Feldbach, M. Kirm, A. Maaroos, H. Mändar, S. Vielhauer, Synthesis and luminescence properties of Ce3+ doped nanoporous 12CaO·7Al2O3 powders and ceramics, Opt. Mater. 32 (2010) 784–788, https://doi.org/10.1016/J.OPTMAT.2009.11.014.
[154] E. Tõldsepp, E. Feldbach, M. Kirm, Synthesis, characterization and luminescence properties of Pr3+-doped C12A7 and C3A, J. Ceram. Sci. Technol. 4 (2013) 77–84, https://doi.org/10.4416/JCST2012-00039A.
[155] R.D. Deslattes, E.G. Kassler, P. Indelicato, L. De Billy, E. Lindroth, J. Anton, X-ray transition energies: new approach to a comprehensive evaluation, Rev. Mod. Phys. 75 (2003) 35, https://doi.org/10.1103/RevModPhys.75.35.
[156] J. Li, W. Zhang, K. Garbev, P.J.M. Monteiro, Coordination environment of Si in calcium silicate hydrates, silicate minerals, and blast furnace slags: a XANES database, Cem. Concr. Res. 143 (2021) 106376, https://doi.org/10.1016/J.CEMCONRES.2021.106376.
[157] Y. Yan, B. Ma, G.D. Miron, D.A. Kulik, K. Scrivener, B. Lothenbach, Al uptake in calcium silicate hydrate and the effect of alkali hydroxide, Cem. Concr. Res. 162 (2022) 106957, https://doi.org/10.1016/J.CEMCONRES.2022.106957.
[158] M. Vespa, R. Dähn, T. Huthwelker, E. Wieland, Soft X-ray absorption near-edge investigations of Mg-containing mineral phases relevant for cementitious materials, Phys. Chem. Earth, Parts A/B/C 99 (2017) 168–174, https://doi.org/10.1016/J.PCE.2017.03.006.
[159] K. Inoue, Y. Nishiki, K. Fukushi, R. Suma, T. Sato, H. Sakuma, K. Tamura, S. Yokoyama, M. Shimbashi, T. Mizukami, K. Unami, Y. Noji, T. Kitajima, S. Fukaya, Y. Takeichi, S. Yamashita, H. Suga, Y. Takahashi, Systematic comparison of Mg K-edge XANES spectra of magnesium-bearing clay minerals and magnesium silicate hydrates: a promising tool for identifying magnesium silicate hydrate in natural samples, Appl. Clay Sci. 245 (2023) 107152, https://doi.org/10.1016/J.CLAY.2023.107152.
[160] X. Ke, V.A. Baki, A.I. Large, G. Held, B. Walkley, J. Li, Atomic-scale characterisation of sodium aluminosilicate hydrates (N-A-S-H) and Mg-substituted N(-M)-A-S-H using XANES, Appl. Geochem. 147 (2022) 105515, https://doi.org/10.1016/J.APGEOCHEM.2022.105515.
[161] S.M. Clark, G.R. Morrison, W.D. Shi, The use of scanning transmission X-ray microscopy for the real-time study of cement hydration, Cem. Concr. Res. 29 (1999) 1099–1102, https://doi.org/10.1016/S0008-8846(99)00091-5.
[162] S.R. Chae, J. Moon, S. Yoon, S. Bae, P. Levitz, R. Winarski, P.J.M. Monteiro, Advanced nanoscale characterization of cement based materials using X-ray synchrotron radiation: a review, Int. J. Concr. Struct. Mater. 7 (2013) 95–110, https://doi.org/10.1007/S40069-013-0036-1.
[163] K.E. Kurtis, P.J.M. Monteiro, J.T. Brown, W. Meyer-Ilse, Imaging of ASR gel by soft X-ray microscopy, Cem. Concr. Res. 28 (1998) 411–421, https://doi.org/10.1016/S0008-8846(97)00274-3.
[164] G. Geng, J. Li, Y.-S. Yu, D.A. Shapiro, D.A.L. Kilcoyne, P.J.M. Monteiro, Nanometer-resolved spectroscopic study reveals the conversion mechanism of CaO·Al2O3·10H2O to 2CaO·Al2O3·8H2O and 3CaO·Al2O3·6H2O at an elevated temperature, Cryst. Growth Des. 17 (2017) 4246–4253, https://doi.org/10.1021/acs.cgd.7b00553.
[165] J. Li, K. Xu, G. Geng, H.E. Mason, Determine the coordination of Al and Si of Fe-rich fly ash: the challenge in NMR and how we probe its heterogeneity using X-ray spectromicroscopy, Cem. Concr. Res. 161 (2022) 106947, https://doi.org/10.1016/J.CEMCONRES.2022.106947.
[166] M. Thasfiquzzaman, H. Nguyen, T. Mansikkala, M. Huttula, I. Beinik, J. Schwenke, K. Thånell, A.P. Hitchcock, P. Kinnunen, M. Patanen, Characterization of hydrated magnesium carbonate materials with synchrotron radiation-based scanning transmission X-ray spectromicroscopy, Mater. Adv. 5 (2024) 5167–5178, https://doi.org/10.1039/D4MA00044G.
[167] E. Wieland, R. Dähn, M. Vespa, B. Lothenbach, Micro-spectroscopic investigation of Al and S speciation in hardened cement paste, Cem. Concr. Res. 40 (2010) 885–891, https://doi.org/10.1016/J.CEMCONRES.2010.02.001.
[168] G. Geng, Z. Shi, A. Leemann, C. Borca, T. Huthwelker, K. Glazyrin, I.V. Pekov, S. Churakov, B. Lothenbach, R. Dähn, E. Wieland, Atomistic structure of alkali-silica reaction products refined from X-ray diffraction and micro X-ray absorption data, Cem. Concr. Res. 129 (2020) 105958, https://doi.org/10.1016/J.CEMCONRES.2019.105958.
[169] T. Vehmas, V. Montoya, M.C. Alonso, R. Vašíček, E. Rastrick, S. Gaboreau, P. Večerník, M. Leivo, E. Holt, N. Fink, N. Ait Mouheb, J. Svoboda, D. Read, R. Červinka, R. Vasconcelos, C. Corkhill, Characterization of Cebama low-pH reference concrete and assessment of its alteration with representative waters in radioactive waste repositories, Appl. Geochemistry 121 (2020) 104703, https://doi.org/10.1016/J.APGEOCHEM.2020.104703.
[170] A.M. Scheidegger, M. Vespa, D. Grolimund, E. Wieland, M. Harfouche, I. Bonhoure, R. Dähn, The use of (micro)-X-ray absorption spectroscopy in cement research, Waste Manag. 26 (2006) 699–705, https://doi.org/10.1016/J.WASMAN.2006.01.032.
[171] J. Stietz, S. Amayri, V. Häußler, D. Prieur, T. Reich, Uptake of Pu(IV) by hardened cement paste in the presence of gluconate at high and low ionic strengths, Front. Nucl. Eng. 2 (2023) 1268767, https://doi.org/10.3389/FNUEN.2023.1268767.
[172] M. Vespa, R. Dähn, D. Grolimund, E. Wieland, A.M. Scheidegger, Spectroscopic investigation of Ni speciation in hardened cement paste, Environ. Sci. Technol. 40 (2006) 2275–2282, https://doi.org/10.1021/ES052240Q.
[173] A. Mancini, E. Wieland, G. Geng, B. Lothenbach, B. Wehrli, R. Dähn, Fe(II) interaction with cement phases: method development, wet chemical studies and X-ray absorption spectroscopy, J. Colloid Interface Sci. 588 (2021) 692–704, https://doi.org/10.1016/J.JCIS.2020.11.085.
[174] B. Ma, A. Fernandez-Martinez, B. Madé, N. Findling, E. Markelova, E. Salas-Colera, T.G.G. Maffeis, A.R. Lewis, D. Tisserand, S. Bureau, L. Charlet, XANES-based determination of redox potentials imposed by steel corrosion products in

cement-based media, Environ. Sci. Technol. 52 (2018) 11931–11940, https://doi.org/10.1021/ACS.EST.8B03236.
[175] X. Gaona, R. Dähn, J. Tits, A.C. Scheinost, E. Wieland, Uptake of Np(IV) by C-S-H phases and cement paste: an EXAFS study, Environ. Sci. Technol. 45 (2011) 8765–8771, https://doi.org/10.1021/ES2012897.
[176] J. Stietz, S. Amayri, V. Häußler, R. Scholze, T. Reich, The uptake of actinides by hardened cement paste in high-salinity pore water, Minerals 13 (2023) 1380, https://doi.org/10.3390/MIN13111380.
[177] P.G. Allen, J.J. Bucher, M.A. Denecke, N.M. Edelstein, N. Kaltsoyannis, H. Nitsche, T. Reich, D.K. Shuh, Application of synchrotron radiation techniques to chemical issues in the environmental sciences, in: Synchrotron Radiat. Tech. Ind. Chem. Mater. Sci, Springer, Boston, MA, 1996, pp. 169–185, https://doi.org/10.1007/978-1-4615-5837-8_12.
[178] P.G. Allen, G.S. Siemering, D.K. Shuh, J.J. Bucher, N.M. Edelstein, C.A. Langton, B. Clark, T. Reich, M.A. Denecke, Technetium speciation in cement waste forms determined by X-ray absorption fine structure spectroscopy, Radiochim. Acta 76 (1997) 77–86, https://doi.org/10.1524/RACT.1997.76.12.77.
[179] A.A. Almeida, C.C. Dos Santos, R.M.M. Santos, E. Elkaim, A. Beauvois, S. H. Pulcinelli, V. Briois, C.V. Santilli, Relevance of layered double hydroxides and their derived mixed oxides nanoparticles in the crystallization of cement hydration phases: a time-resolved study of the kinetic mechanism, Constr. Build. Mater. 506 (2026) 144886, https://doi.org/10.1016/J.CONBUILDMAT.2025.144886.
[180] M. Vespa, R. Dähn, D. Grolimund, E. Wieland, A.M. Scheidegger, Co speciation in hardened cement paste: a macro- and micro-spectroscopic investigation, Environ. Sci. Technol. 41 (2007) 1902–1908, https://doi.org/10.1021/ES0624568.
[181] P. Mandaliev, R. Dähn, B. Wehrli, E. Wieland, Macro- and microspectroscopic study of Nd (III) uptake mechanisms in hardened cement paste, Environ. Sci. Technol. 43 (2009) 8462–8468, https://doi.org/10.1021/ES902016Q.
[182] A. Peys, V. Isteri, J. Yliniemi, A.S. Yorkshire, P.N. Lemougna, C. Utton, J.L. Provis, R. Snellings, T. Hanein, Sustainable iron-rich cements: raw material sources and binder types, Cem. Concr. Res. 157 (2022) 106834, https://doi.org/10.1016/J.CEMCONRES.2022.106834.
[183] A. Baral, C. Pesce, A.S. Yorkshire, Z. Zhakiyeva, R. Snellings, T. Hanein, J. L. Provis, A. Peys, Research characterisation of iron-rich cementitious materials, Cem. Concr. Res. 177 (2024) 107419, https://doi.org/10.1016/j.cemconres.2023.107419.
[184] E. Wieland, G.D. Miron, B. Ma, G. Geng, B. Lothenbach, Speciation of iron(II/III) at the iron-cement interface: a review, Mater. Struct. 56 (2023) 1–24, https://doi.org/10.1617/S11527-023-02115-X.
[185] A. Mancini, E. Wieland, G. Geng, R. Dähn, J. Skibsted, B. Wehrli, B. Lothenbach, Fe(III) uptake by calcium silicate hydrates, Appl. Geochemistry 113 (2020) 104460, https://doi.org/10.1016/J.APGEOCHEM.2019.104460.
[186] M. Vespa, E. Wieland, R. Dähn, B. Lothenbach, Identification of the thermodynamically stable Fe-containing phase in aged cement pastes, J. Am. Ceram. Soc. 98 (2015) 2286–2294, https://doi.org/10.1111/jace.13542.
[187] J.L. Provis, V. Rose, S.A.B. And, J.S.J.V. Deventer, High-resolution nanoprobe X-ray fluorescence characterization of heterogeneous calcium and heavy metal distributions in alkali-activated fly ash, Langmuir 25 (2009) 11897–11904, https://doi.org/10.1021/la901560h.
[188] S.A. Bernal, V. Rose, J.L. Provis, The fate of iron in blast furnace slag particles during alkali-activation, Mater. Chem. Phys. 146 (2014) 1–5, https://doi.org/10.1016/J.MATCHEMPHYS.2014.03.017.
[189] Q. Hu, M. Aboustait, T. Kim, M.T. Ley, J.W. Bullard, G. Scherer, J.C. Hanan, V. Rose, R. Winarski, J. Gelb, Direct measurements of 3d structure, chemistry and mass density during the induction period of C3s hydration, Cem. Concr. Res. 89 (2016) 14–26, https://doi.org/10.1016/j.cemconres.2016.07.008.
[190] M. Moradian, Q. Hu, M. Aboustait, M.T. Ley, J.C. Hanan, X. Xiao, V. Rose, R. Winarski, G.W. Scherer, Multi-scale observations of structure and chemical composition changes of portland cement systems during hydration, Constr. Build. Mater. 212 (2019) 486–499, https://doi.org/10.1016/j.conbuildmat.2019.04.013.
[191] G.A. van Riessen, G.N. Hinsley, C.M. Kewish, A. van Riessen, Visualising geopolymerisation processes using scanning X-ray diffraction and fluorescence microscopy, Materials (Basel) 17 (2024) 5896, https://doi.org/10.3390/MA17235896.
[192] M.N. Muhamad, P. Barnes, C.H. Fentiman, D. Hausermann, H. Pollmann, S. Rashid, A time-resolved synchrotron energy dispersive diffraction study of the dynamic aspects of the synthesis of ettringite during minepacking, Cem. Concr. Res. 23 (1993) 267–272, https://doi.org/10.1016/0008-8846(93)90091-M.
[193] P. Barnes, S.M. Clark, D. Häusermann, C.H. Fentiman, M.N. Muhamad, E. Henderson, S. Rashid, Time-resolved studies of the early hydration of cements using synchrontron energy-dispersive diffraction, Phase Transit. 39 (1992) 117–128, https://doi.org/10.1080/01411599208203475.
[194] J.L. Provis, J.S.J. van Deventer, Geopolymerisation kinetics. 1. In situ energy-dispersive X-ray diffractometry, Chem. Eng. Sci. 62 (2007) 2309–2317, https://doi.org/10.1016/J.CES.2007.01.027.
[195] J.L. Provis, J.S.J. Van Deventer, Direct measurement of the kinetics of geopolymerisation by in-situ energy dispersive X-ray diffractometry, J. Mater. Sci. 42 (2007) 2974–2981, https://doi.org/10.1007/S10853-006-0548-Z.
[196] P. Barnes, S. Colston, B. Craster, C. Hall, A. Jupe, S. Jacques, J. Cockcroft, S. Morgan, M. Johnson, D. O'Connor, M. Bellotto, Time- and space-resolved dynamic studies on ceramic and cementitious materials, J. Synchrotron Radiat. 7 (2000) 167–177, https://doi.org/10.1107/S0909049500003137.
[197] N.N. Naik, A.C. Jupe, S.R. Stock, A.P. Wilkinson, P.L. Lee, K.E. Kurtis, Sulfate attack monitored by microCT and EDXRD: influence of cement type, water-to-cement ratio, and aggregate, Cem. Concr. Res. 36 (2006) 144–159, https://doi.org/10.1016/J.CEMCONRES.2005.06.004.
[198] W. Huda, R. Brad Abrahams, X-ray-based medical imaging and resolution, Am. J. Roentgenol. 204 (2015) W393–W397, https://doi.org/10.2214/AJR.14.13126.
[199] N.E. Omori, A.D. Bobitan, A. Vamvakeros, A.M. Beale, S.D.M. Jacques, Recent developments in X-ray diffraction/scattering computed tomography for materials science, Philos. Trans. R. Soc. A. 381 (2023) 2259, https://doi.org/10.1098/RSTA.2022.0350.
[200] P. Bleuet, E. Welcomme, E. Dooryhée, J. Susini, J.L. Hodeau, P. Walter, Probing the structure of heterogeneous diluted materials by diffraction tomography, Nat. Mater. 7 (2008) 468–472, https://doi.org/10.1038/nmat2168.
[201] C. Hall, P. Barnes, J.K. Cockcroft, S.L. Colston, D. Häusermann, S.D.M. Jacques, A. C. Jupe, M. Kunz, Synchrotron energy-dispersive X-ray diffraction tomography, Nucl. Instruments Methods Phys. Res. Sect. B Beam Interact. with Mater. Atoms 140 (1998) 253–257, https://doi.org/10.1016/S0168-583X(97)00994-4.
[202] L. Valentini, M.C. Dalconi, M. Parisatto, G. Cruciani, G. Artioli, IUCr, towards three-dimensional quantitative reconstruction of cement microstructure by X-ray diffraction microtomography, J. Appl. Cryst. 44 (2011) 272–280, https://doi.org/10.1107/S0021889810054701.
[203] M. Voltolini, M.C. Dalconi, G. Artioli, M. Parisatto, L. Valentini, V. Russo, A. Bonnin, R. Tucoulou, Understanding cement hydration at the microscale: new opportunities from 'pencil-beam' synchrotron X-ray diffraction tomography, J. Appl. Cryst. 46 (2013) 142–152, https://doi.org/10.1107/S0021889812046985.
[204] G. Artioli, T. Cerulli, G. Cruciani, M.C. Dalconi, G. Ferrari, M. Parisatto, A. Rack, R. Tucoulou, X-ray diffraction microtomography (XRD-CT), a novel tool for non-invasive mapping of phase development in cement materials, Anal. Bioanal. Chem. 397 (2010) 2131–2136, https://doi.org/10.1007/s00216-010-3649-0.
[205] G. Artioli, L. Valentini, M. Voltolini, M.C. Dalconi, G. Ferrari, V. Russo, Direct imaging of nucleation mechanisms by synchrotron diffraction micro-tomography: superplasticizer-induced change of C–S–H nucleation in cement, Cryst. Growth Des. 15 (2015) 20–23, https://doi.org/10.1021/cg501466z.
[206] F. Claret, S. Grangeon, A. Loschetter, C. Tournassat, W. De Nolf, N. Harker, F. Boulahya, S. Gaboreau, Y. Linard, X. Bourbon, A. Fernandez-Martinez, J. Wright, Deciphering mineralogical changes and carbonation development during hydration and ageing of a consolidated ternary blended cement paste, IUCrJ 5 (2018) 150–157, https://doi.org/10.1107/S205225251701836X.
[207] Z. Yue, Z. Su, P.P. Paul, A.T.M. Marsh, A. Macente, M. Di Michiel, J.L. Provis, P. J. Withers, S.A. Bernal, 3D crystalline phase and pore structure evolution upon CO2 exposure in sodium sulfate-activated cement pastes, Cem. Concr. Res. 187 (2025) 107716, https://doi.org/10.1016/J.CEMCONRES.2024.107716.
[208] Z. Su, Z. Yue, A.T.M. Marsh, M. Di Michiel, T.L. Burnett, J.L. Provis, P.P. Paul, S. A. Bernal, P.J. Withers, 4D quantification of C-(A)-S-H and Mg-Al LDH phase alterations and microstructural evolution during accelerated carbonation of alkali-activated slag pastes, Cem. Concr. Res. 198 (2025) 108009, https://doi.org/10.1016/J.CEMCONRES.2025.108009.
[209] C. Hall, S.L. Colston, A.C. Jupe, S.D.M. Jacques, R. Livingston, A.O.A. Ramadan, A.W. Amde, P. Barnes, Non-destructive tomographic energy-dispersive diffraction imaging of the interior of bulk concrete, Cem. Concr. Res. 30 (2000) 491–495, https://doi.org/10.1016/S0008-8846(00)00206-4.
[210] A. Gonzalez-Saborido, M. Tyrer, S.D.M. Jacques, M. Vickers, P. Barnes, Development of time-resolved 3D-diffraction-tomography to study ongoing carbonation in concrete, in: 12th Int. Congr. Chem. Cem. Proc., Montreal, Canada, 2007, pp. 159–165.
[211] S. Lu, E.N. Landis, D.T. Keane, X-ray microtomographic studies of pore structure and permeability in Portland cement concrete, Mater. Struct. Constr. 39 (2006) 611–620, https://doi.org/10.1617/S11527-006-9099-7.
[212] E. Gallucci, K.L. Scrivener, A. Groso, M. Stampanoni, G. Margaritondo, 3D experimental investigation of the microstructure of cement pastes using synchrotron X-ray microtomography (μCT), Cem. Concr. Res. 37 (2007) 360–368, https://doi.org/10.1016/j.cemconres.2006.10.012.
[213] M.B. Leite, P.J.M. Monteiro, Microstructural analysis of recycled concrete using X-ray microtomography, Cem. Concr. Res. 81 (2016) 38–48, https://doi.org/10.1016/J.CEMCONRES.2015.11.010.
[214] E.N. Landis, E.N. Nagy, D.T. Keane, G. Nagy, Technique to measure 3D work-of-fracture of concrete in compression, J. Eng. Mech. 125 (1999) 599–605, https://doi.org/10.1061/(ASCE)0733-9399(1999)125:6(599).
[215] K. Xu, A.S. Tremsin, J. Li, D.M. Ushizima, C.A. Davy, A. Bouterf, Y.T. Su, M. Marroccoli, A.M. Mauro, M. Osanna, A. Telesca, P.J.M. Monteiro, Microstructure and water absorption of ancient concrete from Pompeii: an integrated synchrotron microtomography and neutron radiography characterization, Cem. Concr. Res. 139 (2021) 106282, https://doi.org/10.1016/J.CEMCONRES.2020.106282.
[216] M.A. Homel, J. Iyer, S.J. Semnani, E.B. Herbold, Mesoscale model and X-ray computed micro-tomographic imaging of damage progression in ultra-high-performance concrete, Cem. Concr. Res. 157 (2022) 106799, https://doi.org/10.1016/J.CEMCONRES.2022.106799.
[217] T. Deboodt, D. Wildenschild, J.H. Ideker, O.B. Isgor, Comparison of thresholding techniques for quantifying Portland cement hydrates using synchrotron microtomography, Construct. Build Mater. 266 (2021) 121109, https://doi.org/10.1016/j.conbuildmat.2020.121109.
[218] T. Deboodt, D. Wildenschild, J.H. Ideker, O.B. Isgor, Use of iodine for improving phase quantification using x-ray tomography, Cem. Concr. Res. 116 (2019) 102–112, https://doi.org/10.1016/J.CEMCONRES.2018.11.004.

[219] M.A.B. Promentilla, T. Sugiyama, T. Hitomi, N. Takeda, Characterizing the 3D pore structure of hardened cement paste with synchrotron microtomography, J. Adv. Concrete Technol. 6 (2008) 273–286, https://doi.org/10.3151/jact.6.273.
[220] M.A.B. Promentilla, T. Sugiyama, T. Hitomi, N. Takeda, Quantification of tortuosity in hardened cement pastes using synchrotron-based X-ray computed microtomography, Cem. Concr. Res. 39 (2009) 548–557, https://doi.org/10.1016/j.cemconres.2009.03.005.
[221] T. Sugiyama, M.A.B. Promentilla, T. Hitomi, N. Takeda, Application of synchrotron microtomography for pore structure characterization of deteriorated cementitious materials due to leaching, Cem. Concr. Res. 40 (2010) 1265–1270, https://doi.org/10.1016/j.cemconres.2009.10.009.
[222] J.L. Provis, R.J. Myers, C.E. White, V. Rose, J.S.J. van Deventer, X-ray microtomography shows pore structure and tortuosity in alkali-activated binders, Cem. Concr. Res. 42 (2012) 855–864, https://doi.org/10.1016/J.CEMCONRES.2012.03.004.
[223] J.E. Vigor, D.P. Prentice, X. Xiao, S.A. Bernal, J.L. Provis, The pore structure and water absorption in Portland/slag blended hardened cement paste determined by synchrotron X-ray microtomography and neutron radiography, RSC Adv. 14 (2024) 4389–4405, https://doi.org/10.1039/D3RA06489A.
[224] N. Marinoni, M. Voltolini, M.A.T.M. Broekmans, L. Mancini, P.J.M. Monteiro, N. Rotiroti, E. Ferrari, A. Bernasconi, A combined synchrotron radiation micro computed tomography and micro X-ray diffraction study on deleterious alkali-silica reaction, J. Mater. Sci. 50 (2015) 7985–7997, https://doi.org/10.1007/S10853-015-9364-7.
[225] D. Hernández-Cruz, C.W. Hargis, J. Dominowski, M.J. Radler, P.J.M. Monteiro, Fiber reinforced mortar affected by alkali-silica reaction: a study by synchrotron microtomography, Cem. Concr. Compos. 68 (2016) 123–130, https://doi.org/10.1016/j.cemconcomp.2016.02.003.
[226] L.G. Butler, J.W. Owens, F.K. Cartledge, R.L. Kurtz, G.R. Byerly, A.J. Wales, P. L. Bryant, E.F. Emery, B. Dowd, X. Xie, Synchrotron X-ray microtomography, electron probe microanalysis, and NMR of toluene waste in cement, Environ. Sci. Technol. 34 (2000) 3269–3275, https://doi.org/10.1021/ES990450V.
[227] C.A. Stitt, M. Hart, N.J. Harker, K.R. Hallam, J. MacFarlane, A. Banos, C. Paraskevoulakos, E. Butcher, C. Padovani, T.B. Scott, Nuclear waste viewed in a new light; a synchrotron study of uranium encapsulated in grout, J. Hazard. Mater. 285 (2015) 221–227, https://doi.org/10.1016/J.JHAZMAT.2014.11.035.
[228] C. Paraskevoulakos, C.A. Stitt, K.R. Hallam, A. Banos, M. Leal Olloqui, C.P. Jones, G. Griffiths, A.M. Adamska, J. Jowsey, T.B. Scott, Monitoring the degradation of nuclear waste packages induced by interior metallic corrosion using synchrotron X-ray tomography, Constr. Build. Mater. 215 (2019) 90–103, https://doi.org/10.1016/J.CONBUILDMAT.2019.04.178.
[229] I.M.R. Bernal, S. Shirani, A. Cuesta, I. Santacruz, M.A.G. Aranda, Phase and microstructure evolutions in LC3 binders by multi-technique approach including synchrotron microtomography, Construct. Build Mater. 300 (2021) 124054, https://doi.org/10.1016/j.conbuildmat.2021.124054.
[230] S. Shirani, A. Cuesta, A. Morales-Cantero, A.G. De la Torre, M.P. Olbinado, M.A. G. Aranda, Influence of curing temperature on belite cement hydration: a comparative study with Portland cement, Cem. Concr. Res. 147 (2021) 106499, https://doi.org/10.1016/j.cemconres.2021.106499.
[231] M.C. Schlegel, U. Mueller, U. Panne, F. Emmerling, Deciphering the sulfate attack of cementitious materials by high-resolution micro-X-ray diffraction, Anal. Chem. 83 (2011) 3744–3749, https://doi.org/10.1021/ac200181g.
[232] J. Stroh, M.C. Schlegel, E.F. Irassar, B. Meng, F. Emmerling, Applying high resolution SyXRD analysis on sulfate attacked concrete field samples, Cem. Concr. Res. 66 (2014) 19–26, https://doi.org/10.1016/J.CEMCONRES.2014.07.015.
[233] J. Pouya, M. Neji, L. De Windt, F. Péralès, A. Socié, J. Corvisier, Investigating chemical and cracking processes in cement paste exposed to a low external sulfate attack with emphasis on the contribution of gypsum, Construct. Build Mater. 413 (2024) 134845, https://doi.org/10.1016/J.CONBUILDMAT.2023.134845.
[234] M.C. Schlegel, J. Stroh, K. Malaga, B. Meng, U. Panne, F. Emmerling, Pathway of a damaging mechanism – analyzing chloride attack by synchrotron based X-ray diffraction, Solid State Sci. 44 (2015) 45–54, https://doi.org/10.1016/J.SOLIDSTATESCIENCES.2015.03.021.
[235] J. Stroh, B. Meng, F. Emmerling, Deterioration of hardened cement paste under combined sulphate-chloride attack investigated by synchrotron XRD, Solid State Sci. 56 (2016) 29–44, https://doi.org/10.1016/J.SOLIDSTATESCIENCES.2016.04.002.
[236] M. Zajac, I. Maruyama, A. Iizuka, J. Skibsted, Enforced carbonation of cementitious materials, Cem. Concr. Res. 174 (2023) 107285, https://doi.org/10.1016/j.cemconres.2023.107285.
[237] X. Fu, A. Guerini, D. Zampini, A.F. Rotta Loria, Storing CO2 while strengthening concrete by carbonating its cement in suspension, Commun. Mater. 5 (1) (2024) 109, https://doi.org/10.1038/s43246-024-00546-9.
[238] Z. Chen, T. Zhang, Y. Wu, I. Madsen, J. Ma, K. Sagoe-Crentsil, A. Neild, W. Duan, In-situ XRD study of the effects of amino acids on the carbonation kinetics of cementitious calcium silicates, Cem. Concr. Res. 193 (2025) 107879, https://doi.org/10.1016/J.CEMCONRES.2025.107879.
[239] V. Hérault, E. Foy, É. Charon, G. Touzé, C.C.D. Coumes, S. Poyet, C. Chevallard, M.A. Levenstein, Cement-on-a-chip: a microreactor for operando studies of the carbonation curing of cementitious materials, Lab Chip 25 (2025) 6475–6489, https://doi.org/10.1039/D5LC00638D.
[240] Q. Qiu, A state-of-the-art review on the carbonation process in cementitious materials: fundamentals and characterization techniques, Construct. Build Mater. 247 (2020) 118503, https://doi.org/10.1016/J.CONBUILDMAT.2020.118503.
[241] J. Han, Y. Liang, W. Sun, W. Liu, S. Wang, Microstructure modification of carbonated cement paste with six kinds of modern microscopic instruments, J. Mater. Civ. Eng. 27 (2015) 1–14, https://doi.org/10.1061/(asce)mt.1943-5533.0001210.
[242] X. Miao, L. Zhang, Y. Wang, L. Wang, X. Fu, M. Gan, X. Li, Characterisation of wellbore cement microstructure alteration under geologic carbon storage using X-ray computed micro-tomography: a framework for fast CT image registration and carbonate shell morphology quantification, Cem. Concr. Compos. 108 (2020) 103524, https://doi.org/10.1016/J.CEMCONCOMP.2020.103524.
[243] J.S. Kim, K.S. Youm, J.H. Lim, T.S. Han, Effect of carbonation on cement paste microstructure characterized by micro-computed tomography, Construct. Build Mater. 263 (2020) 120079, https://doi.org/10.1016/j.conbuildmat.2020.120079.
[244] B. Cordonnier, M. Cotte, D. Eakins, M. Krisch, P. Lee, S. Lyonnard, G. Martínez-Criado, J. McCarthy, A. Rack, Novel access modes at the ESRF–EBS, Synchrotron Radiat. News. 38 (2025) 14–19, https://doi.org/10.1080/08940886.2025.2560289.
[245] Z. Su, Z. Yue, P.P. Paul, X. Liu, A.T.M. Marsh, C. Unluer, J.L. Provis, T.L. Burnett, S.A. Bernal, P.J. Withers, 4D imaging of microstructural evolution in alkali-activated slag cement pastes: linking pore-network topology to performance, Cem. Concr. Compos. 166 (2026) 106382, https://doi.org/10.1016/J.CEMCONCOMP.2025.106382.
[246] P. Zhang, F.H. Wittmann, P. Lura, H.S. Müller, S. Han, T. Zhao, Application of neutron imaging to investigate fundamental aspects of durability of cement-based materials: a review, Cem. Concr. Res. 108 (2018) 152–166, https://doi.org/10.1016/J.CEMCONRES.2018.03.003.
[247] E. Rossi, S. Governo, M. Shakoorioskooie, Q. Zhan, S. Mundra, D. Mannes, A. Kaestner, U. Angst, X-ray computed tomography to observe the presence of water in macropores of cementitious materials, RILEM Tech. Lett. 8 (2023) 165–175, https://doi.org/10.21809/RILEMTECHLETT.2023.190.
[248] L. Yang, Y. Zhang, Z. Liu, P. Zhao, C. Liu, In-situ tracking of water transport in cement paste using X-ray computed tomography combined with CsCl enhancing, Mater. Lett. 160 (2015) 381–383, https://doi.org/10.1016/J.MATLET.2015.08.011.
[249] Y. Peng, G. Zhao, Y. Qi, Q. Zeng, In-situ assessment of the water-penetration resistance of polymer modified cement mortars by μ-XCT, SEM and EDS, Cem. Concr. Compos. 114 (2020) 103821, https://doi.org/10.1016/J.CEMCONCOMP.2020.103821.
[250] E.A. Chavez Panduro, M. Torsæter, K. Gawel, R. Bjørge, A. Gibaud, Y. Yang, S. Bruns, Y. Zheng, H.O. Sørensen, D.W. Breiby, In-situ X-ray tomography study of cement exposed to CO2 saturated brine, Environ. Sci. Technol. 51 (2017) 9344–9351, https://doi.org/10.1021/ACS.EST.6B06534.
[251] E.A. Chavez Panduro, B. Cordonnier, K. Gawel, I. Børve, J. Iyer, S.A. Carroll, L. Michels, M. Rogowska, J.A. McBeck, H.O. Sørensen, S.D.C. Walsh, F. Renard, A. Gibaud, M. Torsæter, D.W. Breiby, Real time 3D observations of Portland cement carbonation at CO2 storage conditions, Environ. Sci. Technol. 54 (2020) 8323–8332, https://doi.org/10.1021/ACS.EST.0C00578.
[252] F. Renard, B. Cordonnier, D.K. Dysthe, E. Boller, P. Tafforeau, A. Rack, A deformation rig for synchrotron micro-tomography studies of geomaterials under conditions down to 10 km depth in the Earth, J. Synchrotron Radiat. 23 (2016) 1030–1034, https://doi.org/10.1107/S1600577516008730.
[253] DIFFRAC.TOPAS - Bruker. https://www.bruker.com/en/products-and-solutions/diffractometers-and-x-ray-microscopes/x-ray-diffractometers/diffrac-suite-software/diffrac-topas.html, 2025. (Accessed 26 May 2025).
[254] B.H. Toby, R.B. Von Dreele, IUCr, GSAS-II: the genesis of a modern open-source all purpose crystallography software package, J. Appl. Cryst. 46 (2013) 544–549, https://doi.org/10.1107/S0021889813003531.
[255] J.H. O'Donnell, R.B. Von Dreele, M.K.Y. Chan, B.H. Toby, A scripting interface for GSAS-II, J. Appl. Cryst. 51 (2018) 1244–1250, https://doi.org/10.1107/S1600576718008075.
[256] J. Schindelin, I. Arganda-Carreras, E. Frise, V. Kaynig, M. Longair, T. Pietzsch, S. Preibisch, C. Rueden, S. Saalfeld, B. Schmid, J.-Y.Y. Tinevez, D.J. White, V. Hartenstein, K. Eliceiri, P. Tomancak, A. Cardona, Fiji: an open-source platform for biological-image analysis, Nat. Methods 9 (2012) 676–682, https://doi.org/10.1038/nmeth.2019.
[257] IPSDK explorer. https://www.reactivip.com/ipsdk-explorer-en/, 2025. (Accessed 26 May 2025).
[258] M. Gendron, J.-F. Fontaine, B. Provencher, E. Yen, N. Piché, M. Marsh, Centralizing digital resources for data management, processing, and analysis for enterprise scale imaging research, Microsc. Microanal. 27 (2021) 1084–1085, https://doi.org/10.1017/S1431927621004086.
[259] T. Simonnet, S. Grangeon, F. Claret, N. Maubec, M.D. Fall, R. Harba, B. Galerne, Phase quantification using deep neural network processing of XRD patterns, IUCrJ 11 (2024) 859–870, https://doi.org/10.1107/S2052252524006766.
[260] V. Poline, R.R.P. Purushottam Raj Purohit, P. Bordet, N. Blanc, P. Martinetto, Neural networks for rapid phase quantification of cultural heritage X-ray powder diffraction data, J. Appl. Cryst. 57 (2024) 831–841, https://doi.org/10.1107/S1600576724003704/.
[261] N.I. Prasianakis, AI-enhanced X-ray diffraction analysis: towards real-time mineral phase identification and quantification, IUCrJ 11 (2024) 647–648, https://doi.org/10.1107/S2052252524008157.
[262] C. Wang, X. Li, R. Wan, J. Chen, J. Ye, K. Li, A. Li, R. Tai, A. Sepe, Accelerating imaging research at large-scale scientific facilities through scientific computing, J. Synchrotron Radiat. 31 (2024) 1317–1326, https://doi.org/10.1107/S1600577524007239.
[263] E. Maire, P.J. Withers, Quantitative X-ray tomography, Int. Mater. Rev. 59 (2014) 1–43, https://doi.org/10.1179/1743280413Y.0000000023.

[264] M.M. Thakur, S. Enright, R.C. Hurley, Phase segmentation in X-ray CT images of concrete with implications for mesoscale modeling, Constr. Build. Mater. 403 (2023) 133033, https://doi.org/10.1016/J.CONBUILDMAT.2023.133033.
[265] I. Arganda-Carreras, V. Kaynig, C. Rueden, K.W. Eliceiri, J. Schindelin, A. Cardona, H.S. Seung, Trainable Weka Segmentation: a machine learning tool for microscopy pixel classification, Bioinformatics 33 (2017) 2424–2426, https://doi.org/10.1093/bioinformatics/btx180.
[266] Avizo software|materials characterization software. https://www.thermofisher.com/es/en/home/electron-microscopy/products/software-em-3d-vis/avizo-software.html, 2025. (Accessed 15 May 2025).
[267] F.W.K. Khudhur, A. MacEnte, J.M. MacDonald, L. Daly, Image-based analysis of weathered slag for calculation of transport properties and passive carbon capture, Microsc. Microanal. 28 (2022) 1514–1525, https://doi.org/10.1017/S1431927622000915.
[268] Dragonfly tutorials. https://dragonfly.comet.tech/en/resources/user-tutorials, 2025. (Accessed 8 January 2026).
[269] IPSDK: tutos & scripts - Reactiv IP. https://www.reactivip.com/support-tutos-scripts/, 2025. (Accessed 8 January 2026).
[270] IPSDK: smart image processing - YouTube. https://www.youtube.com/@ipsdk_explorer/videos, 2025. (Accessed 8 January 2026).
[271] P.K.M. Tung, A.Y. Halim, H. Wang, A. Rich, C. Marjo, K. Regenauer-Lieb, Deep-XFCT: deep learning 3D-mineral liberation analysis with micro-X-ray fluorescence and computed tomography, Energies 15 (2022) 5326, https://doi.org/10.3390/EN15155326.
[272] J.R.A. Godinho, A. Hassanzadeh, T. Heinig, 3D quantitative mineral characterization of particles using X-ray computed tomography, Nat. Resour. Res. 32 (2023) 479–499, https://doi.org/10.1007/S11053-023-10169-5.
[273] A. Kornilov, I. Safonov, I. Yakimchuk, A review of watershed implementations for segmentation of volumetric images, J. Imaging 8 (2022) 127, https://doi.org/10.3390/JIMAGING8050127.
[274] R.L. Mitchell, A. Holwell, G. Torelli, J. Provis, K. Selvaranjan, D. Geddes, A. Yorkshire, S. Kearney, Cements and concretes materials characterisation using machine-learning-based reconstruction and 3D quantitative mineralogy via X-ray microscopy, J. Microsc. 294 (2024) 137–145, https://doi.org/10.1111/JMI.13278.
[275] S. Shirani, A. Cuesta, I. Santacruz, A.G. De la Torre, A. Diaz, P. Trtik, M. Holler, M. A.G. Aranda, X-ray near-field ptychographic nanoimaging of cement pastes, Cem. Concr. Res. 185 (2024) 107622, https://doi.org/10.1016/j.cemconres.2024.107622.
[276] A.D. Parsons, S.W.T. Price, N. Wadeson, M. Basham, A.M. Beale, A.W. Ashton, J.F. W. Mosselmans, P.D. Quinn, Automatic processing of multimodal tomography datasets, J. Synchrotron Radiat. 24 (2017) 248–256, https://doi.org/10.1107/S1600577516017756.
[277] R. Rao, Synchrotrons face a data deluge, Phys. Today (2020), https://doi.org/10.1063/PT.6.2.20200925A.
[278] R. Mokso, C.M. Schlepütz, G. Theidel, H. Billich, E. Schmid, T. Celcer, G. Mikuljan, L. Sala, F. Marone, N. Schlumpf, M. Stampanoni, GigaFRoST: the gigabit fast readout system for tomography, J. Synchrotron Radiat. 24 (2017) 1250–1259, https://doi.org/10.1107/S1600577517013522.
[279] C. Wang, F. Yu, Y. Liu, X. Li, J. Chen, J. Thiyagalingam, A. Sepe, Deploying the Big Data Science Center at the Shanghai Synchrotron Radiation Facility: the first superfacility platform in China, Mach. Learn. Sci. Technol. 2 (2021) 035003, https://doi.org/10.1088/2632-2153/ABE193.
[280] X. Li, Y. Zhang, Y. Liu, P. Li, H. Hu, L. Wang, P. He, Y. Dong, C. Zhang, A high-throughput big-data orchestration and processing system for the High Energy Photon Source, J. Synchrotron Radiat. 30 (2023) 1086–1091, https://doi.org/10.1107/S1600577523006951.
[281] J. Vijayakumar, H. Dejea, A. Mirone, C. Muzelle, J. Meyer, C. Jarnias, K. Dollman, S. Zabler, L. Paolasini, A. Bellier, B. Cordonnier, V. Fernandez, P. Tafforeau, Multiresolution phase-contrast tomography on BM18, a new beamline at the European Synchrotron Radiation Facility, Synchrotron Radiat. News. 37 (2024) 16–25, https://doi.org/10.1080/08940886.2024.2414724.
[282] B. Knoll, F. Keilmann, Near-field probing of vibrational absorption for chemical microscopy, Nature 399 (1999) 134–137, https://doi.org/10.1038/20154.
[283] F. Basquiroto de Souza, C. Zheng, S. Chen, Y. Liu, K. Sagoe-Crentsil, W. Duan, Near-field infrared microscopy: a novel analytic mapping technique to nanocharacterize calcium silicate-based cement materials, Cem. Concr. Res. 147 (2021) 106525, https://doi.org/10.1016/J.CEMCONRES.2021.106525.
[284] H.A. Bechtel, S.C. Johnson, O. Khatib, E.A. Muller, M.B. Raschke, Synchrotron infrared nano-spectroscopy and -imaging, Surf. Sci. Rep. 75 (2020) 100493, https://doi.org/10.1016/J.SURFREP.2020.100493.
[285] T.M. Santos, S. Lordano, R.A. Mayer, L. Volpe, G.M. Rodrigues, B. Meyer, H. Westfahl, R.O. Freitas, Synchrotron infrared nanospectroscopy in fourth-generation storage rings, J. Synchrotron Radiat. 31 (2024) 547–556, https://doi.org/10.1107/S1600577524002364.